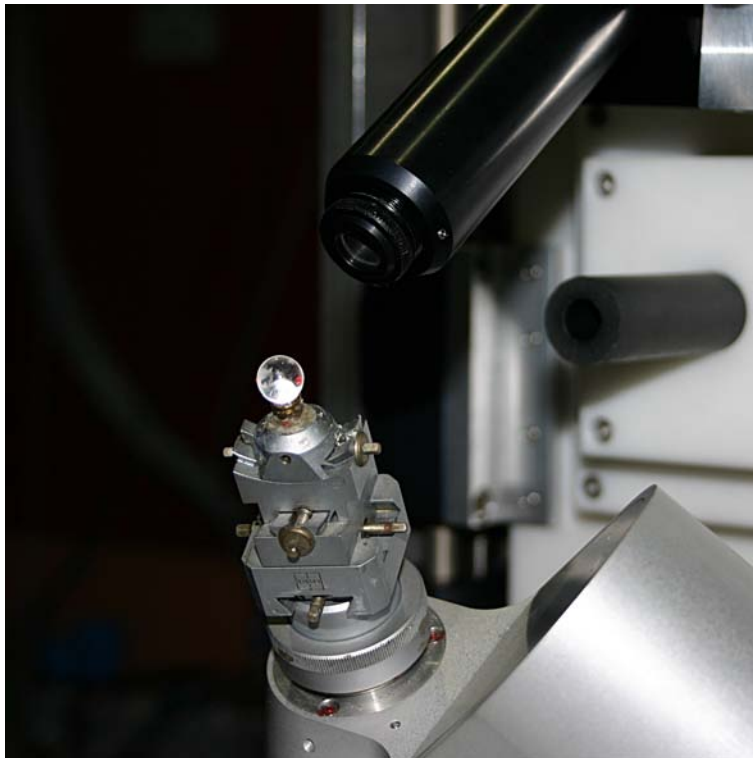


ANNUAL REPORT 2005  
Forschungsneutronenquelle  
Heinz Maier-Leibnitz (FRM II)



cover image: Quartz test sample at the single crystal diffractometer RESI

# Contents

<b>Directors' report</b>	<b>1</b>
<b>The Year in Pictures</b>	<b>2</b>
<b>1 Central services</b>	<b>5</b>
1.1 FRM II in Routine Operation	5
1.2 Neutron flux values and spectra	6
1.3 Reduced Enrichment for FRM II	9
1.4 Detector and Electronics Lab	11
1.5 Sample Environment	12
1.6 IT Services	12
1.7 HELIOS	15
1.8 Hot Neutron Source	16
1.9 Neutron Optics	18
<b>2 Instruments</b>	<b>21</b>
2.1 NEPOMUC	21
2.2 TOF-PAES	22
2.3 PAES	23
2.4 MEPHISTO	24
2.5 MIRA	25
2.6 Simulations for a new neutron guide switch	26
2.7 REFSANS	27
2.8 SPODI	29
2.9 STRESS-SPEC	31
2.10 RESI	33
2.11 Irradiation	34
2.12 SPHERES	37
2.13 PANDA	38
2.14 MAFF	40
2.15 N-REX+	41
2.16 PUMA	43
2.17 NECTAR	44
2.18 SANS-1	46
2.19 ANTARES	48
2.20 Fission Neutron Source	50
2.21 RESEDA	51
<b>3 Scientific Highlights</b>	<b>53</b>
3.1 Magnetic-field induced instability in MnSi	53
3.2 CDBS:Measurements on Mg-Alloys	54
3.3 Stroboscopic Neutron Imaging	55
3.4 Small-angle scattering effects in radiography	57
3.5 TOFTOF: Dynamics of melts	59
3.6 TRISP:Phonon Linewidths in Pb	60

---

<b>4 Facts and Figures</b>	<b>62</b>
4.1 User Program	62
4.1.1 User support	63
4.2 Public relations	65
4.3 Committees	68
4.4 Staff	74
4.5 Publications	77
<b>Imprint</b>	<b>79</b>

## Directors' report

### Successful Start of Routine Operation at FRM II

The outstanding event of the past year was certainly the beginning of the routine operation of FRM II. After having completed the nuclear commissioning in 2004 the Bavarian regulator gave the permission for routine operation of FRM II on April 22, 2005. As a consequence, the Technische Universität München took over FRM II from the general contractor Siemens/Framatome ANP on April 25, 2005. We would like to express our sincere thanks to the staff of Siemens/Framatome ANP that has built a safe and extremely powerful neutron source. At the same time the general contractor was released from his nuclear co-responsibility, which went over exclusively into the hands of the Technische Universität München up from this date. Immediately after, the 2nd fuel element was put into the core position. On Tuesday, May 2, FRM II reached its nominal power of 20 MW and the first neutrons were delivered to the users. Altogether, FRM II operated for 3 full cycles in 2005. The 52-day-rhythm for each cycle was only interrupted for a short period, among others due to two extremely strong thunderstorms, which interrupted the current supply in the region around Garching. The regular maintenance interval after the 3rd cycle was finished in due time. At the very end of 2005 the 5th fuel element was loaded into the core in order to start the 5th cycle on January 5, 2006.

The neutron fluxes at the instruments are fulfilling more than our expectations. The neutron beams which

come from the cold source through the neutron guides to the positions at the instruments have been characterized in great detail. Some of them are the most intensive ones world wide. By the end of 2005, 14 beam instruments were in operation. We expect 5 further instruments to start routine operation in 2006. 278 proposals were submitted in 2 proposal rounds in 2005. Beam time was overbooked by a factor of 2 on the average. About 32 % of the beam requests came from research groups outside of Germany.

The silicon doping, the pneumatic rabbit system and other irradiation facilities are routinely serving our industrial clients by a very pure thermal neutron spectrum and suppression of fast neutron flux by factors between  $10^3$  -  $10^5$ . Single crystalline silicon rods of a diameter of 20 cm to 50 cm in height show the demanded homogeneous doping needed by the semiconductor industry. Industry also booked experimental time at beam instruments like the strain scanner StressSPEC and the radiography station ANTARES. The Centre for Industrial Applications (IAZ) welcomed its first lodger in 2005. Offices and laboratories will be used for the production of radio pharmaceuticals.

Furthermore FRM II participated in the open house on the Garching campus last year. As usual a maximum of 500 visitors were guided through the nuclear and experimental facilities.

In June 2005 the construction work for the combined experimental and office building housing for the FZ-Jülich

outstation was started. In early January 2006 the 1800  $m^2$  large base concrete plate was cast at a Bavarian winter temperature of about  $-10^\circ$  C. The first occupants are expected to move in during December 2006. This building was also in the centre of a dispute with our antagonists accusing FRM II of illegally drilling holes into the outer reactor wall in order to feed particle beams into the new experimental hall. In late December, during a visit to the location, the Mayor of Garching and the members of the City Parliament convinced themselves that all of these accusals would withstand a verification.


Prof. Schreckenbach, who had begun to structure the operation group in 1999 and become the successor of the project manager Dr. Axmann in 2002, finished the construction and started FRM II successfully. On December 31, 2005 the term of Prof. Klaus Schreckenbach as Technical Director of FRM II ended. Routinely he handed over the steering wheel to Dr. Ingo Neuhaus. Dr. Ingo Neuhaus studied Mechanical and Nuclear Engineering at the RWTH Aachen, received his PhD for studying plutonium reduction by using thorium based fuel in PWR. Before joining the FRM-II staff in April 2005 Dr. Neuhaus was responsible for the nuclear operation of the Jülich heavy water research reactor.

Colleagues, users and friends of FRM II wish to express their thanks to Prof. Schreckenbach on the occasion of a Farewell Colloquium which will take place on May 15, 2006.



Guido Engelke

Winfried Petry



Klaus Schreckenbach

## The Year in Pictures



**14 April 05:** The Centre for Industrial Users (IAZ) has been completed.



**3 June 06:** ANTARES receiving visitors from the Bavarian Ministry of Culture, Research and Arts, MD Ulrich Wilhelm and Dr. Ulrike Kirste, and the first scientific user at ANTARES: Dr. Meneske Bastürk, Atomic Institute, Vienna (center); group left: Veronika Vitzthum, ANTARES staff, Prof. Schreckenbach, Technical Director FRM II, Dr. Ingo Neuhaus, designated Technical Director, and Dr. Burkhard Schillinger, head of ANTARES.



**6 May 05:** The very first users at FRM II: Dr. Klaus Habicht / BENSC (far left) and Pegor Aynajian, Diploma student at MPI Stuttgart (far right) at the NRSE-TAS instrument together with Prof. Petry (FRM II) and Kathrin Buchner, MPI.



**17 March 2005:** Visitors from the Federal Ministry of Education and Research (BMBF): Dr. Beatrix Vierkorn-Rudolph and State Secretary W.-M. Catenhusen (right).



**25 April 05:** Siemens handing over the Neutron Research facility to the Technische Universität München: Prof. Schreckenbach, Technical Director FRM II, Mr. Eisenbeiß, Head of the Administration ZA1, and Mr. Engelke, Administrative Director FRM II, signing the transfer documents.



**24 November 05:** Inauguration of N-REX+ operated by the Max-Planck-Institute Stuttgart: Prof. Petry; Prof. Dosch, MPI Stuttgart; Dr. Ulrike Kirste, Bavarian Ministry of Science, Research and Arts; Dr. Rainer Gastl, Max-Planck-Society; Dr.-Ing. Kuch, Management TUM.



**27 April 05:** Celebrating the successful transfer: MDgt. Dr. Brandmair, Bavarian Ministry for Environment, Health and Consumer Protection; Prof. Schilling, University Management; Prof. Schreckenbach, Technical Director FRM II; Mr. Grolle, Framatome ANP; Mrs. Marzin, Administration TUM; Prof. Petry, Scientific Director, Mr. Eisenbeiß, Head of the Administration at Garching; Mr. Donath, Mr. Gyr, Mr. Falke, Mr. Bergmann, Framatome ANP (2nd row, from left to right); Mr. Novak and Mr. Landgraf, Framatome ANP GmbH (1st row).



**20 December 05:** Prof. Petry guiding the members of the Garching town council through the research reactor: On his right Mayor Manfred Solbrig and Mayor Hannelore Gabor (far right) and Walter Kratzl (far left), Manfred Kick and Annette Knott.



**7 October 05:** Freunde und Förderer der TU München visiting the FRM II (from left to right): Dr. Eva Sandmann, Dipl.-Ing. Wolfgang Kling, Robin Kling, Dr. Volker Jung, Heide Jung, (from left to right) and Dr. Horst Nasko, Johannes Ortner, Maximilian Grauvogl



**20 December 05:** Prof. Dr. Dr. hc. mult. W. A. Herrmann, president of the TUM, welcomes members of the Garching town council at the FRM II





# 1 Central services

## 1.1 FRM II in Routine Operation

**K. Schreckenbach**<sup>1</sup>

<sup>1</sup>Forschungsmittelnquelle Heinz Maier-Leibnitz (FRM II), TU München

Following the successful nuclear start-up of the FRM II in 2004 with one full reactor cycle, extensive reports on the results were prepared and submitted to the regulatory body (StMUGV). In addition, various technical improvements were carried out especially at the beam tubes, the neutron guides and the operation of the cold source. Based on these reports, the completion of the technical improvements and the fulfilment of obligations arising from the operation licence the StMUGV granted the approval for routine operation on April 22, 2005.

During the construction and the nuclear start-up TUM and the general contractor Siemens/Framatome were the common holder of the nuclear licence and the nuclear responsibility for the FRM II. After the approval for routine operation Siemens/Framatome left this responsibility on April 14, 2005. Further on TUM is the only holder of the nuclear licence and is working on its own responsibility. The change over was worked out smoothly and the contractor remained on-site only for the completion of still open technical im-

provements.

Following the approval for routine operation the second fuel element was immediately placed in the operational position. After start-up tests full power was achieved on May 2, 2005. Three full reactor cycles (52 days at 20 MW) were scheduled for 2005. This goal was accomplished on December 19, 2005 when the fourth reactor cycle was finished. The three cycles were running from 2/5 to 24/6/2005, 12/7/ to 8/9/2005, and 26/10/ to 19/12/2005.

There were only short interruptions within the cycles. They were caused by two strong thunderstorms with a break of the external power supply. Other interruptions were due to planned short stops and minor problems with measurement units.

The long reactor shutdown from September 9, 2005 to October 15, 2005 was used for the extensive maintenance program and for work at neutron guides and radiation shielding. With the expe-

rience of 2005 we are quite optimistic that 5 full reactor cycles are technically possible in 2006. A new fuel element was already placed in December 2006 for the early start of the fifth cycle in 2006.

At the end of 2005 Prof. K. Schreckenbach finished his term as the first technical Director of the FRM II. He had started at FRM II in May 1999 with organisation of the reactor operation group and passed through the difficult period of the licence for nuclear operation and the nuclear start-up of the FRM II. The designated successor in the responsibility as Technical Director, Dr. Ingo Neuhaus, came to the FRM II in April 2005 for a learning period at the facility, a period which is anyhow obligatory due to the nuclear regulations. I. Neuhaus brought with him a dedicated experience from his former job as head of the Jülich research reactor DIDO. Based on his experience at Jülich and his new experience at the FRM II the regulatory body readily granted him the agreement for his new responsibility.

## 1.2 Neutron flux values and spectra at operating FRM II

A. Röhrmoser<sup>1</sup>

<sup>1</sup>ZWE FRM II, TU München

In April 2005 routine operation of FRM II started. Flux measurements were made in addition to those already performed during the nuclear commissioning phase with the first fuel element in 2004 at different power steps. This report presents a comparison of the measurements and the accompanying calculations.

These measurements were done in and outside the D<sub>2</sub>O-moderator vessel. 30 cm distant from the fuel element the neutron spectrum is quite well thermalised and the very huge part of the vessel serves no more as a moderator but as a storage for the neutrons, the best one we can have. So the name 'moderator' is only half of the truth.

There are several positions in the D<sub>2</sub>O vessel where the usually very well defined thermal neutron spectrum is heavily disturbed, e.g. around strong absorbers as there are the shut down rods, which are withdrawn during op-

eration of FRM II to the upper position of rest or in the region of the strongly absorbing Cd-nose of the vertical beam tube SR11. Further there are some regions of re-thermalisation to lower or higher temperature in the D<sub>2</sub>O. Those areas are restricted to the cold and hot source regions.

The measurements and calculations mentioned now are done with very low background of fast flux with exception of the converter beam tube SR10 as discussed later.

### Irradiation positions in the D<sub>2</sub>O vessel

#### Power determination through flux measurement in the 'high flux rabbit pipe' (HFRP)

The flux at the position in the high flux rabbit pipe HFRP, at 8 cm above mid plane and at a radius of 45 cm, was calculated being perturbed by all other installations in the vessel to  $3.6 \cdot 10^{14} \text{ cm}^{-2} \text{ s}^{-1}$ . The unperturbed flux at the same position was calculated to  $5 \cdot 10^{14} \text{ cm}^{-2} \text{ s}^{-1}$ . But the most important flux depression for the point of measurement originates from the HFRP pipe itself. Including this, the absolute flux for the HFRP position at 20 MW thermal power was calculated to [1]:

$$\Phi_n^{HFRP} = 1.84 \cdot 10^{14} \text{ cm}^{-2} \text{ s}^{-1}$$

The first flux measurements came from gold activation in the high flux rabbit pipe (HFRP) at 10 kW, 160 kW, 2 MW and 5 MW power steps of FRM II during nuclear start up. When extrapolating the measured values to 20 MW thermal power by means of a final comprehensive analysis of all power data, one can derive a best value of measured thermal flux:

$$\Phi_n^{HFRP} = 1.7 \cdot 10^{14} \text{ cm}^{-2} \text{ s}^{-1}$$

Including fast spectrum corrections derived from the calculated data one gets again  $1.8 \cdot 10^{14} \text{ cm}^{-2} \text{ s}^{-1}$ .

The flux measurements in the HFRP positions were also undertaken in order to calibrate the absolute thermal power during the commissioning phase. Two critical items determine the accuracy of this procedure. Firstly, the gold foil activation measurements in the HFRP position have an accuracy of about 10 %, secondly the computer simulations, which make the link between the measured flux at the HFRP position and the maximum neutron fluxes in the moderator, have to rely on the precise 3-D input of all kind of devices in the moderator vessel.

It turned out that despite of the error bars for the gold foil activation analysis this calibration of the absolute power was of great help for power determinations at low power loads. We further asked the question whether the comparison of measured and calculated flux values at the HFRP position can be used to determine the maximum flux level in the moderator vessel. Here, it turned out that a much more reliable determination of the maximum neutron flux stems from reactivity measurements of the reactor in comparison to the predictions by the 3D-simulations of the neutronics in the D<sub>2</sub>O vessel.

Considering all the information the maximum thermal flux values are

$$\Phi_{th}^{max} = 8.0 \cdot 10^{14} \text{ cm}^{-2} \text{ s}^{-1} \text{ unperturbed}$$

$$\Phi_{th}^{max} = 6.4 \cdot 10^{14} \text{ cm}^{-2} \text{ s}^{-1} \text{ perturbed}$$

The perturbed value is of course an average value because perturbation is rather unisotropic around the fuel element due to the different inserts in the moderator vessel.

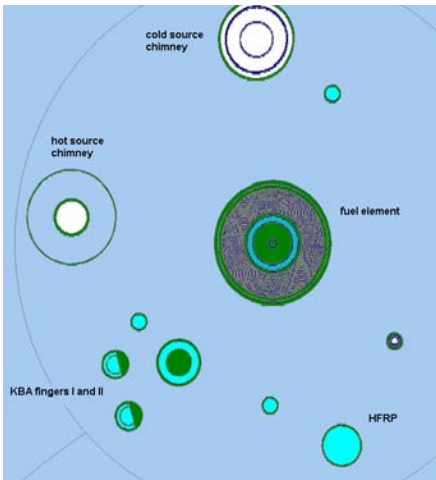


Figure 1.1: Horizontal cut through the D<sub>2</sub>O vessel and the core, 20 cm above core mid plane; the positions of interest are shown, as the (HFRP) pipe and the SDA, which come vertically from the top. Two fingers of the KBA are fed inclined from the top and reach down to this depth. Both are cut at the bottom lid in the picture. Some other installations, like the supply chimneys of the cold and hot source, can be perceived.

**Rabbit systems**

Fig. 1.2 shows the calculated perturbed flux profile  $\Phi_{th}$  at irradiation positions along the two fingers of the KBA. All flux values are calibrated to a thermal reactor power of 20 MW. Each finger provides five irradiation positions, for which the average values are given. For the topmost two positions there also exist measured data [2]. A remarkably good agreement between measurements and calculations has been found for all four measured (2\*2) top positions.

According to the calculations the fast neutron flux is suppressed by two decades at the bottom position 1 and three decades at the end position 5. Measuring the fast flux is clearly more difficult and in this case it gave merely half of the calculated values for the top positions. The calculations are judged to be reliable.

For the somewhat comparable irradiation positions of the pneumatic rabbit system RPA there have already existed more detailed calculations and the self shielding by the pipes is drastically lower than in the described cases HFRP and KBA. So, the officially exhibited values should be rather good [3].

**Silicium doping facility SDA**

The silicon doping facility SDA is located in the  $D_2O$  vessel at a distance of 1 m from the core center. In order to achieve homogeneous doping over the whole volume of single crystals with a height of 50 cm and a variable diameter between 4 to 8 inch, it is necessary to shape the neutron flux profile. Without such measures gradients in flux of at least 10 % would occur between the mid height of a cylinder and its two extremes. This flux homogenizing is obtained by a Ni-cylinder surrounding the silicon blocks having an optimized thickness profile. The here presented calculations are of considerably higher precision than those performed in the licensing phase of FRM II. As a consequence vertical homogeneity could be considerably improved.

The now optimized Ni-liner has a trapezium shape and is better covering the entire silicon blocks to overcome the overall trend of the flux depression at the ends. Figure 1.3 shows the axial flux profiles in a 6"-Si-block, which is now much flatter over the whole block height.

Since the Ni-layer is really thin and shaped, the question can be risen, how precise it can be fabricated. The calculations clearly show that the tolerances for the thickness have to be less than 0.2 mm (preferred 0.1 mm) in order to achieve homogeneity.

Very last results showed that an easier solution could be regarded dismissing any thin and shaped absorber layer. When shaping the width of the  $H_2O$  channel, surrounding the silicon block, a comparable flux shaping can be obtained without changes to the overall geometry of the SDA facility. The manufacturing would be quite uncomplicated, having no questions about the achievable precision or any absorber burn up.

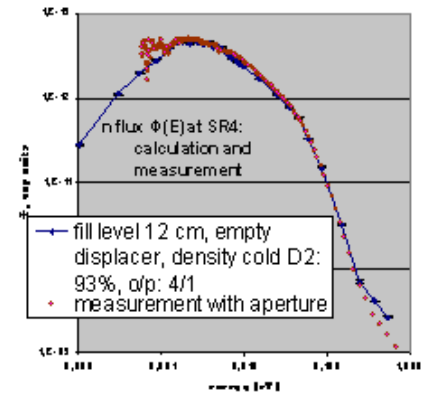


Figure 1.4: n-current  $j_n(E)$  at SR4 end position; comparison of measured (red points) and 3d-calculated (blue dots) spectra.

**Flux values at beam tubes**

FRM II is furnished with a series of beam tubes for the scientific usage. Three beam tubes (SR 1,2,4) are fed by the cold source (CNS) of FRM II at 40 cm distance to the core central axis. The biggest beam tube SR1 supplies six neutron guides which feed the neutrons into an external experimental hall. The other two cold beam tubes lead into the reactor hall.

**Cold Spectrum at SR4**

Beam tube SR4 allows measurements of the spectrum at an end position with direct view onto the cold source surface. The measurements were done at full power of FRM II close to the end of the nuclear commissioning phase. Figure 1.4 shows the measured and the calculated spectra for this end position.

Fig. 1.4 shows an excellent agreement between the measured and calculated spectrum over three decades in energy; the calculated values extend even one extra decade down to 0.1 meV. To reach that perfect agreement several parameters had to be fine-tuned in an iterative procedure. The most important ones were the exact geometry and the filling of the cold source. For instance, the cold source apparently was filled to a level of 12 cm, the displacer was empty and a density of 93% was assumed for

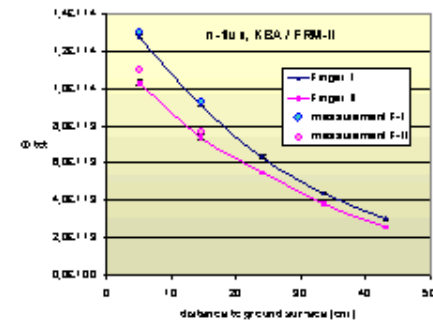


Figure 1.2:  $\Phi_{th}$  at KBA position along the two fingers after a 3D-calculation. For the two top positions exist measurements (light colored dots).

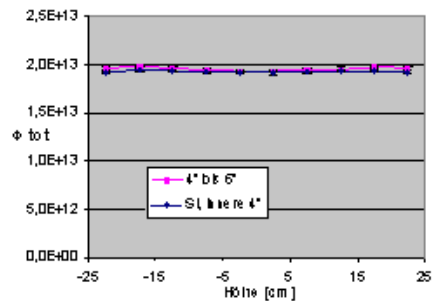


Figure 1.3: calculated axial flux shape in a 6"-Si-block in the SDA facility.

the liquid  $D_2$ . Together with these parameter studies, measurements of the spectrum at SR4 may serve to precisely characterize the filling conditions of the cold source. Fig. 1.4 also clearly reveals the characteristic undermoderation of the FRM II cold source.

Measured data turn out to be less reliable below neutron energies of 1 meV. In this area and even down to far lower energies only calculations provide reliable data. Because the calculations so nicely meet the spectral measurements at SR4, it is concluded that the calculations are of similar reliability for the two other cold beam holes SR1 and SR2, where measurements are not feasible. These calculations are the basis for a prediction of the flux properties at the output side of the cold beam tubes and complex neutron guide systems of operating FRM II.

### Source flux for the neutron guide hall

For further calculations an interface was constituted in form of a source file, which provides all the specific particle tracks as start data. In this case the generated source file is a collection of neutron tracks entering SR1 with flight direction towards the exit. Each single track is stored with exact position, direction, energy and weight. The calculations were run for more than a week on a dedicated computer, so the statistical variance is really low. Figures 1.5 and 1.6 show the distribution of the cold neutrons entering SR1 from such files for particular fill levels of the NCS:

1. The extreme case of a fill level FSt of the NCS of only 1.6 cm above center at a very low power of 200 kW. Due to insufficient heating the displacer volume is not evaporated. The NCS contains 13 l  $D_2$ .
2. A more usual operational case with a fill level of the NCS of 10 cm above center.

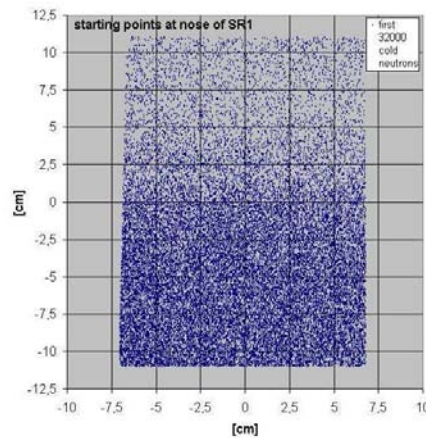


Figure 1.5: Distribution of cold neutrons entering the nose SR1 with flight direction towards the exit in the case of 200 kW reactor power with 13 l  $D_2$  in the CNS.

One can recognize in figure 1.5 and curve 'FSt +2 cm' in figure 1.6 that the lower part of the nose is better illuminated by cold neutrons than the upper part. The tracks are summed up horizontally and lead to the distributions of figure 1.6 over the nose height for both cases.

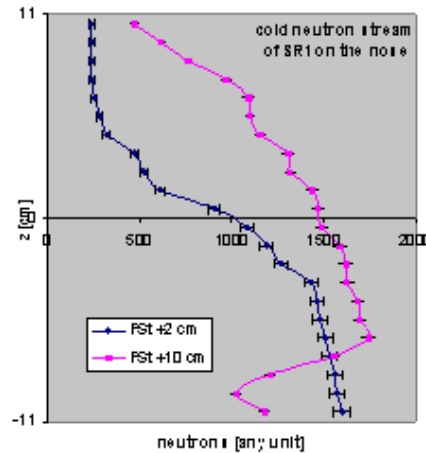


Figure 1.6: Calculated density distribution of cold neutrons entering SR1 with flight direction towards the exit as function of the height position on the nose for the two operational cases but normalized to the same reactor power and begin of cycle. Caused by the density step between vapor to liquid  $D_2$  surfaces a sharp decrease is observed in both cases.

For the extreme low power case 1) (blue curve) the distribution is very asymmetrical. Under more usual operational conditions (viola curve) the displacer in the CNS is evaporated and the cold SR1 neutrons at the nose arrive more symmetrically and more from the center of the CNS. This nicely confirms the idea of a flux gain due to the 'cavity effect'. Normalized to the same nominal power case 2) delivers 32 % more neutrons in comparison to case 1).

### Converter facility SKA

A comparable neutron and also  $\gamma$  source file was generated in beam tube SR10 for the converter facility SKA. Emphasis was put on the exact incorporation of the complex geometry of a converter facility. The total thermal power of the SKA is now calculated to about 70 kW. Further calculations which concentrate on dose values at a phantom at the beam exit use this source files as particle start data.

These calculations are now an important input for the qualification of the tumor therapy by fast neutrons required by the German rules for medical facilities.

- [1] FRM II. *Zu erwartende Neutronen-Messsignale während der nuklearen Inbetriebsetzung (IBS) des FRM II, OPA313.*
- [2] *Annual Report FRM II 2003*, 66.
- [3] *Annual Report FRM 2004*, 63.

## 1.3 Reduced Enrichment for FRM II

A. Röhrmoser<sup>1</sup>, W. Petry<sup>1</sup>, N. Wieschalla<sup>1</sup>

<sup>1</sup>ZWE FRM II, TU München

In 2001 an 'Agreement between the Federal Republic of Germany and the Free State of Bavaria on the Conversion of FRM II was written down and finally signed after the final operating license was granted in May 2003. This compromise is part of the final nuclear license and aims for the development of a new medium enriched fuel element until the end of the year 2010 (MEU, not more than 50% U-235; at the present high enriched fuel with 93% U-235 is used.). The TUM has established an international working group to meet this target. The planning is split into three periods:

1. Search for the fuel type, perform irradiations of fuel plates
2. Further test irradiations, final decision on the fuel type and design of the fuel element
3. Fabrication of the fuel element and licensing

It goes without saying that all the phases have to be accompanied by extensive calculations on a MEU fuel, to decide on the necessary uranium density for a conversion, to do parameter studies and to search for possible alternative pathways. The first 2 1/2-year period is ending with the year 2005. For phase 1 it was intended to be able to do a pre-selection of the fuel for a MEU fuel element. Activities had to be performed in the following fields:

- Calculations for the high density fuel(s) for FRM II geometry
- Irradiations of MEU fuel plates of full size
- Active participation in international research programs for dense fuel.

### Calculations with high density fuels

First enrichment studies for a new FRM were performed by TUM during the design phase in the 80'ies; one decade later at beginning of the construction phase for FRM II the RERTR (reduced enrichment for research and test reac-

tors) group at Argonne presented alternative fuel element designs with reduced enrichment. These calculations confirmed that a conversion to LEU was impossible for FRM II without severe geometry changes even with the theoretical limit of uranium metal densities of 19 g/cm<sup>3</sup>.

Any scenario to convert the FRM II has to keep the reactor power constant at 20 MW, to guarantee a duration of the fuel cycle of 52 days and to yield only marginal losses in the neutron flux and quality. For an enrichment of 50% an advanced fuel with high density is required when maintaining the dimensions of the HEU compact core fuel element. It is clear that some penalties arise from any reduced enrichment design for the users, some of which are more obvious, like some loss in flux values or less obvious ones as an increase in the production of Pu from 11g to about 100 g with the less enriched variants.

### Calculations with UMo/Al dispersive and monolithic fuel, actual results

Uranium-molybdenum dispersion fuel (UMo-Al) was and is under research worldwide up to a density of 8.5 gU/cm<sup>3</sup>. Our neutronics calculations were executed with the same numerical scenario and procedures that led to the HEU design of FRM II, where the fuel is U<sub>3</sub>Si<sub>2</sub> and has a maximum density of 3 gU/cm<sup>3</sup> to achieve 1040 MWd of operation with some reserve.

For **UMo/Al dispersive fuel** the result is that the uranium density in the fuel must be at least 7.75 g/cm<sup>3</sup> with an 235-U enrichment of 50%. When taking into account other aspects like the less fortunate power density distribution (s. below) some parameter range for corrections is needed and the minimum density can hardly be below 8.0 g/cm<sup>3</sup>. In total the core contains then 10.8 kg 235-U instead of 7.5 kg in the ac-

tual HEU case. The total U mass is 21.6 kg instead of 8.0 kg now. The important value of the radial form factor is clearly less opportune with the MEU fuel. Particularly the maximum of the heat load in the outer zone is much higher than actually and can not be accepted for a final design. At the same time this would lead to increased values of the maximum of the fission density (FD) in the fuel. Test irradiations have to show what fission densities the new fuel can withstand under conditions comparable to those in a reactor like FRM II.

The thermal flux is depressed by about 8.0% when compared to the actual HEU fuel.

With the availability of **UMo monolithic fuel** the density would be increased again a reasonable step forward. Despite of the technical problems to produce large fuel plates with gradients in fuel density and curved shape first calculations were performed with monolithic fuel of uranium density of 15.1 g/cm<sup>3</sup>. From a theoretically point of view the higher density could be used to further reduce the enrichment for the unchanged core geometry. As it can be derived from the calculations with UMo-Al dispersive fuel the mass of 235-U cannot be regarded to stay constant under the given conditions. Instead the harmful loss of neutrons in the 238-U has to be largely overcompensated for constant FRM II geometry. And this compensation factor will even raise stronger when further reducing the enrichment. This is shown in the figure 1, where the mass of 235U is drawn as a function of the enrichment in the current geometry. The horizontal line at density 19 g/cm<sup>3</sup> indicates the physical limit with metallic uranium. The calculations for 20% enrichment demands a hypothetical density of about 40 g/cm<sup>3</sup>.

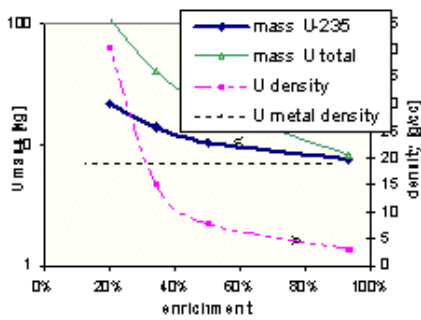


Figure 1.7: Mass of  $^{235}\text{U}$  and U-total (respectively the corresponding U density, right scale) necessary in FRM II to obtain a cycle length of 52 days. In the calculations particular enrichments have been chosen (see dots) and the uranium density has been treated as a variable.

In the case of 34% enrichment, which corresponds to the density of UMo monolithic fuel the mass of uranium in the fuel element would be about 40 kg instead of 8 kg now, thus five times higher. The mass of  $^{235}\text{U}$  would be in the order of 14 kg instead of 7.5 kg now, thus nearly doubled. The radial form factor rises even higher than already in the UMo/Al dispersive fuel case and further density gradients would have to be introduced. A fuel element of that kind still burns not more than 1.3 kg  $^{235}\text{U}$ , i.e. only 9.6% of  $^{235}\text{U}$  would be used, an unacceptable burn-up value. The loss in thermal neutron flux will be clearly more than 10%. The latter results are real penalties, more than marginal ones.

On the other side the high density of UMo monolithic fuel opens new possi-

bilities in the search for a balance between the contradicting demands of decreasing enrichment and highest operational quality of a neutron source. This could mean a better burn up ratio or in other words longing for a longer cycle length for the given FRM II geometry, to compensate the penalty of a lower flux value of 8-10% in the case of 50% enrichment. A raise in the power level is very difficult to achieve because of the less opportune power distribution in the reduced enrichment case.

### Fuel irradiation in phase I

For Phase I it was decided to irradiate four test plates of full size at the MTR reactor OSIRIS/Saclay. For this purpose six plates were produced by CERCA with UMo-Al dispersive fuel (8% wt. Mo). The uranium densities are 7 and  $8\text{g}/\text{cm}^3$ . Two of the  $8\text{g}/\text{cm}^3$  plates contain a Si additive, a possible "diffusion blocker". Before starting irradiation OSIRIS needed an extension of its license for heat flux values in the order of  $300\text{ W}/\text{cm}^2$  for the TUM plates to reach a targeted cladding surface temperature of  $100^\circ\text{C}$ . After some delay with this French licensing the irradiation could finally start 15.9.05 with 4 plates in two different IRIS devices. It is predicted that the aimed density of  $2.3 \cdot 10^{21}$  fissions/ $\text{cm}^3$  can be reached at first after  $3\frac{1}{2}$  cycles for the front plates of each IRIS-device and later for the second plate each device. The 3. cycle (start 15.12.05) shall be finished with the beginning of the year 2005. Me-

chanically thickness scans are done in situ after each cycle to measure the local swelling of the plates.

### Cooperation in UMo monolithic fuel research

The alternative of monolithic UMo fuel is presently under study at the RERTR Program. One of the main challenges with this very high density fuel is the fabrication of full size plates. So far only two test irradiations of small mini-plates have been performed. In August 2005 TUM and CEA/CERCA have signed a contract for 'Cooperation in development for UMo-monolithic fuel plates'. As soon as plates with this monolithic fuel can be fabricated a common TUM/CEA/CERCA irradiation experiment will be launched at OSIRIS.

### Metallographic studies

TUM contributes to high density fuel research. Actually the build up of the harmful UMo-Al interdiffusion layer during irradiation has to be better explained. In a new approach TUM irradiates UMo samples by a heavy ion beam in order to simulate irradiation induced diffusion as it takes place during fuel burn up. This study should reveal whether the diffusion is mainly caused by the fission product projectiles or rather stems from the thermal treatment during irradiation and could in general allow rather cheap metallographic studies.

## 1.4 Detector and Electronics Lab

I. Defendi<sup>1</sup>, S. Egerland<sup>1</sup>, A. Kastenmüller<sup>1</sup>, M. Mühlbauer<sup>1</sup>, M. Panradl<sup>1</sup>, T. Schöffel<sup>1</sup>, K. Zeitelhack<sup>1</sup>

<sup>1</sup>ZWE FRM II, TU München

The main activities of the lab in 2005 were governed by the commissioning of new scientific instruments. A variety of detectors and readout systems as well as electronic components for the instrument control were brought into operation. A few examples are reported.

The Detector and Electronics Lab is strongly involved in the neutron flux calibration and the study of neutron beam quality at the individual instruments. In this framework a scintillator based neutron camera for sample and neutron optical component adjustment has been developed presented in section 2.

Apart from service and maintenance the study of new developments and technologies is regarded as an important task of the lab. With the Physics Department (E18) of the TU München, the lab collaborates in the development of a N<sub>2</sub> based 2d-position sensitive neutron beam monitor for high flux application [1]. In addition, the lab enforced its activities within the NMI3-JRA2 (MILAND) project with the investigation of an ASIC based individual channel readout for MWPC or MSGC.

### Instrument Control and Readout Electronics

A new power supply and control system for the guiding field magnets of the beam line was developed and installed at the positron beam facility NEPO-MUC. The system contains 60 voltage controlled high current sources ( $I = 0 - 10\text{ A}$ ,  $U_{max} = 2.3\text{ V}$ ), which can be individually accessed by a microcontroller. The system can be operated completely remote controlled or in a manual mode.

The backbone of the FRM II data acquisition hardware for single neutron detectors is built by a whole family of PCI/cPCI-based DAQ-boards for

counting, Time-of-Flight measurement or pulse height analysis using the M-module standard [2]. It has been expanded by new modules specifically developed for the thermal single crystal diffractometer *RESI* and the single crystal diffractometer for hot neutrons *HEiDi*. The boards allow multiframe counting controlled by the detector arm movement and include an angular normalization.

Within the Joint European NMI3-JRA2 (MILAND) project the lab participates in the development of a fast medium resolution ( $\approx 1\text{ mm}$ ) neutron detector. One important difficulty to deal with is the unprecedented density of readout channels to be implemented in a limited space. We therefore evaluate the possible use of integrated circuits (ASICs) for an individual readout of single wires/strips. In a survey on ASIC's applicable to MILAND four interesting candidates were identified and investigated [3].

### Detectors

A proper adjustment of neutron optical components like focusing guides,

collimators or monochromators is of great importance for the performance of the scientific instruments. Continuing a development of the tomography group at FRM II [4], we designed a compact neutron sensitive camera for on-line beam inspection, which covers the neutron flux range  $10^5 - 10^8\text{ n/cm}^2/\text{s}$ . The camera is based on a 0.3 mm thick <sup>6</sup>LiF/ZnS scintillator with optical CCD-readout. Its field of view is  $98 \times 65\text{ mm}$  with a resolution of approximately 0.15 mm. Fig 1.8 shows the camera and the associated power supply. First measurements with neutron beam are scheduled for January 2006.

- [1] Rummel, S. *Diplomarbeit, Physikdepartment E18, Technische Universität München.*
- [2] Zeitelhack, K., *et al. FRM-II annual report, 6–7.*
- [3] Mühlbauer, M. *Diplomarbeit, Physikdepartment E21, Technische Universität München.*
- [4] Guerard, B., *et al. NMI3-JRA2 "MILAND" annual report.*



Figure 1.8: <sup>6</sup>LiF/ZnS scintillator based neutron camera with optical CCD-readout.

## 1.5 Sample Environment

J. Peters<sup>1</sup>, H. Kolb<sup>1</sup>, A. Schmidt<sup>1</sup>, A. Pscheidt<sup>1</sup>, J. Wenzlaff<sup>1</sup>

<sup>1</sup>ZWE FRM II, TU München

In 2005 the sample environment group faced its first year characterized by routine operation. Standard FRM II sample environment equipment like closed cycle top loading cryostats (CCR) and high temperature furnaces were successful in operation. A CCR combined with a 3He-insert developed at the FRM II stood the test in a high-pressure experiment on the Triple Axis Neutron Resonance Spin Echo Instrument.

In addition to the support of instrumentalists and users intensive work was done on the further development, improvement and completion of our sample environment equipment. Dedicated to the TOF TOF spectrometer a medium temperature furnace was designed and manufactured for applications like investigation of colloidal drug delivery systems using a commer-

cial available thermostat ( $-20^{\circ}\text{C} < T < 200^{\circ}\text{C}$ ).



Figure 1.9: Medium Temperature Device

## 1.6 IT Services

H. Wenninger<sup>1</sup>, L. Bornemann<sup>1</sup>, J. Dettbarn<sup>1</sup>, J. Ertl<sup>1</sup>, S. Galinski<sup>1</sup>, H. Gilde<sup>1</sup>, C. Herbster<sup>1</sup>, S. Kreyer<sup>1</sup>, J. Krüger<sup>1</sup>, J. Mittermaier<sup>1</sup>, R. Müller<sup>1</sup>, J. Pulz<sup>1</sup>, C. Rajczak<sup>1</sup>, S. Roth<sup>1</sup>, M. Stowasser<sup>1</sup>, B. Wildmoser<sup>1</sup>

<sup>1</sup>ZWE FRM II, TU München

### Overview

The IT Services groups provide and maintain the software and network infrastructure used at the FRM II.

Major efforts and achievements made in 2005 are

- the new file server “hektor”
- improvements of the DHCP server
- a new printing system
- the new firewall controlling the network between internal networks and the DMZ
- the user room located at the project building
- the migration of our Windows 2000 Servers to Windows Server 2003
- continuous development of

NICOS, TACO and TACO applications

- further efforts of making NeXus available for the instruments

### New file server

In 2004, we reached the capacity limit of our main file server more than once. As this is the central data storage point the proper operation of our client systems very much relies on it. To provide a stable solution with capacity and speed that matches our today’s requirements, we replaced the old system in the first week of 2005.

The new system consists of a dual CPU server provided by Fujitsu-Siemens Computers [1] and a transtec [2] RAID storage system with a gross capacity of 6.4 TByte. The storage sys-

tem is connected via SCSI-U320 to the server. The network connection of the server is a Gigabit Fiber Channel line directly to the main switch. Client access to the storage is provided by means of NFS, CIFS [3], SFTP [4] and FTP.

In addition to UNIX permission bits, fine grained access control for files and directories is supported by POSIX.1e ACLs. Backups of the storage system are taken every night and are transferred to the TSM system at the “Leibniz Rechenzentrum”. The whole system is very stable and reliable and turned out to be a complete success.

### DHCP failover

In the FRM II network, nearly all client computer systems get their IP address by querying our DHCP server. As re-



ported in the last annual report, we have done a lot of testing to build DHCP servers with failover functionality and LDAP based configuration backend.

Due to the encouraging test results with the ISC DHCP distribution [5] we decided to set up the new servers in 2005. We could finally put the system into operation in the first half of 2005. So far we did not encounter any problems. The risk of a DHCP service outage is significantly reduced. The configuration for the DHCP service is currently still stored in a file as we want to test and investigate the LDAP backend a little bit more.

## New print server

As printing is a great demand we have to provide a reliable solution which is able to handle the different types of network printers, their connection methods and device specific options. Our old Line Printer Daemon protocol based system was not able to cope with all these requirements.

We decided to use the Common UNIX Printing System (CUPS) [6]. CUPS uses the Internet Printing Protocol (IPP), described in RFC 2910 and RFC 2911, for managing printers, print jobs, queues and printer classes. Network printer browsing allows CUPS to send printer announcements and offers available printers to requesting clients. CUPS uses PostScript Printer Description (PPD) based printing options for device specific parameters. Backward compatibility is achieved by cups-lpd, a server that supports legacy LPD protocol clients. The LPD protocol is described in RFC 1179.

Access to the new print server for Windows clients is provided by Samba [3]. Samba offers a mechanism called point-n-print to the Windows client in the same way a Windows server itself is doing it. Using this feature, we are able to provide easy access to our printers and to maintain all printer drivers and device specific configurations directly on the print server. Clients with a different operating system can use it without any manual driver installation. In the future we plan to inte-

grate failover mechanisms utilizing two or more CUPS servers and CUPS printer classes.

## New Firewall

The Symantec Enterprise Firewall [7] became fully operational at the beginning of 2005. It runs on a Sun Enterprise E250 and Solaris [8] as operating system. It separates the internal networks of the FRM II from the DMZ, and therefore controls all network traffic which leaves or comes into the internal networks.

The main purpose of the firewall is to guarantee security to the networks and to provide network address translation (NAT) of the private IP addresses used in the internal networks to gain access to the internet. Additional features are the application level proxies, which allow protocol inspection transparent to the user.

## User Room

The new user room set up in the FRM II project building is intended for quick and easy network access for scientific users visiting the FRM II. Currently it consists of six Pentium4 computers with 17" TFT monitors.

The operating system used is FreeBSD [9], a UNIX derivative. Software installed on the systems includes the window manager WindowMaker [10] and the web browsers Mozilla [11], Opera [12] and Firefox [13]. The office suite OpenOffice [14] and the image manipulation program Gimp [15] are available.

To simplify maintenance of the operating system and all other software, everything is installed at a single location for all systems. The computers boot from network by means of PXE and mount all necessary directories utilizing the network file system (NFS). The user PCs can be used by every person with a FRM II network account.

## Upgrade from Windows 2000 Server to Windows Server 2003

At the FRM II, the operating network is based on an Active Directory structure running on Windows 2000 Server. Due to limited support of Windows 2000 we decided to upgrade all domain controllers and raise the functional level to Windows Server 2003 [16].

The benefits of the Windows Server 2003 environment are improved security, easier to use management services and the ability to rename the Active Directory domain which we did later that year. The upgrade and rename process was completed successfully without any bigger problems.

## Database for the FRM II Main Entrance

At the main entrance of the FRM II many events like the allocation and return of keys, cars entering and leaving the reactor compound or the change of the guards have to be recorded. Until February 2005 this was done on paper. It was decided to switch to a network based client/server system.

On the client's side the guard can use a web browser to connect to the server. A PHP [17] script provides the frontend to a MySQL [18] database on the server, in which all events are stored. This solution allows backup, archiving and easy access to stored data.

## TACO

In 2005 we focused on improving and stabilizing the TACO based system [19] (in close cooperation with the software development group of the ESRF) as well as on the development of new device servers for new instrument control hardware.

Improvements made on the TACO distribution:

- use of fully qualified host names inside TACO to allow the use of TACO device servers across different DNS zones
- installation and startup of the system itself

Due to the stabilization and the improvements of the system, more and more instruments at the FRM II switch to a TACO based instrument control system. At the moment the instruments PUMA, PANDA, HEiDi, RESI, MIRA, RESEDA and REFSANS are using TACO.

The modularity of TACO enables us to respond quickly to new requirements of the instruments. A lot of device drivers were written in 2005. By the help of our own development tool “tacodevel” we were able to implement and test new devicedrivers in a timely manner. It took us only some hours up to some days, depending on the complexity of the hardware, the quality of documentation and hardware details to integrate a new device server into the instrument control software. Most of the time (about 70 %) was required for testing the software and fixing problems with hardware (mal-)functions.

## TACO Diagnostics

The purpose of TACO Diagnostics is to conveniently monitor all parameters offered by a TACO [19] server.

The program shows the actual values delivered by the TACO server (see figure 1.10). Different states of a TACO device are shown by different colours of the digits. Originally the program was developed in the Linux environment, but it can be ported without problems to other operating systems like \*BSD,



Figure 1.10: Screenshot of TACO Diagnostics MacOS or Windows, as it is written in C++ and using the Qt3 library [20] which is available on all major platforms.

## NICOS

Our main goal of the developments made on NICOS was the improvement of the NICOS client usability. In cooperation with the responsible instrument scientists and engineers as well as the instrument users working with NICOS we implemented the following improvements:

- A syntax check before executing commands as well as scripts to avoid runtime errors of long running scripts (typically over night runs).
- A plot window to display the currently measured data was developed.
- The user interface was simplified. The main activities of the user can now be done in a single window, and the users may see the current state of the instrument and the progress of their experiment.

Due to the satisfying experience with the client/server concept of NICOS more instruments will be outfitted with the system in the course of 2006.

## NeXus

With the scope of the standard neutron data format and the appropriate tools continuously evolving, the support and usage of NeXus [21] at FRM II has been extended likewise. Two different approaches have been followed to generate NeXus files. First the “anything-to-NeXus” converter NXtranslate was used in conjunction with instrument specific template files to produce NeXus data from the existing ASCII files. For that purpose the appropriate retrieval plugins, which actually do the translation job, have been written.

Alternatively data of the NICOS scan routines can be directly written into NeXus structures utilizing the NeXus python API developed at FRM II. In this case according to the NICOS routines a generic class deals with writing raw scan data whereas instrument specific data is output by corresponding subclasses.

In both cases, the NeXus instrument definitions had to be designed and had

to be adapted to satisfy the needs of the experimentators on the one hand and to retain NeXus compliance as far as possible on the other hand. Up to now, the instruments MIRA, TOFTOE, HEiDi, PUMA and PANDA can deliver NeXus files as an option.

- [1] Fujitsu-Siemens Computers. <http://www.fujitsu-siemens.de/>.
- [2] transtec AG. <http://www.transtec.de/>.
- [3] Tridgell, A., *et al.* The Samba Project. <http://www.samba.org/>.
- [4] The OpenBSD Project. OpenSSH. <http://www.openssh.org/>.
- [5] Internet Systems Consortium. Dynamic Host Configuration Protocol distribution. <http://www.isc.org/sw/dhcp/>.
- [6] Easy Software Products. Common UNIX Printing System. <http://www.cups.org/>.
- [7] Symantec Enterprise Firewall. <http://www.symantec.com/Products/enterprise?c=prodinfo&refId=853>.
- [8] Solaris Enterprise System. <http://www.sun.com/software/solaris/index.jsp>.
- [9] The FreeBSD Project. FreeBSD. <http://www.freebsd.org/>.
- [10] others, A. K. Window Maker. <http://www.windowmaker.org/>.
- [11] Mozilla Foundation. Mozilla Suite. <http://www.mozilla.org/products/mozilla1.x/>.
- [12] Opera Software ASA. Opera. <http://www.opera.com/>.
- [13] Mozilla Foundation. Firefox. <http://www.mozilla.com/firefox/>.
- [14] Sun Microsystems. OpenOffice.org. <http://www.openoffice.org/>.

- [15] The GIMP Team. The GIMP. <http://www.gimp.org/>.
- [16] Microsoft Corporation. Windows Server 2003. <http://www.microsoft.com/windowsserver2003/default.aspx>.
- [17] The PHP Group. PHP: Hypertext Preprocessor. <http://www.php.net/>.
- [18] MySQL AB. MySQL RMDB. <http://www.mysql.com/>.
- [19] Götz, A., *et al.* TACO distributed control system. <http://sourceforge.net/projects/taco>.
- [20] Trolltech AS. Qt. <http://www.trolltech.com/products/qt/index.html>.
- [21] NeXus International Advisory Committee. NeXus Data Format for Neutron, X-ray & Muon Science. <http://www.nexus.anl.gov/>.

## 1.7 Polarized $^3\text{He}$ gas on the way to neutron instruments at the FRM II

S. Masalovich<sup>1</sup>, O. Lykhvar<sup>1</sup>, G. Borchert<sup>1</sup>, W. Petry<sup>1,2</sup>

<sup>1</sup>ZWE FRM II, TU München

<sup>2</sup>TU München, Physik Department, E13

In January 2005 HELIOS (IC-Automation GmbH), the facility for large-scale production of highly polarized  $^3\text{He}$  gas, has been put into operation at the FRM II. The measurements that have been done during the year 2005 confirmed the reproducible steady-state  $^3\text{He}$  polarization of about 78% and about 27 bar·litre/day production rate at 72% gas polarization.

With the aim to utilize this highly polarized  $^3\text{He}$  gas at the neutron instruments, gas can be compressed up to 5.3 bar into detachable cells and transported to the experiment. The main tasks in 2005 therefore were:

- to get the experience in production of cells capable to keep gas polarization for a long time (days);
- to build the transporter with a highly homogeneous magnetic field.



Figure 1.11: NSF cell coated with metallic Cs.

### Cells

Polarization of the gas stored in the cell decreases with time as:

$$P_{\text{He}}(t) = P_{\text{He}}(0) \cdot e^{-\frac{t}{T_1}}$$

This results from

- magnetic interaction of atoms with magnetic impurities (whatever they are) on the surface and in the bulk of the cell,
- inhomogeneous magnetic guiding field (field gradient),
- dipole-dipole interaction.

Thus the total relaxation rate (inverse relaxation time,  $T_1$ ) can be written as a sum:

$$\frac{1}{T_1} = \frac{1}{T_1^{\text{wall}}} + \frac{1}{T_1^{\text{gr}}} + \frac{1}{T_1^{\text{dd}}}$$

Here the relaxation rate related to the interaction with inhomogeneous magnetic guiding field and dipole-dipole interaction can be estimated with the following formulas:

$$\frac{1}{T_1^{\text{gr}} [\text{h}]} = 1.7 \cdot 10^4 \left( \frac{|\nabla|\vec{B}_\perp|}{B_0} \frac{1}{[\text{cm}]} \right)^2 \cdot \frac{1}{p [\text{bar}]}$$

and

$$\frac{1}{T_1^{\text{dd}} [\text{h}]} \approx \frac{p [\text{bar}]}{800}$$

while the relaxation rate related to the interaction with the walls is entirely the result of a proper choice of the cell material and the quality of the surface cleaning.

Two neutron spin filters (NSF) have been prepared and tested in the year

2005. These NSF are based on the quartz cells built in 2004, which were now thoroughly cleaned up and coated with pure metallic cesium (Fig. 1.11).

Cesium in one cell was then accidentally oxidized. With the aim to compare, the relaxation time has been measured for both cells:

- Cell #1 (Cs-coated, accidentally oxidized)  $T_1 = (75 \pm 3) \text{h}$ ;
- Cell #2 (Cs-coated)  $T_1 = (267 \pm 17) \text{h}$ .

Cell #2 shows the relaxation time comparable with the best relaxation time reported by other groups for the quartz cells.

The neutron transmission for the empty cells (quartz windows with 8mm total thickness) has been measured to be:

- $T_n = 0.84$  at  $\lambda = 1.5\text{\AA}$ ;
- $T_n = 0.90$  at  $\lambda = 9.7\text{\AA}$ .

Next cells will be built according to the requirements of the neutron instruments.

### Transporter

To preserve gas polarization while transporting it from the HELIOS lab to a neutron instrument the special transporter has been developed and built in 2005. The transporter (Fig. 1.12) is based on a circular solenoid powered with two battery cells 4.5V each.

The parameters of the solenoid were chosen to provide a homogeneous magnetic field in the central area (sized to cover the volume of the NSF cell) with

homogeneity of around

$$\frac{\nabla |\vec{B}_\perp|}{B_0} \simeq 7 \cdot 10^{-4} \text{ cm}^{-1}$$

that could ensure the relaxation time related to the magnetic field inhomogeneity about  $T_1 \simeq 100h$ .

This solenoid is shielded with mu-metal tube against the environmental magnetic fields. The parameters of the tube were also chosen to ensure the best homogeneity in the central area when acting together with activated magnetic field in the solenoid. The solenoid can be pulled out of the mu-metal tube and placed in the guiding field of HELIOS to ensure the loss-free replacement of the NSF cell with newly polarized  $^3\text{He}$  gas into the solenoid.

The whole magnetic system is assembled on a PVC base and protected against mechanical deformation with outer PVC tube. The total weight of the transporter is 11 kg and thus one man can carry it with ease.

The required magnetic homogeneity

of the assembled transporter has been checked with a homemade magnetic mapping system. The final check-up has been performed with polarized  $^3\text{He}$  gas stored in the transporter. The total relaxation time has been measured to be  $T_1 [h] = (110 \pm 8) \cdot p [\text{bar}]$ .

### First application to neutron experiments

The first application of polarized  $^3\text{He}$  gas at the FRM II has been performed at the reflectometer MIRA in November 2005. Gas polarized at HELIOS has been used in the test measurements with the new device developed and built at ILL (France). This device, based on polarized  $^3\text{He}$  gas, combines two tools, neutron polarizer (analyzer) and spin-flipper, into one unit. The test measurements confirmed the high efficiency of this device and, at the same time, verified the ability to provide a highly polarized  $^3\text{He}$  gas for neutron experiments at the FRM II. The very first measurement

on the neutron beam revealed the gas polarization 65% at the instrument.



Figure 1.12: Transporter for polarized  $^3\text{He}$  gas.

## 1.8 Hot Neutron Source

C. Müller<sup>1</sup>, E. Gutmiedl<sup>1</sup>, M. Meven<sup>1</sup>  
<sup>1</sup>ZWE FRM II, TU München

The beam tube SR9 is directed to the vessel of the hot neutron source (HNS) and provides a single crystal diffractometer called HeiDi [1] with hot neutrons of energies between 0.1 to 1 eV.

The HNS shifts the thermal neutron spectrum from the reactor to higher energies. This will be achieved by a hot moderator, which is placed in the  $D_2O$ -reflector tank close to the thermal neutron flux maximum.

A cylinder made out of nuclear-grade graphite is the essential part of the HNS. This graphite moderator will be heated by gamma radiation of the reactor core to temperatures above 2000 °C. To achieve these high temperatures, several layers of carbon fiber and a rigid hemisphere of bounded carbon fiber thermally insulate the moderator. Both types of insulation also have the task to fix the hot moderator in the center to avoid the contact with the "cold" walls.

The moderator and the insulation are enclosed in two vessels made of Zircaloy 4 [2]. The small space between both vessels is filled with helium gas of 3 bars. The helium pressure is permanently monitored. Hence there are two barriers, which safely separate the hot moderator from air and water.

Figure 1.13 shows a cross section of the hot neutron source vessel, the hot moderator and the thermal insulation.

Due to the extremely harsh environmental conditions (e.g. high graphite temperature, chemical reactivity and nuclear radiation), the temperature of the hot moderator is very difficult to measure. Thermocouples and pyrometers are not suitable in this case. Therefore a purpose-built noise thermometer was installed to measure the temperature of the hot graphite (figure 1.13). A noise thermometer [3] is a contact thermometer and is not affected by changes

of the sensor. It measures the white noise of the electrical resistance and determines the absolute temperature. The noise sensor was developed and tested at the Technische Universität München. The data acquisition system of the noise thermometer was delivered from the

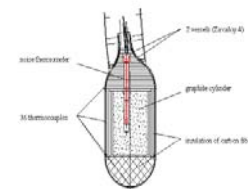


Figure 1.13: Cross section of source vessel with graphite cylinder and carbon insulation.

Forschungszentrum Jülich, ZEL in Germany.

Further design details of the hot neutron source can be found in [4].

## Temperature transients of the hot moderator

At full reactor power (20 MW) the moderator reaches a maximum temperature of 2030 °C (3690 °F). The following figure 1.14 will give an idea how long it takes to get the maximal temperature and to cool down.

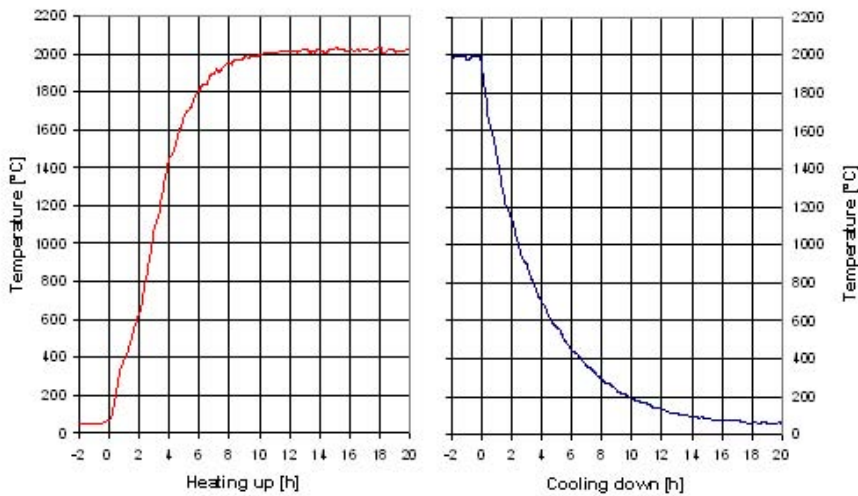


Figure 1.14: Temperature transients of the hot moderator measured by noise thermometer at 20 MW reactor power. The maximum temperature will be achieved within 12 hours (red curve). After shutting down the reactor, it takes more than 20 hours to cool down to room temperature (blue curve).

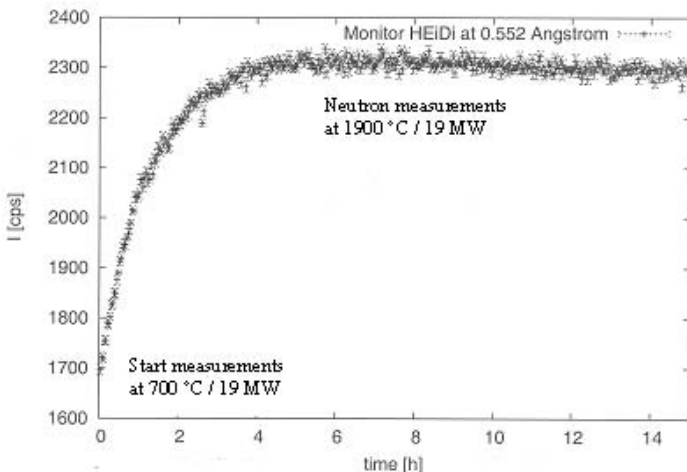


Figure 1.15: Heat-Up effect of hot neutron source at 19MW reactor power

## Heat-Up effect of the hot neutron source

The relative long time needed to reach temperature was used to measure the heat-up effect of the hot neutron source (Figure 1.15). At the beginning of the measurements the reactor was powered up to 19 MW and then kept constant. The temperature of the hot moderator reached 700 °C and a monitor counted 1700 neutrons per second at a wavelength of 0.552 Angström. Six hours later, the source reached a tempera-

ture of 1900 °C and the counts raised to 2300 neutrons per second. This demonstrates the task of the hot neutron source to shift thermal neutrons to higher energies.

It is intended to repeat these measurements on full reactor power (20MW) and with different wavelengths. These measurements are supposed to start with the "cold" HNS at 0 MW.

By doing that, we expect to get a more detailed overview of the spectral efficiency / gainfactor of the HNS, which is expected to be about 7 at its maximum.

- [1] Meven, M., Hibsich, F., Heger, G. *Annual Report 2003 ZWE FRM-II*.
- [2] Gutmiedl, E., A., S. In *Proceedings of the IGORR 8 Meeting* (Munich, 2001).
- [3] Brixy, H. *Noise Thermometers in Sensors*, volume 4 (VCH Verlag, 1990).
- [4] Müller, C., Gutmiedl, E. *Annual Report 2003 ZWE FRM-II*.

## 1.9 The new Neutron Guide of FRM-II: NL 4a, NL 4b and NL 2a-o

Ch. Breunig<sup>1</sup>, E. Kahle<sup>1</sup>, R. Schwikowski<sup>1</sup>, G.L. Borchert<sup>1</sup>, H. Türck<sup>1</sup>, D. Hohl<sup>2</sup>, S. Semecky<sup>3</sup>, A. Ioffe<sup>4</sup>, M. Monkenbusch<sup>4</sup>, O. Holderer<sup>4</sup>

<sup>1</sup>ZWE FRM-II, TU München

<sup>2</sup>Technische Dienstleistungen, München

<sup>3</sup>Kommunikationstechnik, München

<sup>4</sup>IFE, Forschungszentrum Jülich

### The new Neutron Guides NL 4a and NL 4b

In continuation of the work reported in Annual Report 2004, pages 11 ff. we accomplished the construction of the neutron guide (NG) NL4a between the high speed shutter close to the casemate wall and the selector gap in the NG hall (see Fig. 1.16), and the according section of NG NL4b between the fast shutter and the entrance of the PGAA bunker (see Fig. 1.16).

In both cases the NG had to penetrate the wall between the casemate and the NG hall. Therefore the wall had to be opened and the heavy concrete blocks were rearranged to give passage for the NGs. The glass elements of the NGs have been mounted on top of the corresponding steel bars. The adjustment of the NG was performed by means of theodolites reaching high mechanical tolerances. Maximum displacement of two consequent glass elements is less than  $10\mu\text{m}$ , angular mismatch less than 15arcs and less than 45arcs in horizontal and vertical direction, respectively. As in this section the glass NGs have to be vacuum tight all consequent glass tube elements were glued together. The final element was equipped with an Al window that withstands the vacuum pressure and is transparent for neutrons. All NGs could be shown to keep the vacuum up to  $2 \times 10^{-2}$  mbar.

In the casemate region, the NGs were enclosed in 10 cm thick borated PE plates, in the NG hall they have been jacketed by a sandwich of 5 mm borated epoxy and 9cm thick lead (see Fig. 1.16).



Figure 1.16: View of NGs NL4a (to the right) and NL4b (to the left) in the NG hall during the installation period. NL4a is completely enwrapped with lead ending at the position of the selector. For NL4b the glass elements have been adjusted above the bottom lead plate by means of the adjustment frames.

### The new polarising Neutron Guide NL 2a-o

This new NG has been designed by the members of the Jülich Centre for Neutron Science (JCNS). It takes the upper part of the former NL2a cross section,  $B \times H = 44 \times 60 \text{ mm}^2$  at the fast shutter. Within the casemate it has a radius of curvature of 160m horizontally and stays in the casemate section close to NL2a-u so that both NGs had to be coupled to one unit. The coating of the outer wall is FeSi with  $m=3$  while that of the other walls is Ni58,  $m=1.2$ . The NG is enclosed in a magnetic cage consist-

ing of top and bottom plates from iron, connected by columns of permanent magnets NbFeB to maintain a guiding field of about 30mT (see Fig. 1.17). The continuation of the NG is a straight section of 4m that ends at a selector unit. It is coated with Ni58,  $m=1.2$  and enclosed by a magnetic cage similar to that inside the casemate but with a field strength of 5mT. Along the last meter of the NG before the selector the magnetic field is rotated from transversal to longitudinal by means of a magnetic coil with increasing winding density (see Fig. 1.18).

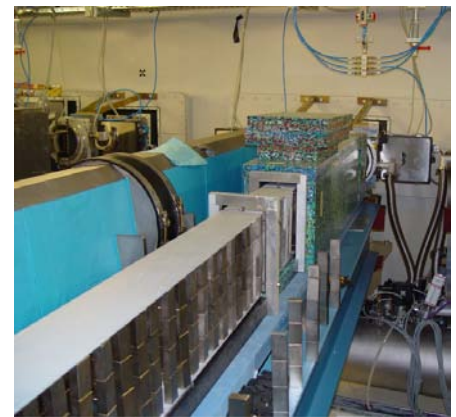


Figure 1.17: The first part of the NG NL2a-o in the casemate. The glass elements are jacketed by the magnetic cage. The top and bottom plates from soft iron are connected by rectangular magnetic columns maintaining a magnetic field of 30mT. For the first element the NG is already en-housed with 10cm thick PE plates.



Figure 1.18: The last part of the NG NL2a-o before the selector gap during the installation period. The glass elements are surrounded by the magnetic coil windings. The NG directly behind the NL2a-o is already enoused with 10cm thick PE plates.





## 2 Instruments

### 2.1 First Experiments at the Positron Beam Facility NEPOMUC

Christoph Hugenschmidt<sup>1,2</sup>, Thomas Brunner<sup>2</sup>, Stefan Legl<sup>2</sup>, Jakob Mayer<sup>2</sup>, Christian Piochacz<sup>1</sup>, Reinhard Repper<sup>1</sup>, Martin Stadlbauer<sup>2</sup>, Klaus Schreckenbach<sup>2,1</sup>

<sup>1</sup>ZWE FRM II, TU München

<sup>2</sup>TU München, Physics Department, E21

#### The mono-energetic positron beam of high intensity at NEPOMUC

In 2005 several positron experiments were performed at the high intensity positron beam facility at NEPOMUC (NEutron induced POsitrone source MU-niCh). After adjustment of the positron beam the beam parameters such as diameter and intensity were determined at the first accessible position outside the biological shield. The positron yield was improved to a maximum beam intensity of  $5 \cdot 10^8$  at a positron energy of 1 keV. The diameter in the longitudinal magnetic guide field of 6 mT was found to be less than 15 mm. We also suc-

ceeded to extract a low-energy positron beam at 15 eV with the world highest intensity of  $4 \cdot 10^7$  moderated positrons per second.

The positron beam facility was extended by several components:  $\mu$ -metal shielding at the straight sections of the beam line, a new adjustable aperture and an adiabatic beam switch in order to divide the beam line into five subsections. With this new switch up to five different positron experiments can be connected to the evacuated beam facility. This beam switch works in the energy range of 15 eV to 1 keV without considerable intensity loss.

#### Positron Experiments at NEPOMUC

The positron beam is extracted at 1 keV for the CDB-spectroscopy, where the beam is focused to 1 mm at the sample position. Several material systems were studied – partially with external users – in order to investigate the chemical surrounding at atomic defects: GaAs(Zn), Fe and Fe-alloys, and Mg-alloys.

The low-energy beam (15 eV) is required for PAES-experiments with low positron induced electron background. With this novel spectrometer positron annihilation induced Auger-electron emission was investigated at the surface of single crystalline silicon and polycrystalline copper. Within a diploma thesis a completely new time-of-flight configuration was connected to the beam line in order to enable PAES-measurements with much higher efficiency, that would lead to two orders of magnitude lower measurement time

This year an apparatus for the production of the negatively charged positronium ( $\text{Ps}^-$ ) was transferred from the Max-Planck-Institute of Nuclear Physics to the FRM II. Recently this experimental set up was connected to the open beam port of the positron beam line in order to determine the diameter of the 500 eV positron beam at the position of the ( $\text{Ps}^-$ ) production target.

The present arrangement of the experiments is shown in figure 2.1.

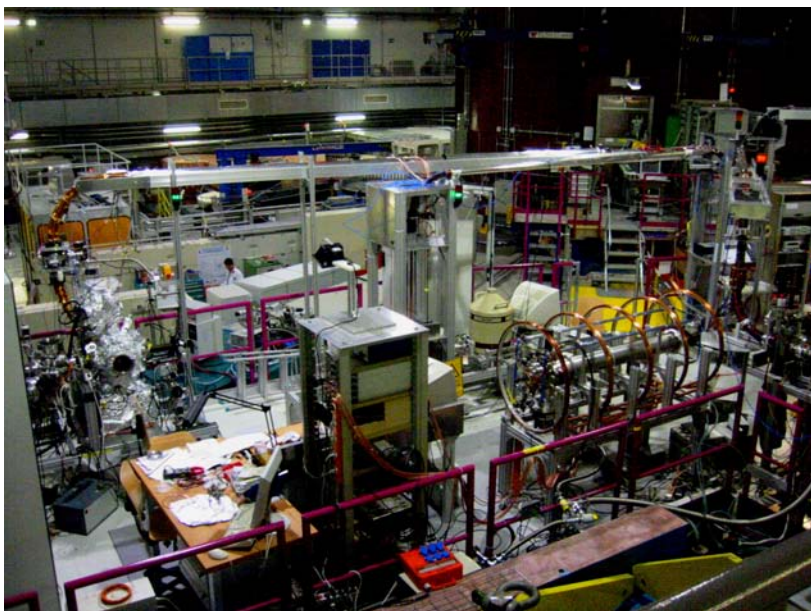


Figure 2.1: Overview of the positron beam facility NEPOMUC and the first installed experiments. CDB spectrometer and the PAES set ups are built and operated by E21/TUM. The ( $\text{Ps}^-$ ) is operated by the Max-Planck-Institute for nuclear physics.

## Outlook

Besides the presented experiments it is planned to install a remoderation device in order to improve the beam

brightness. This will enhance the performance of the scanning positron microscope that will be transferred to the FRMII in a collaboration between the University of the Bundeswehr

(UniBW) and TUM. In addition, a pulsed positron beam system from the UniBW will be connected to the positron beam facility NEPOMUC.

## 2.2 Time of flight spectroscopy of positron induced auger electrons

Stefan Legl<sup>2,1</sup>, Christoph Hugenschmidt<sup>1,2</sup>, Reinhard Repper<sup>1</sup>

<sup>1</sup>ZWE FRM II, TU München

<sup>2</sup>TU München, Physics Department, E21

### Auger electron spectroscopy

Auger electron spectroscopy (AES) is a widely used method in surface physics. X-rays or high energy electrons are used to excite core electrons of a material. These electrons are emitted into vacuum. When electrons from higher shells take their places, binding energy is released and can be transferred to a valence bond electron which is also emitted into vacuum. This so called auger electron has a specific kinetic energy. By analyzing these energies one can determine the elemental composition of the top layers of the sample.

Positron induced auger electron spectroscopy (PAES) uses low energy positron annihilation (15 eV) instead of X-rays or high energy electrons to create the  $e^-$  hole in the inner shell. The following  $e^-$  emission process is the same as in AES.

To analyze the energy of the auger electrons mostly hemispherical energy analyzers are used. Due to their small solid angle (typically  $\geq 0,1\%$ ) and the necessity to scan over certain energy ranges in  $\geq 0.1$  eV steps one needs several hours (using an intense positron source like NEPOMUC at the FRMII) or even weeks (at the lab with a  $\beta^+$ -emitter) to get an auger spectrum [1]. In order to reduce this measurement time to less than one hour we developed a new spectrometer using a time of flight method for analyzing the auger energies. In this spectrometer the count rate of auger electrons is much larger than in conventional analyzers and also a large energy spectrum can be measured simultaneously. A similar spectrometer

was first built at the University of Texas by A. Weiss. [2]

### Experimental setup

Positrons entering the flight tube are deflected in a trochoidal ExB-filter upwards (fig. 2.3). When they leave the filter their longitudinal momentum lies exactly on the axis of the flight tube where also the sample is placed. Additionally the positrons are focussed onto the sample by the magnetic field gradient caused by a strong  $NdFeB_2$  permanent magnet that is placed behind the sample. When a positron annihilates with a core electron two gamma quanta are created (511 keV) and simultaneously the auger electron is emitted. If one of these gamma quanta hits the  $BaF_2$ -detector the timing is started. The auger electron travels through the trochodial filter in the opposite direction of the positron trajectories. Therefore the  $e^-$  is deflected upwards where it hits a micro channel plate (MCP) when it leaves the filter. This MCP creates the stop signal for the timing. The recorded TOF spectrum can be transferred into an energy spectrum of the auger electrons.

The inhomogeneous magnetic field between the sample and the trochodial filter has two important functions. Positrons leaving the filter are captured and adiabatically focussed onto the sample. The second and much more important effect is that all emitted auger electrons from a solid angle of  $2\pi$  (!) are focussed towards the filter. Hence each emitted electron can reach the micro channel plate. The physical explanation for this is the following: Due to conservation of the magnetic moment and conservation of energy, in an inhomogeneous magnetic field longitudinal momentum is converted into transversal momentum (flight direction towards the stronger field) and vice versa (flight direction towards smaller field).

This two effects guarantee a high count rate and together with the ability to measure a large energy range simultaneously we expect a measuring time for a auger spectrum of less than one hour.

### Conclusion and Results

So far the experimental setup has been completed and first measurements at

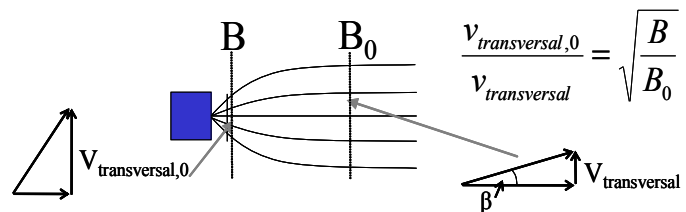


Figure 2.2: Momentum in an inhomogeneous magnetic field.

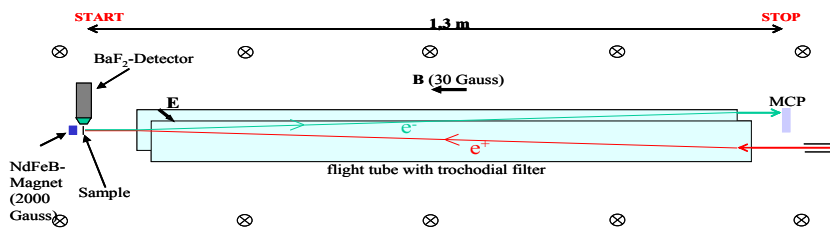


Figure 2.3: Experimental setup of the TOF-PAES.

the intense positron source *NEPOMUC* were performed this year. Focussing positrons on the sample was optimized in a first step. Our measurements showed a number of  $10^7$  positrons per

second hitting the sample, the intensity of the positron beam is also in this range. Therefore, it is concluded that the beam guiding system works extremely efficient. In a second step we

## 2.3 First PAES-measurements at the Positron Beam Facility NEPOMUC

Christoph Hugenschmidt<sup>1,2</sup>, Stefan Legl<sup>2</sup>, Jakob Mayer<sup>2</sup>, Reinhard Repper<sup>1</sup>, Martin Stadlbauer<sup>2</sup>, Benno Straßer<sup>2</sup>, Klaus Schreckenbach<sup>2,1</sup>

<sup>1</sup>ZWE FRM II, TU München

<sup>2</sup>TU München, Physics Department, E21

### Principle of PAES

Auger Electron Spectroscopy (AES) is a commonly used technique in surface science. Since in AES the Auger process is induced by high energy ( $1keV$ ) electrons or X-rays, the spectra contain a large secondary electron background. Hence it is very difficult to identify Auger peaks in the low-energy region.

A new method to initiate the Auger process is the annihilation of low energy (some  $10eV$ ) positrons with electrons. PAES (**P**ositron annihilation induced **A**uger **E**lectron **S**pectroscopy) has several advantages compared to conventional AES: Firstly, there is no

positron induced secondary electron background at  $E_{e^-} > E_{e^+}$  due to the low kinetic energy of the positrons. Secondly, tightly bound adsorbates at the surface are barely destroyed by the incident  $e^+$ -beam. The greatest advantage of PAES is the extremely high surface sensitivity since most of the slow positrons ( $> 90\%$ ) annihilate with electrons of the topmost atomic layer.

The challenge in PAES is to produce a  $e^+$ -beam of high intensity. Since usual laboratory  $e^+$ -sources provide only about  $10^4 \frac{e^+}{s}$ , measurement times of 20 days per spectrum or more are necessary.

### Experimental setup at NEPOMUC

The new positron-beam NEPOMUC at the research reactor FRMII provides a low energy-beam of  $5 \cdot 10^7$  moderated positrons per second at the analysis chamber. Due to the high beam-intensity the measurement time is reduced to several hours. The existing spectrometer (Fig. 2.4) was transferred to the reactor in the end of 2004.

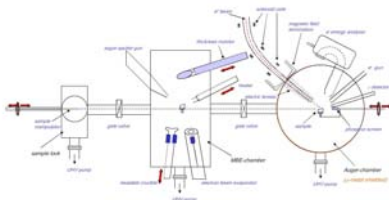


Figure 2.4: A drawing of the PAES-facility at the FRM II.

showed that electrons emitted from the sample reach the MCP. Presently, the electronics is adjusted in order to record first TOF-spectra.

[1] Strasser, B. *Aufbau einer Anlage zu positroneninduzierten Auger-Elektronenspektroskopie*. Ph.D. thesis, Technische Universität München (2002).

[2] Jiang, N. *Design and modeling of a positron annihilation induced auger electron spectrometer with time-of-flight energy analyzer*. Ph.D. thesis, University of Texas at Arlington (1999).

### Measurements and results

There have already been first successful measurements and the results are shown below. The surface sensitivity of the method can be seen at the single-crystal Si-sample (Fig. 2.5). With only one monolayer of copper on it, the Auger-peak of the Si completely vanishes. The other spectrum (Fig. 2.6) shows polycrystalline copper (Ar-sputtered).

The measurement time for all spectra shown was 13 hours and the pressure in the chamber was about  $10^{-9} mbar$ . Unfortunately, the background was higher

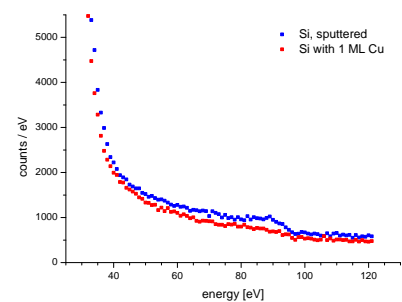


Figure 2.5: Si with PAES.

than expected, that might be attributed to other experiments nearby and insufficient shielding.

## Outlook

In the following year, the aim is to find the true surface sensitivity (qualitatively) for different samples and coatings and to reduce the background. Besides a better shielding, coincident measurement (Auger-electron and annihilation-radiation) of the electrons would be the best way to get a better signal/noise-ratio.

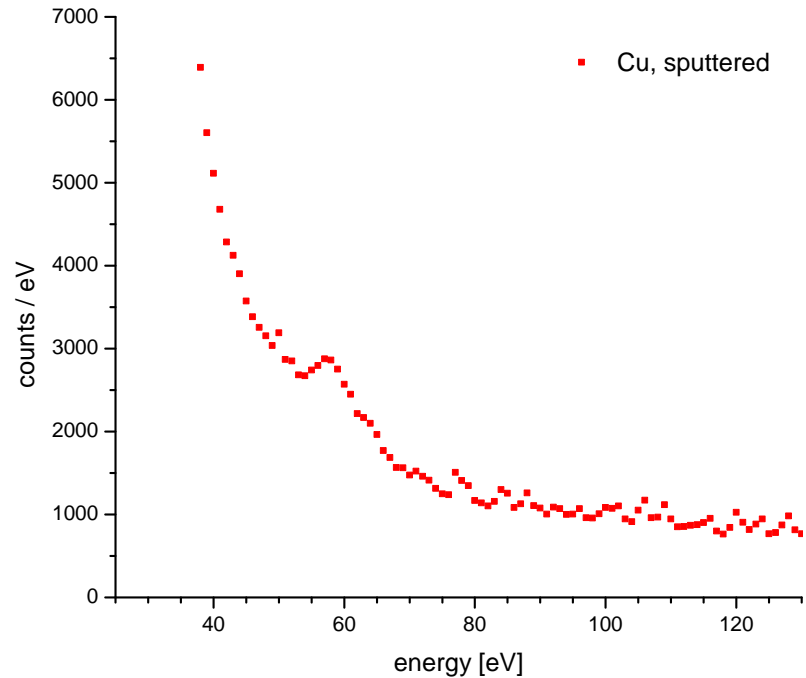


Figure 2.6: Cu with PAES.

## 2.4 MEPHISTO – a measuring facility for particle physics with cold neutrons

D. Rich<sup>1</sup>, H.-F. Wirth<sup>2</sup>, O. Zimmer<sup>2</sup>

<sup>1</sup>ZWE FRM II, TU München

<sup>2</sup>TU München, Physik Department, E 18

### Scientific design

Experiments using cold neutrons address a diverse array of issues in nuclear physics, particle physics, astrophysics, and cosmology. The purpose of MEPHISTO is to provide a versatile facility at which one may conduct such experiments. The bulk of the instrumentation for each experiment is provided and installed by the user (in collaboration with the MEPHISTO team at the FRM II). The instrument itself is designed to optimize the following conditions for the users:

- Maximized neutron fluence
- High neutron polarization (as needed)

- Low backgrounds

### Current status

#### Neutron guide and shielding

Experiments at MEPHISTO are installed at the end of a 30 m, supermirror-coated neutron beamguide, which conducts a neutron fluence of  $\Phi = 6.8 \times 10^9 \text{ n/cm}^2/\text{sec}$  (measured by gold-foil activation in April, 2005) to the experiment. To our best knowledge this is the most intense cold neutron beam for the purpose of fundamental physics. The guide itself is shielded by a combination of polyethylene, lead, and concrete. After the guide, the beam

is typically collimated to a size appropriate to the given experiment, with additional shielding designed accordingly, to minimize the backgrounds at the detectors and in the surrounding environment.

#### Polarizer

A supermirror polarizer is available, but not yet installed, as the experiments conducted in 2005 did not require polarized beam. It is anticipated that the polarizer will be installed, and the neutron beam polarization accurately determined, in 2006.

## Experiments

Two experiments received significant beamtime at MEPHISTO in 2005. The first, designated RASPAD (Russian for “decay”), ran for 1.5 cycles. The second, designated aSPECT (a SPECTrometer to measure the little ‘a’ coefficient in neutron beta decay), also received 1.5 cycles of measuring time.

### RASPAD

The experiment RASPAD was designed to measure the rare radiative branch in neutron beta decay. This is achieved by detection of a triple coincidence among the proton, electron, and photon re-

leased in the neutron decay. A previous measurement at the ILL using the same instrument [1] set an upper bound on this decay branch. A first ever observation of this decay was the goal of the measurement at MEPHISTO. Data analysis is still underway.

### aSPECT

The experiment aSPECT was designed to measure the little ‘a’ coefficient in neutron beta decay, corresponding to the neutrino-electron angular correlation coefficient. This is achieved by the very precise measurement of the energy spectrum of recoil protons from neutron beta decay [2]. This instru-

ment saw beam for the first time anywhere in 2005 at MEPHISTO. The runs to date have been largely development runs, and it is anticipated that the first production runs will be conducted early in 2006.

- [1] Beck, M., Byrne, J., Khafizov, R. U., Kozlov, V. Y., Mostovoi, Y. A., Rozhnov, O. V., Severijns, N., Solovei, V. A. *JETP Letters*, 76, (2002), 392–396.
- [2] Glück, F., Baessler, S., Byrne, J., van der Grinten, M. G. D., Hartmann, F. J., Heil, W., Konorov, I., Petzoldt, G., Sobolev, Y., Zimmer, O. *Eur. Phys. J. A*, 23, (2005), 135–146.

## 2.5 MIRA – The beam line for very cold neutrons at the FRM II

R. Georgii<sup>1</sup>, N. Arend<sup>2</sup>, P. Böni<sup>2</sup>, H. Fußstetter<sup>1</sup>, D. Lamago<sup>1</sup>, S. Mühlbauer<sup>2</sup>, R. Schwikowski<sup>1</sup>

<sup>1</sup>ZWE FRM II, TU München

<sup>2</sup>TU München, Physik-Department, E21

MIRA is a versatile instrument for very cold neutrons (VCN) using neutrons with a wavelength  $\lambda > 8 \text{ \AA}$  (see Fig. 2.7). It is situated at the cold neutron guide NL6b in the neutron guide hall of the FRM II. As the instrument set-up can be changed quickly, MIRA is ideally suited as a testing platform for realising new instrumental set-ups and ideas. In particular, MIRA is unique in its possibilities of combining different neutron scattering methods as:

- Polarized or non-polarized reflectometry.
- Polarized or non-polarized small angle scattering (SANS).
- Classical NRSE (Neutron Resonance Spin Echo) setup as well as using the MIEZE principle.

### Design of the instrument

The instrument is located at the end of a 8 m long curved  $^{58}\text{Ni}$  neutron guide ( $R = 84 \text{ m}$ ) with a cross section of 10 mm x 120 mm. The instrument is fed by means of a wavelength sensitive switch from neutron guide NL6. The radius of curvature of the guide and its coating limit the critical wavelength of



Figure 2.7: Mira equipped with a magnet and a cryostat. In order to reduce scattering by air, the neutrons travel in evacuated tubes before and after the sample.

MIRA to about  $8 \text{ \AA}$ . The monochromator mechanics at the end of the guide is situated inside a massively shielded drum. The multilayer monochromator presently used ( $m = 4.3$ ) allows choosing wavelengths between  $8 \text{ \AA}$  and  $30 \text{ \AA}$ . After monochromatisation the neutrons are then guided through a vacuum tube to the sample position, with the desired sample environment (e.g. low temperatures, magnetic fields). The reflection geometry is vertical, so that  $\theta - 2\theta$  scans can be performed. Further, the sample table is equipped with

a 3D-goniometer for sample orientation. The scattered neutrons are detected either by means of a  $^3\text{He}$  detector or 2-dimensional position sensitive detector (PSD). A slit system of 4 apertures before and behind the monochromator and the sample position is used to define the momentum resolution of MIRA. An optical bench allows quickly changing the different instrumental set-ups.

Furthermore, after the monochromator the neutrons may be polarised. They are guided in a guide field of 60 Gauss provided by permanent magnets. Multilayer bender with a polarization efficiency of 95 % are used for determining the polarisation of the neutrons before and after scattering. All moving parts, the NRSE electronics and the readout of the detectors are fully automated and controlled by the experiment software.

In 2005 MIRA was successfully taken into user operation. In total, 6 proposals, several test and service measurements were performed, for example a test of a switchable polarization  $\text{He}^3$  spin filter for the ILL. 2 diploma theses (The flux line lattice of Niobium by Sebastian Mühlbauer (E21), Entwick-

lung eines positionsempfindlichen Detektors für intensive Neutronenstrahlen by Stefan Rummel, E18) and one Ph.D. thesis (Small angle scattering on MnSi by Daniel Lamago (FRM II) were finished using mainly data from MIRA. Also major parts of the beam time went in another Ph.D. thesis for the development of a double MIEZE spectrometer (Nikolas Arend, E21), which will be finished in 2006.

Wavelength range	8 Å - 30 Å
Monochromatic flux	$4 \cdot 10^5 \text{ Å}^{-1} \text{ s}^{-1} \text{ cm}^{-2}$ at 10 Å
Momentum transfer	$0.005 \text{ Å}^{-1} < Q < 1.1 \text{ Å}^{-1}$
Largest observable length	$0.4 \cdot 10^{-6} \text{ m}$
Angular Resolution	0.05°
Temperature range	180 mK - 2000 K
Available magnets	B < 0.5 T vertical, horizontal B < 10 T vertical
Polarization analysis	2 multilayer benders
Detector	180 mm x 180 mm PSD resolution 1 mm x 2 mm; single $^3\text{He}$ detector

## 2.6 Simulations for a new neutron guide switch for the instrument MIRA

Sebastian Mühlbauer<sup>1</sup>, Peter Böni<sup>1</sup>, Robert Georgii<sup>1,2</sup>

<sup>1</sup>TU München, Physics Department, E21

<sup>2</sup>ZWE FRM II, TU München

### Intention

The instrument MIRA is located at the end of the neutron guide 6B, which is connected to the cold neutron guide NL6-b by means of a wavelength sensitive switch. The neutron flux at the sample position of MIRA was measured recently to be  $4 \cdot 10^5 \text{ cm}^{-2} \text{ s}^{-1}$ . In order to improve the neutron flux, several simulations for a new, improved neutron guide switch were performed, using the program package McStas [1]. A gain factor of 10 can be reached without the usage of neutron focusing devices. Furthermore, by adding neutron focusing devices, gains of 100 compared to the actual flux are achievable. In order to calculate the losses in neutron flux for the NL6 after the rebuilt switch, additional simulations were performed.

### Current neutron guide switch

The first issue to be considered is the actual geometry of the guide switch, as shown in fig. 2.8. A silicon wafer, tilted at an angle of 3° relative to the beam axis is deflecting the neutrons into the neutron guide NL6-b (cross section  $120 \times 10 \text{ mm}$ ), which is inclined towards the guide 6 at an angle of 6°. The silicon wafer reaches 2 cm into the neutron

guide NL6-b and is coated with  $\text{Ni}^{58}$  for the first quarter, supermirror  $m = 2$  [ $\Theta_c^{\text{Ni}}$ ] for the second quarter and supermirror  $m = 3$  [ $\Theta_c^{\text{Ni}}$ ] for the second two quarters of its length. The radius of curvature of the guide is 85 m, the supermirror coating is  $m = 2$  [ $\Theta_c^{\text{Ni}}$ ]. Both, the inclination of the neutron guide NL6-b and the silicon wafer, as well as the radius of curvature of the guide are limiting the cutoff wavelength of the system to 7.7 Å. The maximum of the cold neutron flux of the FRM II cold source is located at 4 Å, therefore only a small fraction of the neutrons can be used at the instrument.

### Improved neutron guide switch

Improving the neutron flux without changing the cross section of the neutron guide ( $120 \times 10 \text{ mm}$ ) makes it necessary to shift the cutoff wavelength of the guide system to a smaller wavelength, i.e. 4 Å. To achieve this goal, both the guide and the switch have to be redesigned. The simulations contained several different geometries of varying inclination angles of the neutron guide, different radii of curvature of the guide and different coatings. Within the bounds of geometrical con-

straints as shown in fig. 2.9 the guide switch can be shifted by several meters

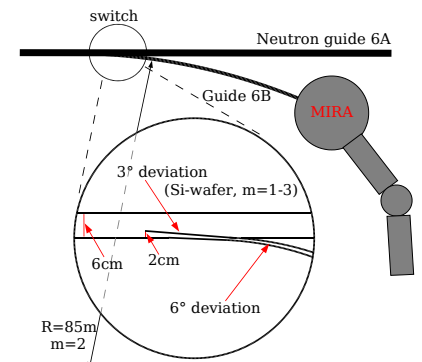


Figure 2.8: Current geometry of the neutron guide switch for NL6/B.

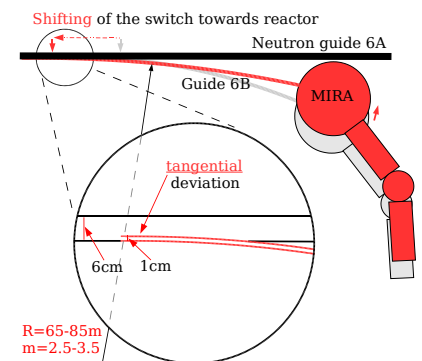


Figure 2.9: Improved geometry of the neutron guide switch for NL6/B.

towards the reactor, as well as the instrument itself can be moved by 35 cm towards the NL6. The results of the simulations are presented in fig. 3.

## Losses for the neutron guide NL 6

In order to make assumptions for the losses of flux of the NL6, the neutrons deflected by the switch were subtracted from the flux inside NL6. As only 1 cm of the cross section of NL6 is shadowed, the maximum loss can be  $\frac{1}{6}$ . Additionally, the divergence of the neutron beam after the switch was analyzed.

## Results

As shown in fig. 2.10, a gain factor in neutron flux of 10 can be reached, shifting the cutoff to shorter wavelengths, while losing only about 12 percent of neutron flux inside the NL6 (shown in the inset of fig. 2.10). Furthermore, shorter wavelengths would give direct access to atomic resolution on MIRA, which is not yet possible with 10 Å.

[1] Nielsen, K., Lefmann, K. *Physica B*, 238. McStas webpage: <http://neutron.risoe.dk/mcstas>.

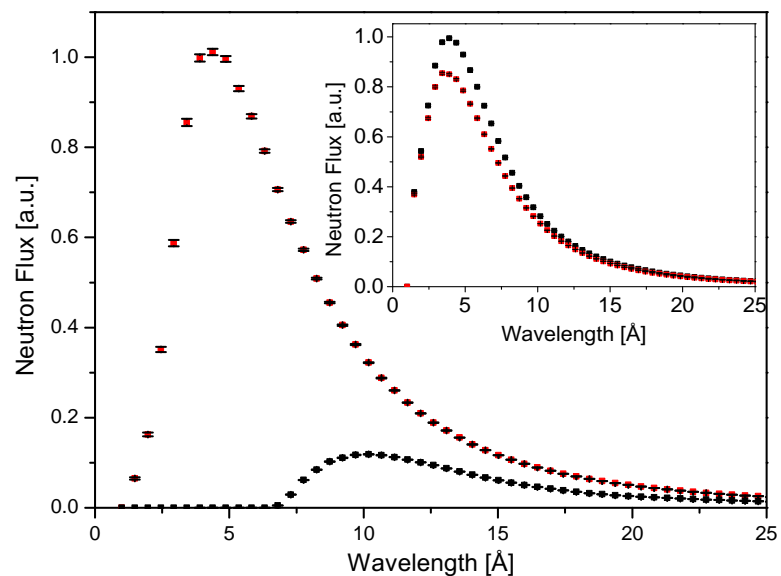


Figure 2.10: Gain factor for a suggested geometry of the new neutron guide switch (tangential deviation,  $R = 80$  m,  $m = 2.5 [\Theta_c^{Ni}]$ , cutoff 4 Å. The inset shows the losses in the guide NL6 for the upper geometry.

## 2.7 Horizontal ToF-Neutron Reflectometer REFSANS at FRM II Munich/Germany: First Tests and Status

R. Kampmann<sup>1</sup>, M. Haese-Seiller<sup>1</sup>, V. Kudryashov<sup>1</sup>, C. Daniel<sup>2</sup>, B. Nickel<sup>3</sup>, J. Rädler<sup>3</sup>, A. Schreyer<sup>1</sup>, E. Sackmann<sup>2</sup>

<sup>1</sup>GKSS Forschungszentrum, Institut für Werkstofforschung, Geesthacht, Germany

<sup>2</sup>TU München, Physik Department, E22

<sup>3</sup>Ludwig-Maximilians-Universität, München, Germany

### Introduction

In 2005 the horizontal reflectometer REFSANS at FRMII in Munich/Germany has successfully been put into operation. It is dedicated to the comprehensive analysis of the air / water interface by means of specular and off-specular reflectivity as well as GISANS measurements [1, 2].

### REFSANS and its main components

The main demands made on REFSANS are to provide excellent conditions for *i*) specular reflectivity, *ii*) grazing incidence (GI-)SANS and *iii*) to allow comprehensive investigations on the air / water interface for biological applications [1, 2]. To meet these demands novel and expensive components have been developed for this horizontal ToF-reflectometer.

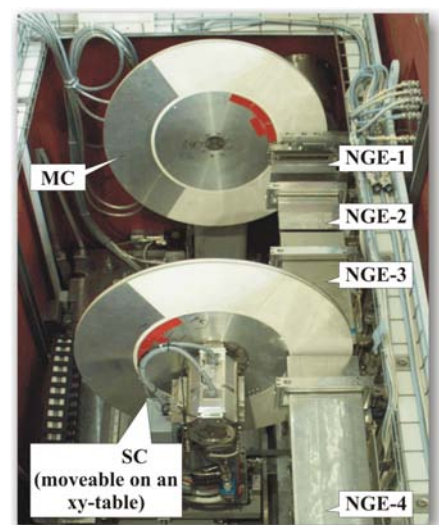


Figure 2.11: View of neutron guide elements (NGE), master chopper and slave chopper in the chopper chamber.

The instrument starts with the master chopper (MC) in the chopper chamber in which the slave chopper (SC) can be positioned in neutron guide gaps at distances between  $\approx 5$  cm and  $\approx 2.1$  m from the MC. Both choppers have double discs to adjust the transmission window between  $0^\circ$  and  $120^\circ$  (Fig. 2.11). They are operated with windows of equal height and the SC opens at the time  $t_0$  when the MC closes with the result that at  $t_0$  the neutron guide between both choppers is filled with neutrons with wavelengths  $\lambda < \lambda_0$  [3]. This expensive design (Fig. 2.12) is needed to meet the demands of specular reflectivity and of GI-SANS comprising high and low  $\lambda$ -resolution.

Neutron guide elements of REFSANS as well as their mechanical support in the chopper and in the beam guide chamber are designed for realizing very different beam geometries. Standard reflectivity measurements are performed with a horizontally slit height-smearred beam and incidence angles of the primary beam of  $\pm 3$ , 12 and 48 mrad (main beam settings in REFSANS). The beam may be guided towards the sample surface from the air or through the substrate [1, 2].

GISANS geometry demands to collimate the beam horizontally and vertically. In this geometry the intensity can strongly be increased by means of focusing 13 partial beams in the detector plane at a distance of  $\sim 9$  m from the sample (Fig. 2.12). This focusing is performed by means of pre-collimating the beams in radially collimating neutron guide channels in the chopper chamber (NGE-3 and -4) and by comb-like diaphragms which can be moved into the beam in between of neutron optical bodies (Fig. 2.12 and 2.13) preventing mixing of neutrons in different partial beams.

The sample environment is designed for experiments at the air / water interface as well as at the air / solid and liquid / solid interface. In all cases one can make use of a microscope in upright or inverted position either for preparation purposes or as a complementary measuring option (e.g. fluorescence techniques). The further equipment

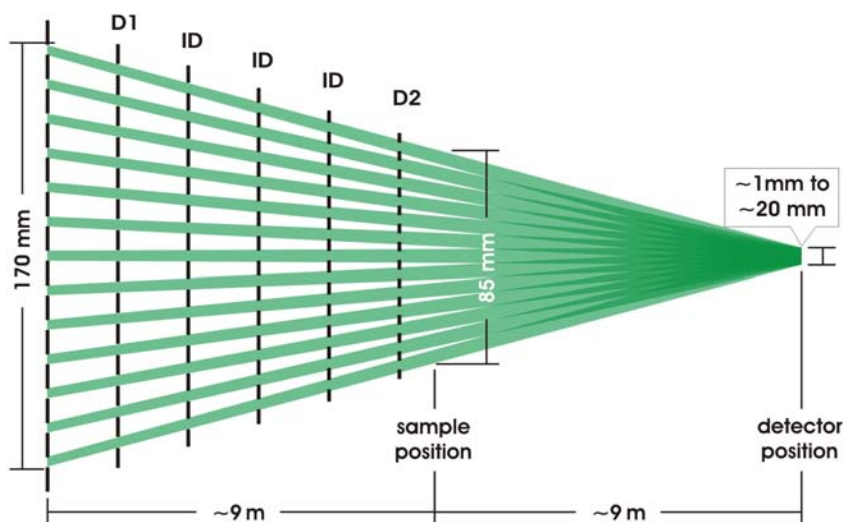


Figure 2.12: Schematic view of the horizontal focusing of up to 13 beams in the detector plane. The beam is pre-collimated in the radial collimator (lower channels in the 0.6 m and 1 m long NGE-3 and -4).

consists of a damping table, a temperature controlled film balance and a set of translational tables ( $x, y, z$ ) together with a three-axis goniometer ( $\chi, \phi, \Omega$ ).

A 2D-position sensitive area detector with an active area of  $500 \text{ mm} \times 500 \text{ mm}$  and a position resolution of  $\approx 2 \text{ mm} \times 3 \text{ mm}$  has successfully been put into operation. With its high quantum efficiency for neutrons and its very low one for gammas the detector meets all requirements for measuring low reflectivity and weak GISANS contributions [4]. Together with a new data acquisition based on the P7888 card from FAST ComTec GmbH the delay-line based 2D-detector allows of maximum count rates of  $\sim 10^6$  n/s.

In the scattering tube the 2D-detector can be positioned at distances between  $\approx 2$  m and  $\approx 12$  m from the sample. The scattering tube can be lifted such that the specularly reflected beam passes its centre for incidence angles between  $\sim 0$  and  $\sim 100$  mrad (Fig. 2.11).

## Status

REFSANS has successfully been put into operation, all components (chopper system, neutron optics, sample environment, 2D-detector, shielding, scattering tube with lifting system and data acquisition system) meet or even surpass their requirements. Test beams have already been guided to the sample demonstrating that the shielding is sufficiently thick. First measurements will be performed at REFSANS in spring 2006 after repairing of some broken elements of neutron guide NL-2b.

## Acknowledgements

The great contribution of the technical department of GKSS to constructing and manufacturing of REFSANS components is gratefully acknowledged. The development of REFSANS has been supported by the German Federal Ministry of Education, Research and Technology (BMBF) under contracts 03-KA5FRM-1 and 03-KAE8X-3.

- [1] Kampmann, R., Haese-Seiller, M., Marmotti, M., Burmester, J., Deriglazov, V., Syromiatnikov, V., Okorokov, A., Frisius, F., Trisl, M., Sackmann, E. *Applied Physics A*, 74,



(2002), 249–251.

- [2] Kampmann, R., Haese-Seiller, M., Kudryashov, V., Deriglazov, V., Syromiatnikov, V., Trisl, M., Toperverg, B., Okorokov, A., Schreyer, A., Sackmann, E. *Physica B*, 335, (2003), 274–277.
- [3] van Well, A. A. *Physica B*, 180-181, (1992), 959–961.
- [4] Kampmann, R., Marmotti, M., Haese-Seiller, M., Kudryashov, V. *Nuclear Instruments and Methods A*, 529, (2004), 342–347.

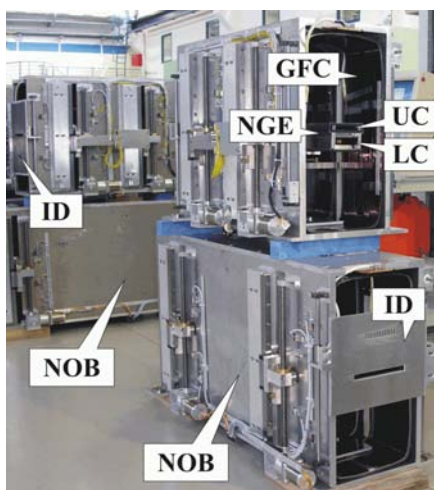


Figure 2.13: View of neutron optical bodies (NOB) ready for being mounted into the beam guide chamber (NGE, UC and LC: neutron guide element and its upper (UC) or lower channel (LC); GFC: guide field coil; ID: interim diaphragms).

## 2.8 Structure Powder Diffractometer SPODI

M. Hoelzel<sup>1</sup>, A. Senyshyn<sup>1</sup>, R. Gilles<sup>2</sup>, B. Krimmer<sup>2</sup>, F. Elf<sup>3</sup>, H. Boysen<sup>4</sup>, H. Fuess<sup>1</sup>

<sup>1</sup>TU Darmstadt, Material- und Geowissenschaften

<sup>2</sup>TU München, ZWE FRM II

<sup>3</sup>Universität Bonn, Mineralogisch-Petrologisches Institut

<sup>4</sup>Ludwig-Maximilians-Universität, Depart. für Geo- und Umweltwissenschaften, München

### Introduction

The Structure Powder Diffractometer SPODI (fig. 2.14) is designed for high resolution powder diffraction. The general concept of SPODI and descriptions of its components have already been published [1, 2, 3, 4, 5]. In this report, the commissioning of the instrumental components as well as measurements during first proposal cycles in 2005 are summarized.

### Results and Discussion

At the beginning of the second reactor cycle, significant improvements in the adjustment of the Ge(551) monochromator have been achieved. Neutron radiography images of the monochromator crystals have been taken using a small circular slit (about 1 mm diameter) at the sample position and an

area detector at various distances between 0.5 and 3 m behind the slit. Beside the image plate detector of SPODI (belonging to the small-angle scattering apparatus), also the CCD camera made by Martin Muehlbauer has been applied for detection. For adjusting the monochromator, all 17 crystals have to be aligned individually according to three axis (i) translation (ii) tilting for vertical focussing and (iii) rotating in the scattering plane. The observed intensity distributions of the spots displayed on the detector were used as a measure for the alignment of the monochromator crystals.

For each of the 80 detectors, which are position sensitive in the vertical direction, the correlation between the position along the detector height and the detector channel number has to be determined individually. Based on long-time vanadium scans carried out al-

ready in the first reactor cycle, a detector calibration file could be established which was implemented in a new detector read-out software. The application of the detector calibration file on the raw data yields the intensity distribution of neutrons vs. scattering angle and detector height.

The different transmissions of the



Figure 2.14: Diffractometer SPODI in the Experimental Hall of FRM II

detector collimators as well as the different efficiencies of the detectors require an intensity correction value for each of the 80 collimator-detector pairs. These intensity correction values have been derived from various vanadium scans at different positionings of the detector array.

In addition to the intensity correction, also corrections for the scattering angles have to be determined for each of the 80 collimator-detector pairs. This is necessary because small mismatches between the orientations of the detector collimators towards the sample position or the detectors cause a deviation of the effective scattering angle from the nominal scattering angle. To determine the offset in the scattering angle for each collimator-detector pair, sequences of measurements of standard samples have been carried out. In these sequences, the positionings of the detector array have been varied in the following way:  $0^\circ$ ,  $-2^\circ$ , .... up to  $-60^\circ$ . From these data, diffraction patterns for the individual collimator-detector pairs have been derived. The diffraction patterns of each detector have been analysed by Rietveld refinement to get a zero-shift value (= offset in scattering angle) for each collimator-detector pair. Various standard samples have been used to achieve enough statistics for the scattering angle correction for each of the 80 collimator-detector pairs.

From the end of the second reactor cycle and throughout the third reactor cycle, measurements of users have been carried out at SPODI.

During this period, the high-temperature furnace as well as the cold-head cryostat have been set into operation at SPODI.

A new data analysing software has been developed to integrate the data along the Debye-Scherrer cones using the full detector height while taking into account the instrumental corrections. Figure 2.15 illustrates a section of the intensity distribution (counts vs. detector height and scattering angle) for a measurement of  $Al_2O_3$  standard. In figure 2.16 corresponding diffraction patterns are shown, obtained by different way: (i) by integration along the Debye-Scherrer cones over the full detector height, (ii) by integration along the vertical direction over the full detector height and (iii) by integration along the vertical direction over 100 mm detector height. The comparison shows that high resolution diffraction along with high intensities can be achieved at SPODI.

Recently, the small-angle scattering apparatus of the Structure Powder Diffractometer has been set into operation. For this purpose, a new Cu(111) monochromator has been installed, yielding 4.08 Angstroms at a monochromator take-off angle of  $155^\circ$ . After adjustment of the monochromatic beam, first test measurements have been performed using circular slits for the collimation and a cooled beryllium filter to cut off lambda-half contributions.

## Acknowledgement

The support of this project by the German BMBF is gratefully acknowledged.

- [1] Gilles, R., Artus, G., Saroun, J., Boysen, H., Fuess, H. *Physica B*, 276-278, (2000), 87.
- [2] Gilles, R., Saroun, J., Boysen, H., Fuess, H. *Proc. HERCULES X Euro Conference*, 282.
- [3] Gilles, R., Krimmer, B., Saroun, J., Boysen, H., Fuess, H. *Mat. Sci. For.*, 378-381, (2001), 282.
- [4] Gilles, R., Krimmer, B., Boysen, H., Fuess, H. *Appl. Phys. A 74 (Suppl.)*, 74, (2002), S148.
- [5] Hoelzel, M., Gilles, R., Schlapp, M., Boysen, H., Fuess, H. *Physica B*, 350, (2004), e671.

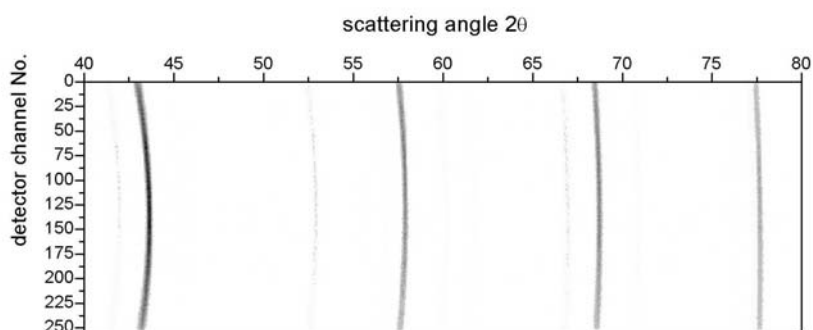


Figure 2.15: 2D intensity distribution for  $Al_2O_3$  standard.

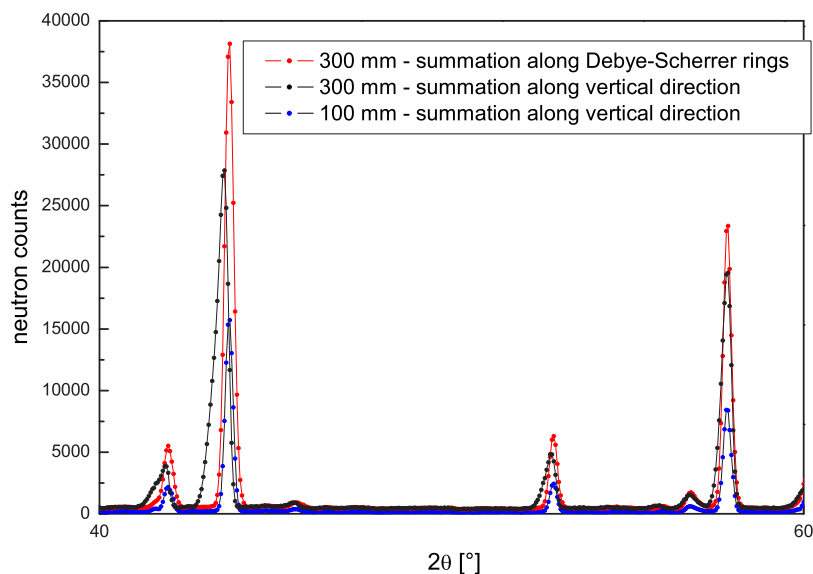


Figure 2.16: Diffraction patterns obtained from the intensity distribution given in fig 2.15, by (i) integration along the Debye-Scherrer cones over the full detector height, (ii) integration along the vertical direction over the full detector height and (iii) integration along the vertical direction over 100 mm.

## 2.9 STRESS-SPEC Materials Science Diffractometer

M. Hofmann<sup>1</sup>, U. Garbe<sup>2</sup>, G.A. Seidl<sup>1</sup>, R. Schneider<sup>3</sup>, J. Rebelo-Kornmeier<sup>3</sup>, R.C. Wimpory<sup>3</sup>

<sup>1</sup>TU München, ZWE FRM II

<sup>2</sup>GKSS, Geesthacht

<sup>3</sup>BENSC, Hahn-Meitner-Institut, Berlin

### Introduction

The Materials Science diffractometer Stress-Spec is located at the thermal beam tube SR3 and is optimized for residual stress analysis and texture measurements of new materials and engineering components. Its main characteristics and components have been described elsewhere [1, 2] and here only the most relevant developments of 2005 will be reviewed.

### New Hardware

The new primary collimators with iron foils were installed and aligned prior to the 2nd reactor cycle. They replaced the existing High Performance Thermo-plastic foil collimators to avoid radia-

tion damage and improve long term stability of the beam line. The interlock system to restrict access to the experimental area while the neutron beam is open was finalised and tested to work according to specifications.

### Commissioning experiments

In the first reactor cycle of 2005 we continued with the commissioning of the instrument. The first experiments included new gold foil measurements at the monochromator position. The measured thermal flux at the monochromator is approx.  $9 \times 10^9$  n/cm<sup>2</sup>/s with a small contribution of fast neutrons ( $E > 0.3$  eV) determined through comparison with gold foils shielded by Cd. The flux at the sam-

ple position was determined with calibrated monitors for all three monochromators at selected wavelengths and monochromator to sample distances (see table 2.2 and figure 2.17). The

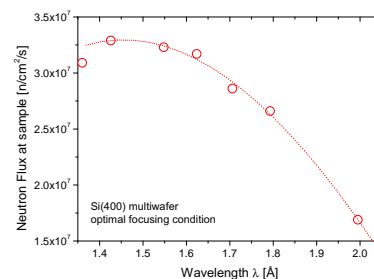


Figure 2.17: Neutron flux at the sample position for optimised focusing of the Si monochromator.

Monochromator	$\lambda$ [Å]	Reflection	Flux [n/cm <sup>2</sup> /s]
Si (400)	1.548	(400)	$3.2 \times 10^7$
PG (002)	1.47	(004)	$9.2 \times 10^7$
Ge (511)	1.516	(511)	$1.4 \times 10^7$

Table 2.2: Measured neutron flux at the sample position of STRESS-SPEC. The monochromator-sample distance was  $L_{MS} = 1.8$  m.

focussing options of the Ge and Si monochromators were also directly investigated using a camera setup borrowed from the tomography group. Moreover we used a perfect Si(100) single crystal to check the homogeneity of all three monochromators and to determine their respective resolution functions. This revealed that in case of the PG monochromator some of the crystals seem to have moved during the installation procedure which will be rectified at the first possible opportunity in 2006. In addition the resolution of the Si(400) and the Ge(511) monochromator was measured using  $Al_2O_3$  and annealed Fe samples at wavelength  $\lambda = 1.81$  Å and 1.516 Å, respectively, showing good agreement with expected values. Values of  $\Delta d/d = \Delta\theta_S/\tan\theta_S$  down to  $2 \cdot 10^{-3}$  can be achieved on STRESS-SPEC.

## Residual Strain

Apart from the start of the user program (see Experimental Reports), several experiments using either Round Robin samples or samples extensively measured at other neutron sources were conducted to compare STRESS-SPEC with other neutron strain scanners and texture diffractometers. Figure 2.18 shows a comparison of two of ferritic steel repair weld round robin samples, which were measured within the frame work of the NET European Network (Network on Neutron Techniques Standardization for Structural Integrity), lead by the Joint Research Centre - Institute for Energy (JRC-IE) in Petten, NL. The specimens are nominally the same and indeed the strain, here in the out-of-plane normal direction, shows excellent agreement. For this measurement, the Si (400) perfectly bent crystal monochromator was selected, with a scattering angle of  $2\theta_S \approx 88.3^\circ$  using the Fe (211) reflection. A

gauge volume of  $2 \times 2 \times 2$  mm<sup>3</sup> was used. Other experiments included determination of the strain values in the VAMAS Round Robin Ring and Plug sample [3], where excellent agreement with tabulated and calculated strain values was achieved in comparably short measurement times. It was possible to achieve experimental uncertainties in strain values  $\epsilon$  of  $1 \times 10^{-4} = 100 \mu\epsilon$  in this Al sample in less than 3 minutes per strain direction using gauge volumes down to  $2 \times 2 \times 2$  mm<sup>3</sup>.

## Texture

The first pole figures (figure 2.19) measured on STRESS-SPEC using standard samples show that global texture analysis [4] is easily feasible. The results and also the time required to measure the pole figures are at least comparable to measurements at the dedicated texture

diffractometer TEX-2 [5]. Our experiments, however, show that in future due to the high neutron flux at STRESS-SPEC in combination with the area detector it will be possible to decrease the data acquisition time for such experiments by at least a factor of 3. A software tool to handle and analyse the data of the two dimensional detector was developed. It also allows to evaluate pole figures of phase mixtures.

## Outlook

In 2006 tests and upgrading of the instrument will continue with the aim to speed up the alignment procedure of the slits for strain measurement using a newly developed automated procedure. For texture measurements the time to position samples has to be decreased. This can be done by adapting the instrument software to take data continuously while rotating the sample around the rotation angle phi.

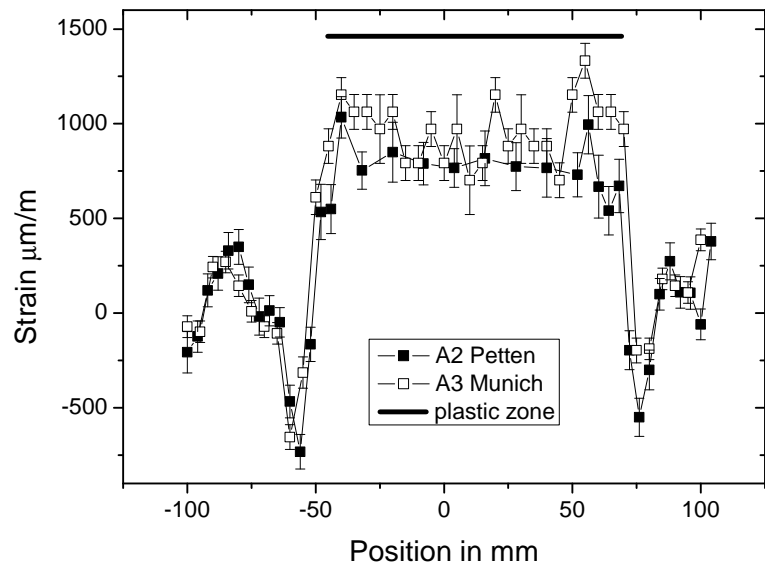


Figure 2.18: Comparison of JRC Petten and STRESS-SPEC measurements on repair weld round robin samples.

- [1] Hofmann, M., Seidl, G., Schneider, R. *Ann. Report FRMII*.
- [2] Hofmann, M., Schneider, R., Seidl, G., Garbe, U., Rebelo-Kornmeier, J., Brokmeier, H. *Physica B*. In press.
- [3] Webster, G. In *Proceedings ICRS-6*, volume 1, 189–196 (Oxford, Institute of Materials, 2000).
- [4] Bunge, H., Wenk, H., Pannetier, J. *Texture Microstruct.*, 5, (1982), 153.
- [5] Brokmeier, H.-G., Zink, U., Schnieber, R., Wittassek, B. *Mat. Sci. Forum*, 273-275, (1998), 277.

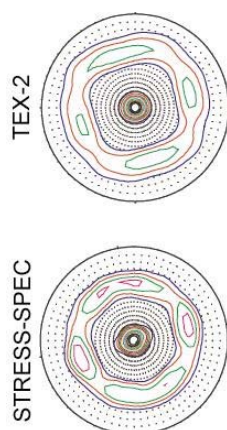


Figure 2.19: Comparison of the (110) - pole figure of the standard Cu sample measured on STRESS-SPEC and TEX-2. Note the better resolved pole figure due to higher resolution in orientation space of STRESS-SPEC.

## 2.10 RESI – The Single Crystal Diffractometer

B. Pedersen<sup>1</sup>, G. Seidl<sup>1</sup>, W. Scherer<sup>2</sup>, F. Frey<sup>3</sup>

<sup>1</sup>ZWE FRMII, TU München

<sup>2</sup>Universität Augsburg, Institut für Physik

<sup>3</sup>Ludwig-Maximilians-Universität München, Sektion Kristallographie, GeoDepartment,

### Introduction

The year 2005 has been the first year with real user service on RESI. The instrument was further adjusted, the second monochromator was successfully commissioned and measurements to characterise the instrument were carried out.

### New components

The main new component installed in 2005 was the Ge-511 monochromator for a wavelength of 1.5 Å. It uses stacks of elastically bend Ge-wafers in the same focusing system as the Cu-422 monochromator.

In the end of 2005 also the second goniometer option consisting of a heavy

tow-circle goniometer with either a tilting head or an eulerian cradle was installed and is currently being commissioned.

The sample environment available at RESI was expanded by an Oxford Cryosystems Cryojet open-flow nitrogen cooler (operating temperature range RT-100K) and an Oxford Diffraction Helijet open-flow helium cooler (operating temperature range 100K - 15K).

### Instrument characteristics

The highly sophisticated monochromator mechanics, which allow adjustment of the individual crystals in three degrees of freedom have proven to be very useful. Using the image plate as a “cam-

era” for neutrons, we were able to focus the monochromatic beam on an area of about 20×30 mm, thereby increasing the flux density on the sample position by approx. a factor of 5 (compared to flat monochromator) to approx.  $1 \cdot 10^6 \text{ n cm}^2 \text{ s}^{-1}$  for the copper monochromator and  $4 \cdot 10^6 \text{ n cm}^2 \text{ s}^{-1}$  for the germanium monochromator.

To determine the resolution function of the instrument, we measured a small piece of a perfect germanium crystal with fine slicing (rotation scan, omega scan width 0.1° per image) using the Cu-422 at 1 Å. From the rocking width of the reflections, we find the expected behavior, with a minimum at 90° theta, where the resolution is 12'. This corresponds to the divergence of the focusing neutron guide. For reflections not

in the diffraction plane, the resolution slightly decreases due to a combination of the curvature of the Ewald sphere and the larger vertical divergence of the incident beam.

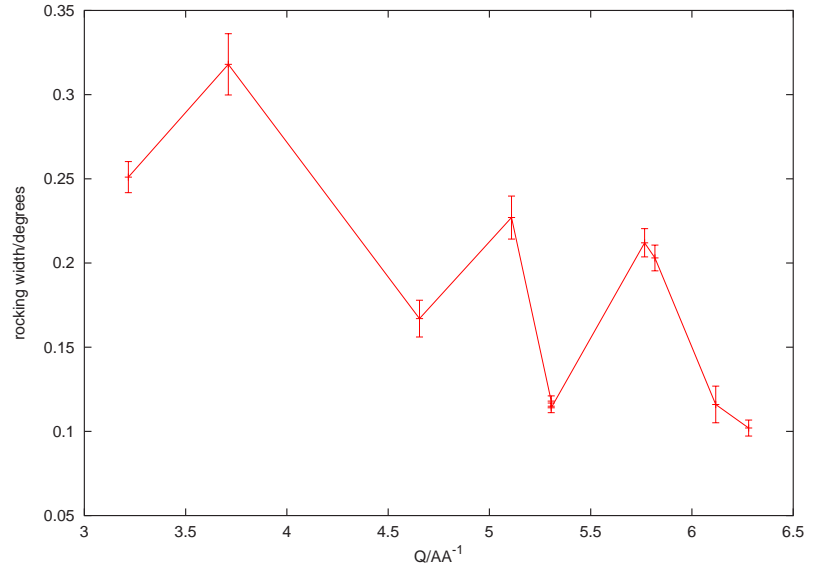


Figure 2.20: Resolution (rocking width, FWHM) of a perfect Ge single crystal, determined from different reflections covering the active detector area.

## 2.11 Irradiation Facilities

H. Gerstenberg<sup>1</sup>, X. Li<sup>1</sup>, G. Langenstück<sup>1</sup>, M. Oberndorfer<sup>1</sup>, A. Richter<sup>1</sup>

<sup>1</sup>ZWE FRM II, TU München

### General

After the successful taking into operation during the nuclear start-up in 2004, the irradiation service of the FRM II has begun its routine operation starting from the second reactor cycle in spring 2005. In addition to the following main facilities:

- the pneumatic rabbit system RPA,
- the capsule irradiation facility KBA,
- the test rig of the silicon doping facility SDA,
- the transport rabbit system TRP serving as quick connection between FRM II and the Institute for Radiochemistry (RCM),

two other new irradiation positions were set into operation in 2005. These are:

Table 2.3: Irradiations at the FRM II in 2005

position	PRA	KBA	SDA	AS	RS	total
irradiation No.	52	77	7	3	1	140

Table 2.4: Neutron flux in some irradiation channels at the FRM II (status 2005)

channel	$\Phi_{th}(1/cm^2s)$	$\Phi_{epi}(1/cm^2s)$	$\Phi_{fast}(1/cm^2s)$
RPA1	$3.6 \times 10^{13}$	$6.7 \times 10^9$	$2.0 \times 10^9$
RPA2	$1.5 \times 10^{13}$	$3.2 \times 10^9$	$4.1 \times 10^8$
RPA3	$4.8 \times 10^{12}$	$7.6 \times 10^8$	$7.2 \times 10^7$
RPA4	$7.3 \times 10^{13}$	$2.4 \times 10^{10}$	$5.6 \times 10^{11}$
RPA5	$3.9 \times 10^{13}$	$1.2 \times 10^{10}$	$5.9 \times 10^9$
RPA6	$7.1 \times 10^{12}$	$1.2 \times 10^9$	$1.5 \times 10^8$
KBA1-1	$1.3 \times 10^{14}$	$2.6 \times 10^{11}$	$3.9 \times 10^{11}$
KBA1-2	$9.3 \times 10^{13}$	$9.9 \times 10^{10}$	$2.0 \times 10^{11}$
KBA2-1	$1.1 \times 10^{14}$	$7.5 \times 10^{10}$	$2.1 \times 10^{11}$
KBA2-2	$7.7 \times 10^{13}$	$3.9 \times 10^{10}$	$1.0 \times 10^{11}$
SDA2	$1.6 \times 10^{13}$	$1.0 \times 10^{11}$	$1.0 \times 10^{10}$
AS	$1.2 \times 10^{13}$	$1.0 \times 10^9$	$1.5 \times 10^{10}$
RS			$1.8 \times 10^{14}$

- the position for short term irradiations of medium volume samples (AS) and
- the high flux irradiation position in the central control rod (RS).

Altogether 140 irradiations were carried out during the three reactor cycles in 2005. Table 2.3 shows the irradiation numbers on each system.

Neutron fluxes were measured again by using the standard flux monitors (Al, Co, Zr, U, Ni) at the beginning of the routine operation in the second reactor cycle. The new flux data are very comparable to the values which were measured during the nuclear commissioning of the reactor in 2004. The detailed results of the neutron flux measurements are shown in table 2.4.

Three new operators have joined the irradiation team in 2005.

### Pneumatic Rabbit System (RPA)

The pneumatic rabbit system consists of six independent irradiation channels, which are suited to be loaded by identical polyethylene capsules. Due to their different positions within the heavy water moderator tank these irradiation channels offer different thermal neutron flux densities, what means flexible irradiation conditions for the users. Beside the irradiations of samples for the neutron activation analysis, some interesting isotopes for the nuclear pharmacy such like  $^{177}\text{Lu}$  and  $^{188}\text{Re}$  were also produced using this system.

### Capsule Irradiation Facility (KBA)

The capsule irradiation facility is a pool water driven rabbit device to be used for long term irradiations. It exhibits two irradiation channels both of which can be loaded by up to five Al irradiation capsules.

For a very special research purpose in the geoscience (fission track analysis), a series of stone samples were irradiated at a low reactor power of 300 kW or 900 kW, so that a desired relatively low neutron fluency could be reached in a reasonable irradiation time. According to the different neutron fluencies the irradiation times were between 9 and 98 minutes. The reactor ran at this low power step normally for only several hours. Altogether 19 low fluency irradiations of this kind were carried out using the KBA in 2005. The longest irradiation on the KBA at full reactor power of 20 MW was 48 hours for a production of  $^{177}\text{Lu}$ . Table 2.5 shows irradiations on the KBA at different reactor powers in 2005.

### Position for Short Term Irradiations of Medium Volume Samples (AS)

This new irradiation position was used for the first time in 2005, so that irradiations of larger volume samples or those requiring a low neutron fluency can also be performed at nominal reactor power at 20 MW. The distance from the centre of the irradiation position to the reactor core is exactly 100 cm. The irradiation pipe is parallel to the fuel element. In comparison to the KBA, the thermal neutron flux here is about one order of magnitude lower. In principle the local neutron flux at the position of the sample can easily be lowered further by varying the irradiation position in the vertical axis in the irradiation pipe because of the change of the vertical neutron flux distribution within the moderator tank. Figure 2.21 shows the design of this irradiation device, which is mounted on the handling bridge during the operation. The position of the sample container can be defined by the length of the nylon string just like fishing. Neutron flux was measured by



Figure 2.21: Design of the irradiation device for the fishing irradiation position.

using  $\text{Au} - \text{Al}$  (1%) wires and  $\text{Ni}$ -foil (99.8%) as flux monitors.

### Irradiation position in the central control rod (RS)

During the 3rd reactor cycle a neutron flux measurement was carried out for the first time in the irradiation position in the control rod, which was optimized mainly to provide a high fast neutron flux. It can, however, only be loaded and unloaded when the reactor is shut down, i.e. after completion of its 52-day cycle. For the flux measurement, the monitors were loaded in an Al-capsule mounted at the end of the control rod in the central channel of the reactor. The fast neutron flux was determined via the reaction  $^{54}\text{Fe}(n,p)^{54}\text{Mn}$ . The result is shown in Tab. 2.4. The fast neutron flux is less than expected. The reason could be the shielding effect of the control rod itself. The typical monitor Ni for the determination of fast neutron flux is here not suitable due to the burn-up effect in

reactor power	300 kW	900 kW	20 MW	total
irradiation No.	5	14	58	77
irradiation time	21-98 min	9-35 min	100s-20d	

Table 2.5: irradiations on the KBA at different reactor powers in 2005.

a very high thermal flux. The determination of thermal and epithermal neutron fluxes could not be performed in this cycle for technical reasons but will be done in one of the next reactor cycles as soon as possible.

Some possible applications in this position are for example the production of the positron source  $^{58}\text{Co}$  or the isotope  $^{188}\text{Re}$  for the nuclear medicine. The isotopes will be produced via the following reactions:

$$^{58}\text{Ni}(n,p)^{58}\text{Co}(T_{1/2} = 78d), \text{ (fast neutron reaction)}$$

$$^{186}\text{W}(n,\gamma)^{187}\text{W}(n,\gamma)^{188}\text{W}(\beta^-)(T_{1/2} = 69d)$$

$$^{187}\text{Re}(T_{1/2} = 17h) \text{ (double neutron capture with thermal neutrons).}$$

Test samples will be irradiated in the next reactor cycles in 2006.

## Silicon doping Facility (SDA)

The neutron flux profile within the silicon ingots in the doping position were successfully determined by using a simplified test rig of the doping facility (SDA-opt) during the system start-up in 2004. Based on the values of the flux measurements, the shape of the Ni-absorber being necessary to reduce the axial inhomogeneity of the neutron flux within the ingot below 5% was calculated and optimised by means of Monte-Carlo calculation. Figure 2.22 shows the cut view of the optimised shape of the Ni-liner.

Two nickel coating samples were analysed by the governmental Material Test Office for Engineering. Above all, the connection between the very thin nickel coating layer and the aluminium carrier was intensively checked through bending test and metallurgical analysis. After the positive examination, a prototype of the nickel absorber pipe was made by the company Leistner in the summer of 2005. Figure 2.23 shows the

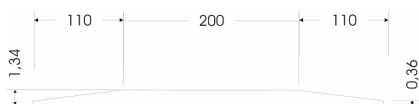


Figure 2.22: cut view of the optimised Ni-liner shape.



Figure 2.23: top) Ni-liner after the coating, bottom) Test doping rig mounted with the first nickel liner after an irradiation in the reactor pool.

test doping rig mounted with the first nickel liner. The neutron flux distribution behind the nickel liner was determined again.

Flux monitors were mounted at 24 positions in a test ingot with a diameter of 6 inches and a length of 500 mm. The results in figure 2.24 show that the axial difference between the middle level and the both edges of the test ingots is less than 5%. The total neutron flux is reduced by about 6% as compared to the use of the pure Al tube due to the absorption by the nickel coating. Test silicon ingots with diameters of 4 and 6 inches from two manufactures were irradiated in the test doping rig with the Ni-liner to check the doping homogeneity.

According to the feed-backs of the clients, the first doping results were extremely positive. Radial resistivity variation is less than 4% ~ 5%. Axial variation is below 3% ~ 4% and seems to be completely hidden in measurement noise. The minority carrier lifetime in Si is high, around 400-700 microseconds, what means a low content of irradiation defects. After adjustment of the calibration factors connecting the irradiation dose to the target resistivity the irradiations met the conditions of the doping specifications very well. The relative axial resistivity deviations within a 6 inches test ingot is shown in figure

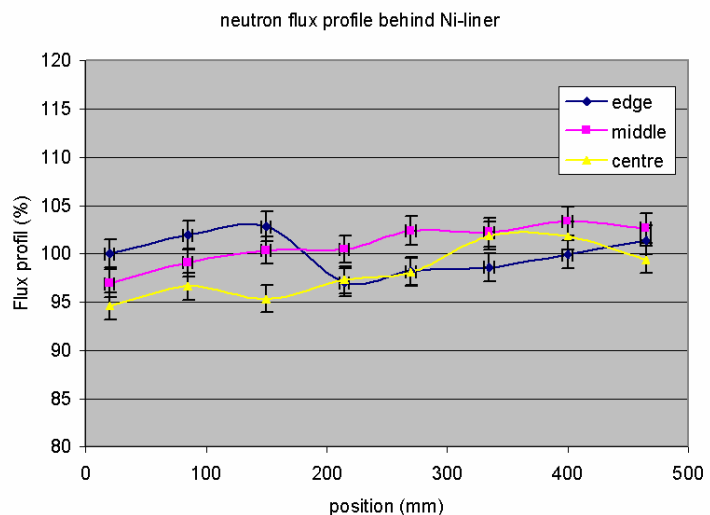


Figure 2.24: Neutron flux profile behind Ni-liner in a 6" ingot.



**2.25.** The first doping batch of 6" Si-ingot for a commercial production was already irradiated before the Christmas 2005. Up to 500 kg Si ingots will be irradiated by using the current manual doping system in the next reactor cycle at the beginning of 2006.

The concept of the final Si doping facility offering a semi automatic operation was already verified by the TÜV Süd in summer of 2005. The installation of important parts has already begun. The final system will be completely installed in the moderator tank in 2006.

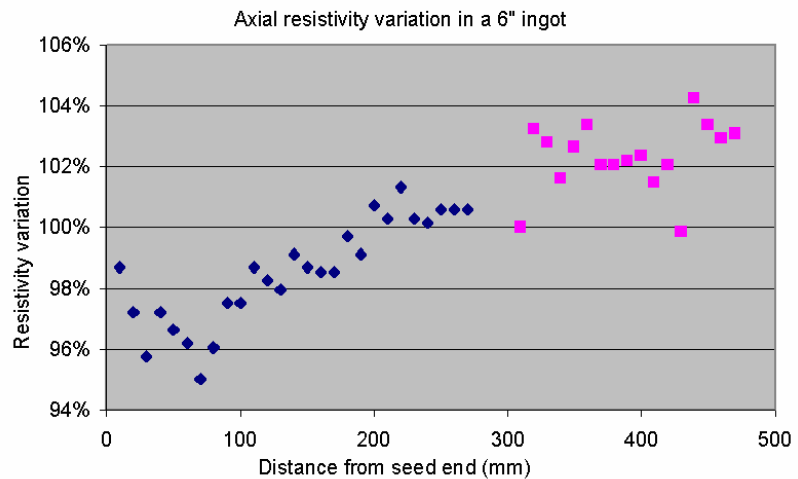


Figure 2.25: Relative axial resistivity deviation within a 6 inches test ingot.

## 2.12 Status of the Backscattering Spectrometer SPHERES

P. Rottländer<sup>1</sup>, J. Wuttke<sup>1</sup>, W. Bünten<sup>1</sup>, M. Prager<sup>1</sup>, D. Richter<sup>1</sup>

<sup>1</sup>Institut für Festkörperforschung, Forschungszentrum Jülich

At first, we wish to announce that the backscattering spectrometer has been renamed from RSSM to SPHERES (SPectrometer with High Energy RESolution). On a more technical side, in the course of the year 2005, the instrument has made the transition from assembly to the early commissioning phase.

SPHERES is the first instrument of the Jülich Centre for Neutron Science (JCNS) with personnel permanently on site in Garching. In autumn 2004 and spring 2005, Peter Rottländer and Wilhelm Bünten moved to Garching, and

in October 2005, Joachim Wuttke joined our team as instrument responsible.

Early in the year, the instrument chamber finally has been closed and the polyethylene and cadmium shielding has been attached to the inside walls. Paint gave a brighter look to the instrument (Fig. 2.26).

The gap between the primary neutron guide and the instrument-specific convergent neutron guide has been filled with the temporary instrument beam shutter, and the selector. Both components were successfully tested before they were surrounded by shield-

ing. Additional shielding measures were also taken for the convergent neutron guide (Fig. 2.27).

For the phase-space transformation chopper, the good news is that we now have a working device which enables us to proceed with commissioning of the instrument. We had to give up the idea of a magnetic bearing because of still unsolved resonance problems. The control circuit of the bearings produces rather well-defined frequencies which could not be damped away. The conventional bearing, originally thought of as backup solution, proved to be more successful: For a short time, it was possible to operate the wheel at full speed (4800 rpm). After a week or so, however, the bearing began to show signs of wear. With replaced bearings, we therefore decided to operate the wheel at 1600 rpm. At this speed, all timing conditions with respect to the neutron times of flight are fulfilled, thus permitting normal operation of the instrument. The phase-space transformation effect will be halved thus giving an intensity increase by a factor of two instead of four. We still pursue the plan



Figure 2.26: The instrument chamber.

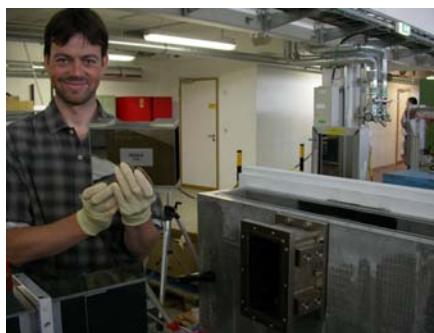


Figure 2.27: The last neutron guide element is inserted.



Figure 2.28: The detectors as mounted in the instrument chamber. On the left there is the chopper vacuum chamber.

of a better performing chopper wheel.

No serious problem was encountered when starting operation of the Doppler monochromator. The vibrations of the Doppler drive were minimal even at the maximum velocity amplitude of 4.7 m/s.

All components being installed, the instrument was optically aligned to about a tenth of a degree with help of a laser beam and mirrors.

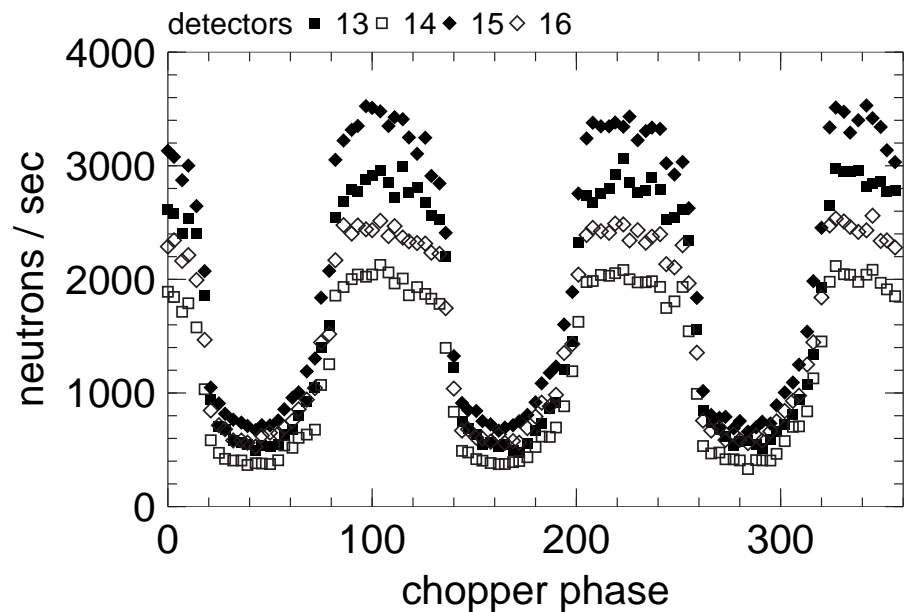


Figure 2.29: Correlation of chopper position and neutron intensity.

Wiring of the instrument and installation of media supply has been partly done and will be completed in 2006, together with the installation of the remaining parts of the safety instrumentation and other components. The detector banks have been installed, and wired (Fig. 2.28). Data acquisition electronics also has been installed and it has been demonstrated that it takes detector counts and angular information of the chopper wheel and the position and velocity of the Doppler monochromator properly.

A gold foil activation analysis has

shown an integral neutron intensity of about  $1 \cdot 10^{10}$  neutrons per second at the end of the convergent neutron guide, just in front of the chopper. The neutrons are spatially homogeneous distributed with a current density of  $1.8 \cdot 10^9$  neutrons per second and  $\text{cm}^2$ . First neutron measurements show opening and closing of the chopper wheel (Fig. 2.29). On the other hand, it was not yet possible to detect the elastic peak of a vanadium sample. The reason is a too high background of neutrons. Reduction of the background will be the foremost problem to solve in 2006.

## 2.13 PANDA – The Cold Three-Axis Spectrometer

P. Link<sup>1</sup>, A. Schneidewind<sup>2</sup>, D. Etzdorf<sup>1</sup>, M. Loewenhaupt<sup>2</sup>

<sup>1</sup>ZWE FRM II, TU München

<sup>2</sup>TU Dresden, Institut für Physik

### Introduction

The last year led us from commissioning of the cold three-axes spectrometer PANDA to first user experiments. Following the start-up of the reactor in May 2005 we completed the magnetic field shielding and did a first spectrometer alignment. We were able to measure the first inelastic signal from a sample

on June 22nd. The succeeding experiments were also used to further improve the instrument. The obtained results showed that PANDA has the expected performance at least for the configurations tested so far.

During cycles 3 and 4 (second half of the year), we run a total number of 12 user experiments delivering 75 days of beamtime (51 days for external users).

In addition, first successful experiments using the 15T cryomagnet were performed.

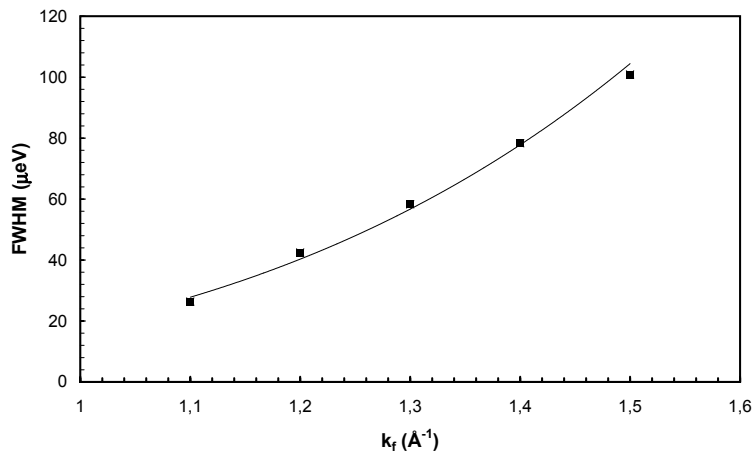


Figure 2.30: Energy resolution obtained from Vanadium scans with flat analyser and monochromator

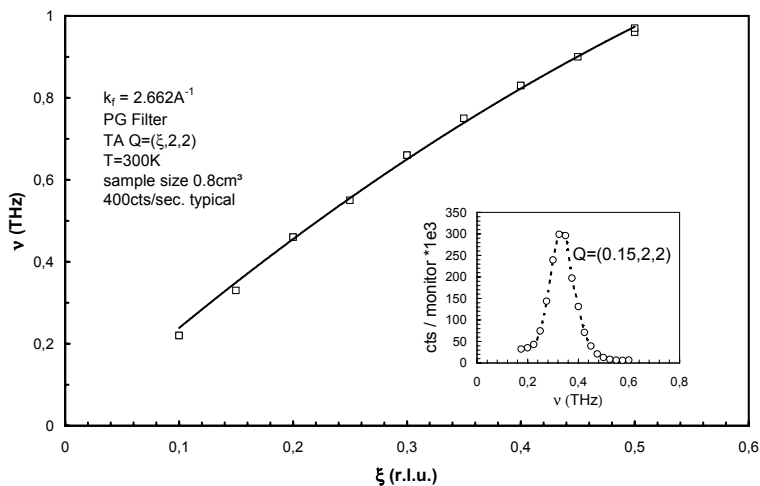


Figure 2.31: test measurement of Pb acoustic phonons.

## Commissioning and first results of the instrument characterisation

PANDA had been designed to match two main aspects of cold TAS performance, a high flux at the sample position and a most flexible set-up concerning resolution and choice of wave vector. Further emphasis has been laid on the usage of the 15T vertical

field magnet as dedicated sample environment. Before inserting the PG002 monochromator we did a Au foil measurement of the white beam flux at the monochromator position. This resulted in a value of  $3.5(5) \cdot 10^9 \text{ n/cm}^2\text{s}$  almost exactly matching the predictions of the MC simulations with MCNP and McStas. From user experiments (as an example of data obtained with PANDA see figure 2.32) we concluded the performance of PANDA being about the same as the up to now leading instru-

ment IN14 at ILL using a comparable instrument set-up. This has been confirmed with Gold foil activation measurements, which yielded a maximum monochromatic flux of about  $5.5 \times 10^7 \text{ n/cm}^2\text{s}$  at the sample position for  $k_i = 2.662 \text{\AA}^{-1}$  with a 6cm PG filter and having the monochromator in the vertically focused mode. Concerning the resolution datasets obtained from a Vanadium standard also fulfil the expectations (see fig. 2.30). Besides the configuration for the small wave vector / high energy resolution mode we also worked at incident wave vectors ranging from  $2 \text{\AA}^{-1}$  to  $3.5 \text{\AA}^{-1}$  to realize medium energy transfers / medium resolution. As a test phonons of a Pb single crystal have been measured in this configuration as shown in figure 2.31.

## Outlook

During the year 2006 the PANDA team will complete the characterisation of the instrument with PG monochromator and analyser and start the installation of the Heusler monochromator and analyser for experiments with polarised neutrons and polarisation analysis. Responding to the high demand of the community for PANDA we want to keep the high level of available beam time for external users under the given conditions.

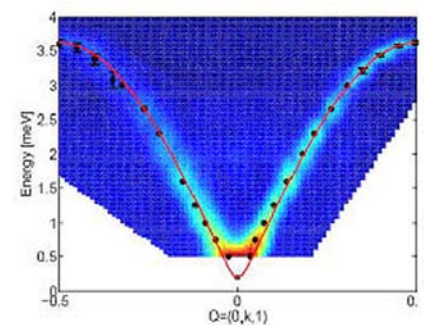


Figure 2.32: Example of inelastic data: spin-wave dispersion of a  $S=1/2$  2D square lattice Heisenberg antiferromagnet (courtesy of M. Kenzelmann and H. Ronnow).

## 2.14 MAFF – Munich Accelerator for Fission Fragments

D. Habs<sup>1,3</sup>, R. Krücken<sup>2,3</sup>, R. Stoepler<sup>3</sup>, M. Groß<sup>1,3</sup>, W. Assmann<sup>1,3</sup>, T. Faestermann<sup>2,3</sup>, R. Großmann<sup>1,3</sup>, Ph. Jüttner<sup>4</sup>, H.-J. Maier<sup>1,3</sup>, P. Maier-Komor<sup>2,3</sup>, F. Nebel<sup>2,3</sup>, M. Schumann<sup>1,3</sup>, J. Szerypo<sup>1,3</sup>, P. G. Thirolf<sup>1,3</sup>, E.-L. Tralmer<sup>4</sup>, E. Zech<sup>2,3</sup>

<sup>1</sup>Dept. f. Physik der LMU München

<sup>2</sup>Physik-Department E12, TU München

<sup>3</sup>Maier-Leibnitz-Laboratorium f. Kern- u. Teilchenphysik

<sup>4</sup>ZWE FRM II, TU München

MAFF, the Munich Accelerator for Fission Fragments, is a reactor based RIB facility, planned to be set up at the FRM II by the group for experimental nuclear physics (Prof. Habs) of the LMU and the TUM physics department E12 (Prof. Krücken).

MAFF aims at providing very intense beams of neutron-rich isotopes to a broad range of nuclear physics experiments as well as applied physics and nuclear medicine [1, 2, 3]. In a first step (MAFF First Beam) the beam will have an energy of 30 keV (low-energy beam), and only  $10^{-3}$  of the final beam intensity will be available in order to start the experiment with a minimum of investment costs. In a second step the full beam intensity corresponding to  $10^{14}$  fissions/s will be made available (MAFF-I) before also the high-energy beamline will be set up, where the ions are post-accelerated to energies adjustable in the range 3.7–5.9 MeV/u.

### Project management and system engineering

Since June 2005 our team is strengthened by a project manager with experience from industry. In the second half of 2005 we solicited quotations for the basic engineering of the main components of MAFF. Several companies submitted a quote and the orders were placed in October. The results shall be delivered until March 2006, providing the basis of the specifications required for the authorisation procedure that will be opened subsequently.

### Trolley Tests

Lens and source trolley are the heart of the MAFF I physics program enabling the production and extraction of rare isotopes. Both trolleys are similar in de-

sign, especially when it comes to the trolley bodies and the traction system. This system is used regularly at the source side and leaves little to no tolerance to failure. Therefore the traction system of the trolley and everything related, like the adjustment system for the trolley and the lock for securing the trolley in its final position as well as the supporting structure have been designed and constructed over the past years and are currently tested. It is planned to use the majority of the constructed parts, in case of successful tests, later on for the MAFF project. To avoid concerns from the TÜV, intricate material tracing has been performed for all crucial components.

Among the tests carried out are:

- Mechanical integrity
- Traction system performance
- Adjustment possibilities
- Comparison of different traction concepts
- Comparison of different lubricants

- Failure simulations

Still in progress are tests concerning:

- Long term tests
- Electrical contacting
- Failure simulations

The performed tests have shown the feasibility of the concept and have been valuable to gain deeper insight on possible failures and their respective probabilities. Design enhancements based on the gained operating experience could be made. Upcoming test will be devoted to long term tests, investigation of the electrical contacting concept and enhanced failure simulations.

### Neutron-flux measurement

A neutron-flux measurement in the neutron guide tunnel was carried out during the 4th power-cycle, to gain better knowledge about the neutron distribution in the neutron guide tunnel during reactor operation. This information is important for MAFF to estimate

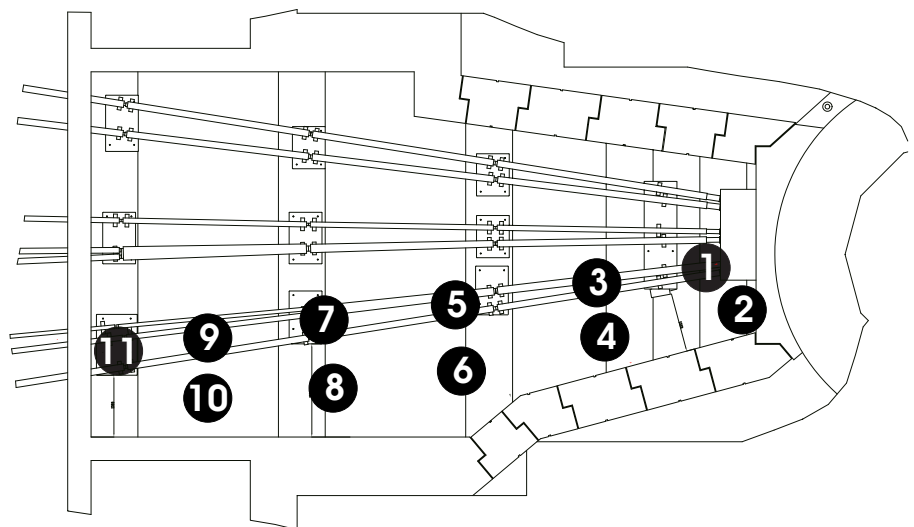


Figure 2.33: Positions of Co and Au samples for determination of the neutron-flux in the neutron guide tunnel.

the amount of neutron induced  $\gamma$ -activation to metal components. The decision if and where stainless steel or aluminium can respectively must be used will be strongly influenced by the outcome of this measurement.

The integral neutron-flux over the whole reactor cycle was determined by placing  $^{59}\text{Co}$  (0,1 g to 1 g) samples on top of neutron guide 1 (NL1) and on the floor in alignment with the beam tube 6 (SR6) as shown in Fig. 2.33.

In addition to the Co samples gold foils ( $\approx 200 \mu\text{g}$ ) have been placed in the same locations, to determine the flux during the last days of the power cycle.

After the end of the reactor cycle the samples have been removed and the neutron-flux at the sample positions has been determined by measuring the  $\gamma$ -activity of the samples.

Preliminary results indicate an average neutron-flux of  $1 \cdot 10^5$  to  $5 \cdot 10^6 \text{ n cm}^{-2} \text{ s}^{-1}$  and hint towards a maximum neutron-flux of  $2 \cdot 10^5$  to  $5 \cdot 10^7 \text{ n cm}^{-2} \text{ s}^{-1}$ .

The neutron-flux is highest next to the reactor shielding and drops towards the end of the neutron guide tunnel, by one to two orders of magnitude.

From the results can be seen that the extensive use of stainless steel in the

neutron guide tunnel especially close to the reactor wall must be objected. A substantiated calculation of the neutron induced  $\gamma$ -activity of MAFF components can now be performed.

- [1] Habs, D., *et al.* MAFF – Physics Case and Technical Description.
- [2] Habs, D., *et al.* *NIM B*, 204, (2003), 739–745.
- [3] Faestermann, T., *et al.* *Nucl. Phys. A*, 746, (2004), 22c–26c.

## 2.15 N-REX<sup>+</sup> – The Materials Science Neutron/X-Ray Reflectometer

A. Rühm<sup>1</sup>, U. Wildgruber<sup>1</sup>, M. M. Nülle<sup>1</sup>, F. Maye<sup>1</sup>, J. Franke<sup>1</sup>, J. Major<sup>1</sup>, H. Dosch<sup>1</sup>

<sup>1</sup>Max-Planck-Institut für Metallforschung, Stuttgart

During the year 2005 the commissioning of the neutron reflectometer with add-on X-ray option, N-REX<sup>+</sup>, (Figure 2.34) has been started and is expected to be finished in the second half of 2006. The instrument has reached a state in which the basic operation mode of unpolarized neutron reflectivity measurement on solid samples is available for first in-house test experiments. N-REX<sup>+</sup> was officially inaugurated on November 24th, 2005.

Figure 2.35 shows a first set of neutron reflectivity data obtained on a 500 Å dPS (deuterated polystyrene) film

on silicon substrate. These measurements are part of a project aimed at proving the suitability and new potential of the SERGIS (spin-echo resolved grazing incidence scattering) technique

for the investigation of dewetting processes in polymer films. Understanding and controlling the dewetting process of polymer films is important as the polymer-island morphology gener-



Figure 2.34: The neutron/X-ray reflectometer N-REX<sup>+</sup> in its present state. The open structure between monochromator, sample and detector allows adoption of extended beam conditioning equipment, e.g. a SERGIS set-up.

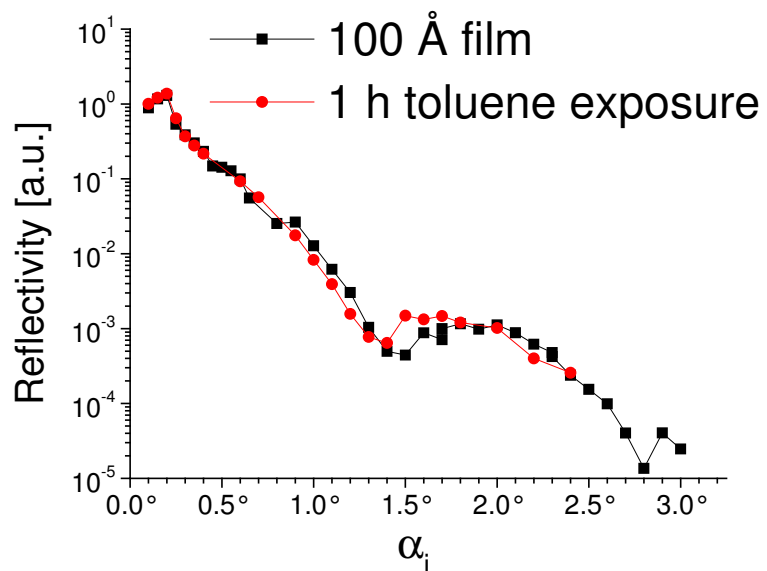


Figure 2.35: Reflectivity curve obtained from 2D detector images on a dPS film on Si substrate. The accessible dynamic range for reflectivity measurements is currently  $10^{-5}$ . This must be improved by one order of magnitude in 2006. A major improvement should be achievable by an enhancement of the current neutron flux of  $2 \cdot 10^4 \text{ neutrons/cm}^2\text{s}$  to the expected optimum value of  $3 \cdot 10^6 \text{ neutrons/cm}^2\text{s}$  (according to the measured white beam characteristics and MCSTAS simulations).

ated in the dewetting process can be exploited to grow nanostructures on surfaces. In the present case, the dewetting process is most easily initiated by exposing the samples to toluene atmosphere [1, 2]. The sample chamber used for this purpose at N-REX<sup>+</sup> is shown in Figure 2.36. It allows to expose the samples to the vapor of the polymer solvent in a computer controlled way, thus enabling in-situ reflectivity measurements during the dewetting process. The chamber exhibits two aluminum and two kapton windows, which will later also enable simultaneous neutron/X-ray experiments. The first two neutron reflectivity curves displayed in Figure 2.35 show the effect of swelling of the

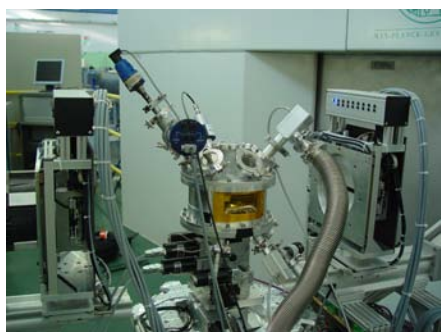


Figure 2.36: Vacuum/vapor sample chamber for simultaneous neutron/X-ray characterization. The chamber comprises two aluminum and two kapton windows at a 90° angle.



Figure 2.37: The compact-source unit of the add-on X-ray reflectometer (EFG, Berlin). This machine can deliver Cu-K $\alpha$  radiation of variable divergence. The beam is rotated around the sample by means of two vertical translation stages. Therefore neutron and X-ray characterization can be performed simultaneously without mutual interference.

Table 2.6: The basic N-REX<sup>+</sup> instrument parameters (for liquid/horizontal sample mode, HOPG monochromator, 20 MW reactor power)

wavelength range	2-6 Å
max. incidence angle	5°
max. exit angle	20°
max. out-of-plane q (specular)	0.55 Å <sup>-1</sup>
max. q (within the reflection plane)	1.35 Å <sup>-1</sup>
max. in-plane q (grazing angle diffraction)	>5.4 Å <sup>-1</sup>
total flux at monochromator	4 · 10 <sup>9</sup> neutrons/cm <sup>2</sup> s
maximum flux at monochromator	4 · 10 <sup>8</sup> neutrons/cm <sup>2</sup> sÅ (at 4 Å)
monochromatic flux for reflectometry at sample	3 · 10 <sup>6</sup> neutrons/cm <sup>2</sup> s (estimated)

polymer film as a consequence of solvent incorporation into the film. After exposure to toluene atmosphere for 1 hour, the first minimum in the reflectivity curve has shifted to smaller grazing incidence angles  $\alpha_i$ , indicating an increase of the film thickness. These measurements shall be amended by GISANS (grazing incidence small angle neutron scattering) and especially SERGIS experiments at a later stage of the commissioning of N-REX<sup>+</sup> to unravel the lateral morphology of dewetted polymer films.

Figure 2.37 shows the compact X-ray source unit of the add-on X-ray reflectometer at N-REX<sup>+</sup>. This unit integrates a Cu-K $\alpha$  sealed tube X-ray source, a focussing mirror optics, a germanium (220) channel-cut monochromator, a slit unit to define the beam size, as well as two vertical translation stages to adjust the incidence angle of the X-ray beam onto the sample surface. A very similar detector unit, which can adopt a scintillation counter or a CCD camera, is already in the manufacturing process. The X-ray reflectometer will thus be completed and available for experiments in summer 2006. Polarization equipment will become available at about the same time. This includes two polarizing mirrors, a bender in combination with a collimator, and a <sup>3</sup>He cell. In combination with spin-echo setup from the EVA reflectometer (Institut Laue Langevin, Grenoble), SERGIS experiments (spin-echo resolved grazing incidence scattering) will then be possible at N-REX<sup>+</sup> [3, 4]. Current

tasks to be completed are: complete installation of all 33 HOPG (highly oriented pyrolytic graphite) monochromator crystals (at present only 7 are installed), flux and background optimization, improvement of the control software, improvement of the preliminary radiation shielding, installation of radiation safety electronics, completion of the motor, encoder, and detector installations. For quantitative instrument parameters of the N-REX<sup>+</sup> reflectometer see the Table 2.6

- [1] Müller-Buschbaum, P., Gutmann, J. S., Stamm, M., Cubitt, R., Cunis, S., von Krosigk, G., Gehrke, R., Petry, W. *Physica B*, 283, (2000), 53–59.
- [2] Müller-Buschbaum, P., Bauer, E., Wunnicke, O., Stamm, M. *J. Phys.: Condens. Matter*, 17, (2005), S363–S386.
- [3] Felcher, G. P., te Velthuis, S. G. E., Major, J., Dosch, H., Anderson, C., Habicht, K., Keller, T. In Anderson, I. S., Guérard, B., editors, *Advances in Neutron Scattering Instrumentation, Proceedings of SPIE*, 164–174 (SPIE Optical Engineering Press, Bellingham, WA, USA, 2002).
- [4] Major, J., Dosch, H., Felcher, G. P., Habicht, K., Keller, T., te Velthuis, S. G. E., Vorobiev, A., Wahl, M. *Physica B*, 336, (2003), 8–15.

## 2.16 PUMA – the thermal triple axis spectrometer

K. Hradil<sup>2</sup>, H. Schneider<sup>2</sup>, J. Neuhaus<sup>1</sup>, G. Eckold<sup>2</sup>

<sup>1</sup>ZWE FRM-II, TU München

<sup>2</sup>Inst. f. Physikal. Chemie, Universität Göttingen

During the year 2005 the three axes spectrometer PUMA started its commissioning phase and performed first 'friendly user' experiments. Problems due to the inefficient primary shielding could be solved by mounting additional shielding elements made from PE in combination with B<sub>4</sub>C in vulcanized rubber. The flux of unwanted epithermal neutrons outside the monochromator drum could be reduced by a factor of 250. The first measurements for characterisation revealed that the performance of the instrument corresponds (extremely) well to the predictions from simulations.

Figure 2.38 shows the instrument in its current status with the mounted additional shielding around the monochromator drum. The shielding consists of 26 individual elements that remove efficiently radiation leaks as well as unwanted background. Whereas the range of the monochromator is not affected by the additional shielding, the sample scattering angle range is now limited to a maximum of 120 degrees. Moreover, additional shielding elements around the sample as well as at the entrance of the analyser system helped a lot to further reduce the background counting rate. An efficient shielding of the experimental area made from a composite structure (iron, PE, B<sub>4</sub>C in vulcanized rubber, lead) allows for a sufficient radioprotection of the surrounding accessible area. Due to the high flux in the focussing mode of the instrument, the beamstop for the direct beam could not be mounted directly at the sample table. Rather it was placed on a separate unit on air pads that can be automatically positioned according to any particular combination of monochromator and scattering angles. The beamstop is made as a sandwich of 3mm LiF, 30cm boron enriched PE and 10 cm lead. Additionally, 5 cm thick lead plates surround the PE part. Test measurements in different instrument configurations have demon-

strated the efficiency of this design. The positioning of the beamstop as an additional axis is implemented within the control software in order to assure the radiation protection requirements.

For the first experiments the PG(002) monochromator bending device build in cooperation with the FRM II and optimised in the workshop of the University Göttingen was available. Figure 2.39 shows the device within the exchange unit in the monochromator drum. The mechanical tests yielded an excellent accuracy and reproducibility of the horizontal and vertical bending.

For optical tests a conventional divergent halogen lamp was used. Reflection of light from the PG(002) crystals reveal an excellent performance of both vertical and the horizontal focussing. After mounting the device within the primary shielding and the adjustment with neutrons, the beam profiles were measured with a CCD camera. Figure 2.40 represents the comparison of the CCD

camera pictures with the McStas simulations which are in very good agreement.

First and preliminary flux measurements have been performed at sample position with horizontal and vertical entrance slits of 10 mm and 130 mm, respectively, using a calibrated monitor along with gold foils. Both methods yielded a flux of  $2.4 \cdot 10^8$  n cm<sup>-2</sup>s<sup>-1</sup> for 1.8 Å neutrons in good agreement with McStas simulations.

During the adjustment of the instrument with neutrons a vanadium sample was used to measure the energy resolution for different incident energies for the PG(002) monochromator (figure 2.41). As expected the results for dE/E are in the range between 2 to 4%.

After only 1 1/2 cycle, all absolute encoders within the monochromator shielding were not working any longer due to radiation damage. Consequently, a new concept for the readout of the positions for the respective



Figure 2.38: View on the triple axes spectrometer PUMA within the experimental hall of FRM-II.

axes was required and implemented within short time in order to continue the user operation. The subsequent re-adjustment and tests of the encoding systems revealed that the required positioning accuracy of  $0.005^\circ$  was maintained.

Despite all the problems during commissioning phase of the instrument, not only first characterisation measurements and inelastic test experiments on phonons from a quartz crystal (not shown here), but also approximately 40 days of cycle 2 and 3 have been assigned to external friendly users. The scientific results obtained and the amount of proposed scientifically high quality experi-

ments not only from new external users proved the excellent performance of the instrument. Detailed information on results of these experiments can be found within the experimental reports.



Figure 2.39: PG(002) monochromator within the change unit in the primary shielding.

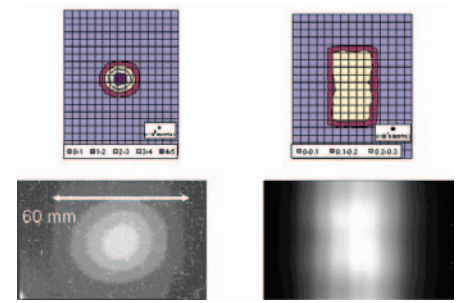


Figure 2.40: Comparison of the beam profile for the PG(002) monochromator for the horizontal/vertical focussed device (left) and the collimator configuration (right) with McStas simulations.

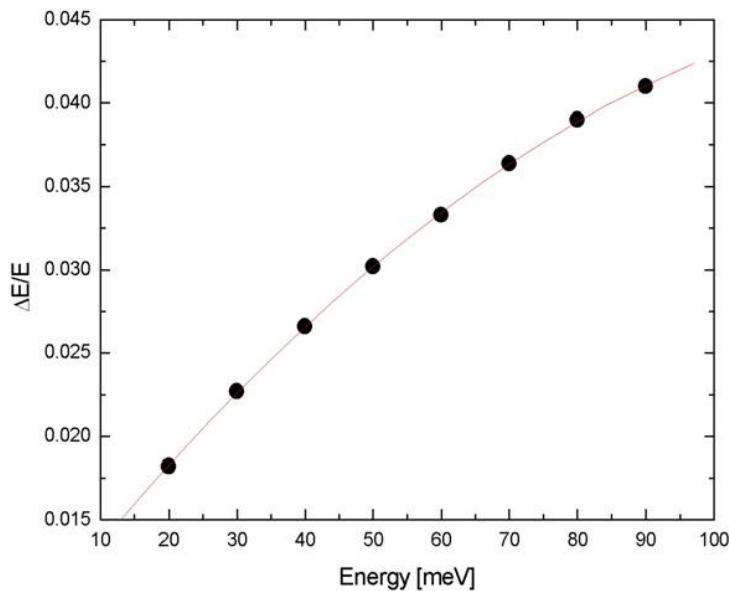


Figure 2.41: Energy resolution curve of the PG(002) monochromator for the double focussing mode.

## 2.17 NECTAR - Neutron Computer Radiography and Tomography facility

T. Bücherl<sup>1</sup>, M. Mühlbauer<sup>1</sup>, Ch. Lierse von Gostomski<sup>1</sup>

<sup>1</sup>Institut für Radiochemie, TU München

### General

The NECTAR facility is set up at the converter facility in the experimental hall (beam tube SR 10). It is using fission

neutrons for radiography and tomography measurements. The available beam time has to be shared with the facility for medical applications (MEDAPP), also located at SR 10.

### Activities

Begin of 2005, the complete hardware of NECTAR, i.e. the manipulator for the samples, the manipulator for the





Figure 2.42: Photograph of the NECTAR facility. Left: Manipulator for the samples. Right: Detector system based on a liquid nitrogen cooled CCD camera.

detector systems and the new constructed beam stop, was set up again after the installation of the overhead travelling crane, including a precise adjustment of all components. The control cabin housing detector electronics and working place was positioned on the back wall of the bunker, the control unit for the manipulator system close to it.

Due to problems in the control electronics of the shutters and filters of the converter facility, no measurement time was available for several months in 2005. But some measurements for the determination of system parameters, for the optimization of the radiography mode and of first users could be performed.

At the end of the year the set up of the second detector system based on 4 single beam detectors was started. It will be mainly used for tomography.

## System Parameters

One important parameter of a radiography system is the  $L/D$  value, where  $L$  is the distance between collimator and sample position and  $D$  the diameter of the circular collimator outlet window. It is a measure of the available resolution. It was determined experimentally by using an iron cylinder (diameter 5 cm, height 2.56 cm) fixed at the sample manipulator and varying the distance between the cylinder and the detector system. A first estimation resulted in  $L/D = 233 \pm 16$ . The relatively large standard deviation may be caused by the contribution of scattered neutrons in the cylindrical object. This has to be

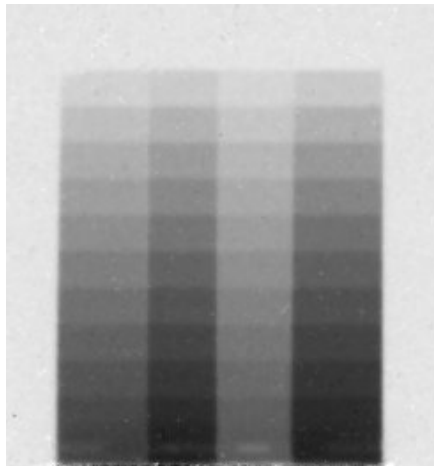


Figure 2.43: Normalized radiograph of a step wedge made of lead, iron, aluminium and polyethylene (from left to right). The depth of the each step increases by 5 mm, i.e. the maximum depth is 50 mm.

investigated in more detail in the next reactor periods.

The fission neutron flux available at the measuring position was estimated by taking into account the modified permanent filter and the collimator with  $L/D=118$  to about  $4.9 \cdot 10^6 \text{ cm}^{-2} \text{ s}^{-1}$ .

## Radiography Mode

The actual challenge in optimization the radiography (and tomography) mode is the improvement of the detection efficiency of the fission neutrons. Due to the low cross sections of scintillator and converter materials and their limited applicable thicknesses only a small fraction of the incoming fission neutrons contribute to the signal in the detector. Furthermore, when using scintillators moderated neutrons (e.g. when passing the sample) may superimpose this signal resulting in distorted and often useless radiographs.

First investigations of different scintillators and converters for the optimized conversion of incoming fission neutrons in visible light while being highly insensitive for neutrons with lower energies have been performed. Actually a pp-converter gives the best results, but further improvement might be possible.

## Applications

For industrial purposes studies on the applicability of neutron radiography on large gear boxes (side lengths up to 40 cm), motors (diameter larger than 12 cm) and on large turbine blades (ca. 20 cm in height and up to 12 cm in depth) have been performed, especially the latter very successfully.

The NECTAR facility was also used by an external client for the testing of electronic components on fast neutron sensitivity.

## Outlook

With the availability of fission neutrons the measurements of the system parameters will continue with higher precision as well as the optimization of the radiography mode, specially the improvement of detection efficiency. The main focus in 2006 will be the installation of the tomography mode for routine application.

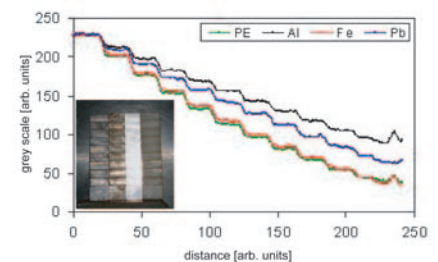


Figure 2.44: Intensity plot of the individual materials of the step wedge (small photograph) derived from the normalized radiograph.



Figure 2.45: Left: Photograph of a motor.  
Right: Normalized fission neutron radiograph of the motor.

## 2.18 The new small-angle scattering instrument SANS-1 at the FRM II

R. Gilles<sup>1</sup>, B. Krimmer<sup>1</sup>, A. Ostermann<sup>1</sup>, C. Schanzer<sup>2</sup>, O. Nette<sup>3</sup>, A. Vogel<sup>3</sup>, R. Kampmann<sup>3</sup>, A. Schreyer<sup>3</sup>, W. Petry<sup>1</sup>

<sup>1</sup>ZWE FRM II, TU München

<sup>2</sup>Paul Scherrer Institut, Villigen, Switzerland

<sup>3</sup>GKSS Forschungszentrum, Geesthacht

The new small-angle scattering instrument SANS-1, a project of the Technische Universität München and the GKSS in Geesthacht is currently build at the new Foschungs-Neutronenquelle Heinz Maier-Leibnitz (FRM II)[1, 2, 3]. This contribution describes the concept and the technical features of the instrument. The first task was to implement the instrument in the park of other instruments in the neutron guide hall of FRM II. Monte Carlo simulations with the program McStas were performed to optimize the neutron guide system and the positioning of the instrument according the available space. The design of the instrument allows it to include additional components in the future in a flexible way.

Parameters of the new SANS-1 instrument (Fig. 2.46):

- cross section of neutron guide 50 x 50 mm<sup>2</sup> - vertically S-shaped neutron guide, R = 480 m (second part of S-shaped neutron guide is curved in horizontal with R = 2100 m) - supermirrors with m = 1.2 - 2.0 - collimation length of 20 m: a) neutron guide, b) slit system, c) polarisation option, d) focusing elements e) chopper option for future ap-

plications - maximum sample to detector distance 20 m, - detector area 1 x 1 m<sup>2</sup>, lateral movement 0.5 m - Q-range: Qmin < 10<sup>-2</sup> nm<sup>-1</sup>, Qmax 16 nm<sup>-1</sup>

A comparison of different neutron guide systems (single curved and S-shaped types) shows a few advantages

for S-shaped neutron guides if similar flux at the sample position is compared (see fig. 2.47). The latter neutron guide provides a sharp wavelength cut off at  $\lambda < 3 \text{ \AA}$  for a collimation part with neutron guide and apertures as well. Single curved neutron guides forward these

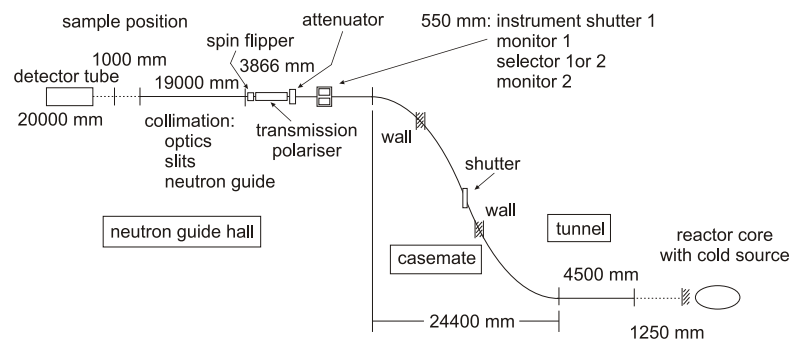


Figure 2.46: Schematic drawing of the new SANS-1 instrument

useless neutrons below 3 Å to the selector position which results in a higher background. Fig. 2.48 and fig. 2.49 show the intensity and divergence distribution for the two types of neutron guides. The difference in the intensity distribution is small with slightly higher intensity (5%) at the sample position for the S-shaped neutron guide. The asymmetry in the intensity distribution after the collimation section (Fig. 2.48) due to the curvature is very similar for both guide systems. A more pronounced difference is visible in the divergence profiles. The standard single curved guide shows a clear asymmetry between the horizontal and vertical divergence in comparison to the S-shaped neutron guide.

Another advantageous consequence of the vertical S-shaped neutron guide is an increase of the height of the neutron beam centre to 1.5 m, which allows a higher degree of freedom for different sample environments. Last but not least only the vertical S-shaped guide allows an adequate positioning of the instrument in the neutron guide hall.

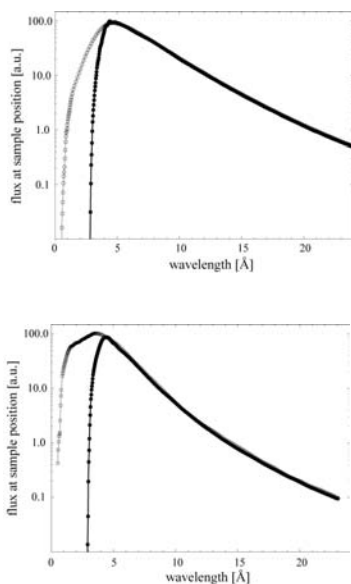


Figure 2.47: Comparison of intensity versus wavelength between a single curved (open circles) and an S-shaped (closed circles) neutron guide. Top: The collimation part (19m) contains a neutron guide of Ni58. Bottom: The collimation part contains 50 x 50 mm<sup>2</sup> apertures.

The set up of the S-shaped neutron guide (Fig. 2.50) was the main task of this year and was done by the neutron optic group (Prof. G. Borchert, C. Breunig, E. Kahle) and H. Tuerck as well as by the company GHS. At the same time the construction and building of the selector tower and the instrument shutter was done by the construction group of F. Tralmer and the workshop of the TU Munich.

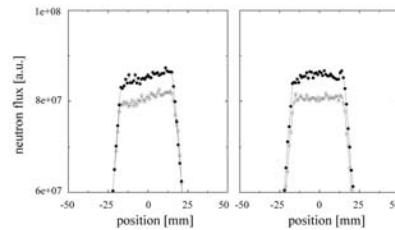


Figure 2.48: Intensity distribution at the end of the collimation system with guide (19 m) of a horizontal single curved neutron guide (open circles) and of a vertical S-shaped neutron guide (closed circles). Left: Sum along the horizontal direction for the S-shaped guide and the vertical direction for the single curved guide. Right: Sum along the vertical direction for the S-shaped guide and along the horizontal direction for the single curved guide. A wavelength of 4.7 Å was used in the simulation.

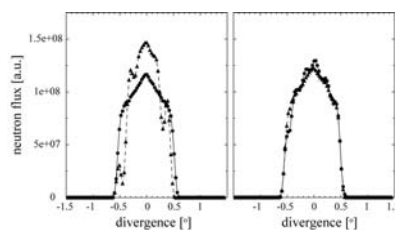


Figure 2.49: Divergence distribution at the end of the collimation system with guide 19 m of a horizontal single curved neutron guide (left) and of a vertical S-shaped neutron guide (right) for the horizontal divergence (triangles, dashed line) and the vertical divergence (circles, solid line). A wavelength of 4.7 Å was used in the simulation.



Figure 2.50: End position of the S-shaped neutron guide NL 4a for the SANS-1 instrument.

Recently a co-operation with GKSS (the group of Prof. A. Schreyer) has started. GKSS takes over the construction and building of the collimation system. The collimation system consists of four tracks for optic elements and a polariser at the beginning. A chopper system is foreseen in the collimation part as an option for future.

- [1] Gilles, R., Schanzer, C., Petry, W., Eckold, G. In *Proceedings of German Neutron Scattering Conference* (Dresden, 2004).
- [2] Gilles, R., Schanzer, C., Petry, W., Eckold, G. In *Proceedings of CANSAS-IV Meeting* (RAL: Chilton, Didcot, Oxfordshire, England, 2004).
- [3] Gilles, R., Ostermann, A., Schanzer, C., Krimmer, B., Petry, W. *Physica B*. In print.

## 2.19 Multiple radiation measurements at the radiography facility ANTARES

Burkhard Schillinger<sup>1,2</sup>, Elbio Calzada<sup>1,2</sup>, Martin Mühlbauer<sup>2</sup>, Michael Schulz<sup>2</sup>

<sup>1</sup>ZWE FRM II, TU München

<sup>2</sup>TU München, Physics Department, E21

<sup>3</sup>Institut Laue-Langevin, Grenoble, France

Although the neutron radiography and tomography facility ANTARES is designed for measurements with thermal and cold neutrons, the use of additional filters and an X-ray tube allows for measurements with epithermal neutrons, with 300 kV X-rays and with gamma.

### Thermal and cold neutrons

ANTARES (Fig. 2.51) is situated at the beam line SR4b, facing the cold source of the reactor. A vertical secondary shutter contains two steel collimators of 1m length and roughly 20 mm and 40 mm diameter to optimize between high resolution and high flux (Fig. 2.52).

Fig. 2.53 shows a neutron radiography of a pressure reducer. Thermal and cold neutrons are ideally suited to penetrate thick layers of Aluminium and to show organic compounds like sealants, O-rings and adhesives. Fig. 2.54 shows a neutron radiography of an oil-filled pump. The oil layer is practically im-

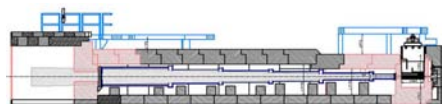


Figure 2.51: Vertical cross section of the ANTARES facility.

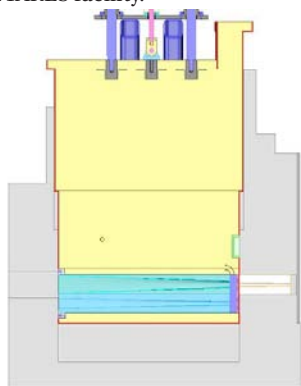


Figure 2.52: Vertical cross section of secondary shutter.

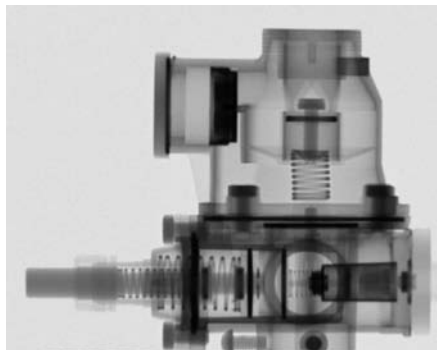


Figure 2.53: Thermal/cold neutron radiography of a pressure reducer.



Figure 2.54: Thermal/cold neutron radiography of an oil-filled pump.

penetrable for cold neutrons, and also the steel parts show a lot of attenuation. On the top left, a plastic plug is visible in a valve.

### Epithermal neutrons

After the secondary shutter, a filter wheel with different pinhole diaphragms is installed. One of the positions is equipped with a 2mm Cadmium sheet (Fig. 2.54), which will absorb all neutrons with energies below 0.4 eV. The scintillation screen employed in the detection system is sufficiently sensitive for epithermal neutrons as well, although the measuring time increases by

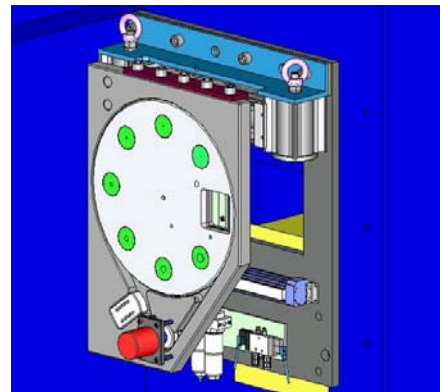


Figure 2.55: The selector wheel with the Cadmium filter.

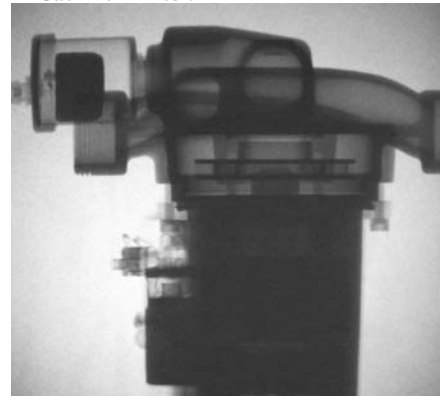


Figure 2.56: Epithermal neutron radiography of the pump.

a factor of ten. In Fig. 2.55, the steel parts show better penetration, and some outlines are visible through the oil.

### Gamma radiation

Between the secondary shutter and the filter wheel, a pneumatic fast shutter (Fig. 2.57) is installed to shut off the thermal and cold flux during short breaks such as repositioning or rotating of the sample or data readout times in order to keep the sample activation as low as possible. It consists of a container filled with boron carbide. The shutter will absorb all cold and

thermal and a wide range of epithermal neutrons, but can be easily penetrated by fast neutrons and gamma radiation originating from the reactor core and from the neutron absorption in the beam tube nozzle. The prompt gamma radiation from neutron capture in Aluminium has a very high energy up to 8 MeV. If the neutron scintillation screen is replaced by a standard medical X-ray scintillation screen made of Gadolinium oxysulfide, we can obtain gamma radiographies with a very high penetration also for steel (Fig. 2.58). The efficiency of the screen drops towards high energies, due to the exposure time is in the order of minutes. Fig. 2.58 shows high penetration even for the steel body of the pump, the plastic body in the valve is faintly outlined, probably due to some remaining sensitivity for fast neutrons, the oil filling is virtually invisible. Some fingerprints on the scintillation screen were removed only after the measurement.

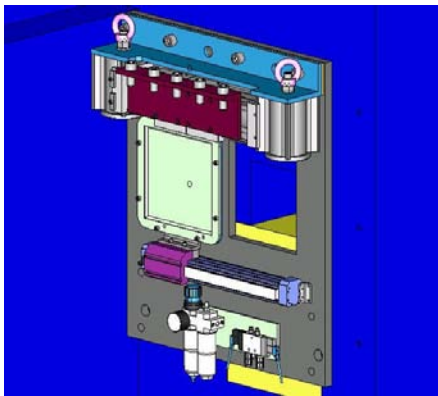


Figure 2.57: The Boron Carbide fast shutter.

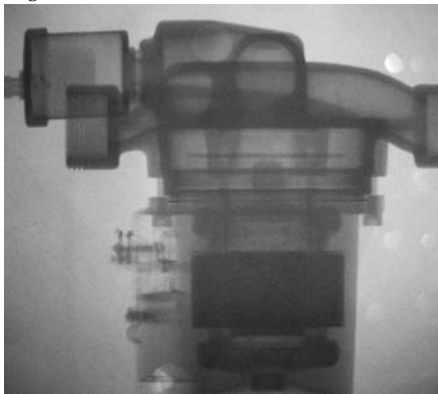


Figure 2.58: Gamma radiography of the pump.

## X-ray tube

For standard measurements, a removable 320kV X-ray tube (fig. 2.59) has been mounted on a sliding system between the filter wheel and the flight tube.

With the X-ray scintillation screen mentioned above, high-quality X-ray images can be obtained in about 30 seconds measuring time. Fig. 2.60 shows a ski boot as an example. The positioning of the tube in the beam path in 12m distance wastes a lot of X-ray intensity, but assures exactly the same quasi-parallel beam geometry as for neutrons. Images recorded that way can be superposed to neutron images without the need for any adjustment or registering. Fig. 2.61, 2.62 and 2.63 show a photo, a neutron and X-ray radiography of a printed circuit board, Fig. 2.64 shows the X-ray image subtracted from the neutron image.

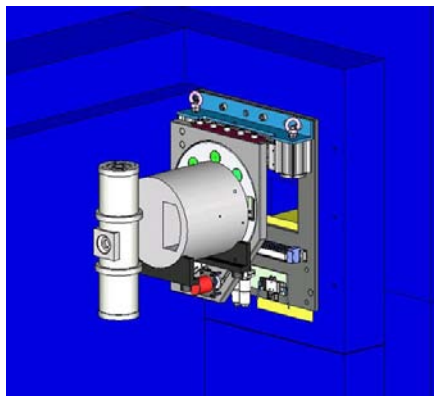


Figure 2.59: The X-ray tube in the beam path.



Figure 2.60: X-ray radiography of a ski boot.

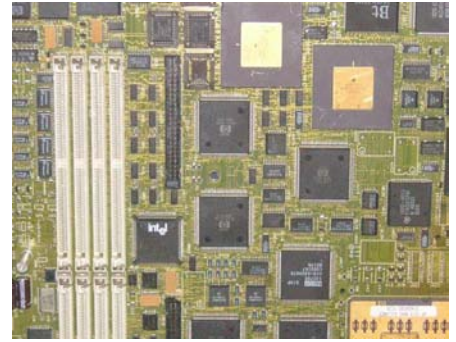


Figure 2.61: Photo of a computer board.

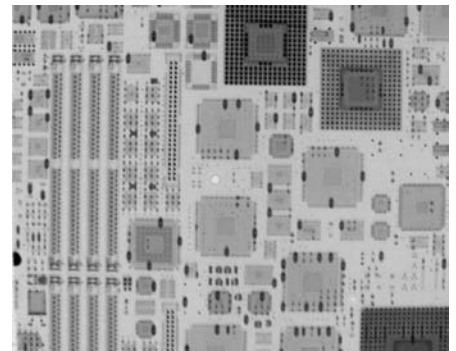


Figure 2.62: X-ray radiography.

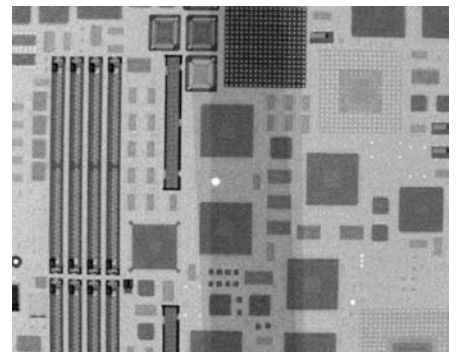


Figure 2.63: Neutron radiography.

## Conclusion

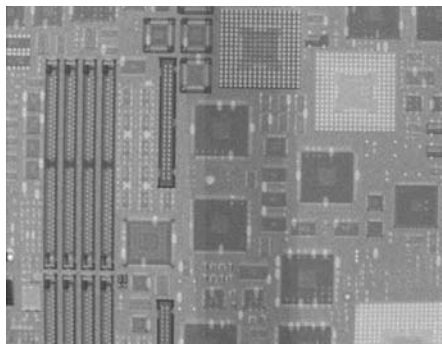


Figure 2.64: The X-ray image subtracted from the neutron image.

ANTARES offers a multitude of possibilities for measurement with different radiations, which can be selected according to the problem at hand. While the instrument is of course optimized for thermal and cold neutrons, a lot of additional information can be obtained with different radiations. All images are perfectly congruent and can be superposed without further adjustment.

## 2.20 The Fission Neutron Source (Converter facility)

F.M. Wagner<sup>1</sup>, A. Kastenmüller<sup>1</sup>, B. Loeper<sup>1</sup>, S. Kampfer<sup>1</sup>, W. Waschkowski<sup>1</sup>

<sup>1</sup>ZWE FRM-II, TU München

During the whole year 2005, the irradiation facility at beam tube SR10 was optimized with respect to the modelling of the beam and the functional safety of shutters, collimator, and other components. The beam filters and the 40-leaf collimator have been completed, documented as parts of a medical product, and successfully tested.

The facility was examined according to the Medical Devices Act, MPG, with respect to the functional, mechanical, and electrical safety and other criteria with external experts in order to furnish it with the CE safety mark. The expected successful completion of this procedure in early 2006 will allow to apply formally for a license for medical use in radiation cancer therapy.

The development of a new filter combination for therapy, and the evaluation of the beam quality by extensive MCNP calculations with the as-built data have been accomplished. By use of dose measurements in an automatic

water phantom, a data set for the irradiation of patients has been worked out. Complementary measurements of some special features of the treatment beam, i.e., the spectral flux distribution, have been prepared.

Figure 2.65 shows the medical irradiation room with the collimator exit and the treatment couch. In comparison with the former therapy facility at FRM, the advantages of the new facility are

- a large cross section of the beam up to 20x30 cm,
- a higher dose rate,
- easier patient positioning due to the height of the beam and the larger irradiation room
- a second irradiation room for the radiography and tomography facilities (see NECTAR).

External clients have used the beam for the systematic testing of the radiation sensitivity of electronic components.



Figure 2.65: The medical irradiation room with the collimator exit and the treatment couch.

## 2.21 First Spin Echo Signal at RESEDA

W. Häußler<sup>1</sup>, D. Streibl<sup>1</sup>, R. Schwikowski<sup>1</sup>, H. Wagensohn<sup>1</sup>, P. Böni<sup>2</sup>

<sup>1</sup>ZWE FRM-II, TU München

<sup>2</sup>TU-München Physik Department E21

Despite meager manpower (1 scientist, half-time technician) when compared with such a demanding instrument, we succeeded to produce the first spin echo signal at the quasielastic Neutron Resonance Spin Echo spectrometer RESEDA in November 2005.

Commissioning of RESEDA was delayed until then, because of high radiation background. Neutron guide and selector housing are shared with the instrument NOSPEC which is not yet built, in contrast to previous plans. We therefore had to build an additional shielding, in order to remove an opening in the selector shielding, which had been foreseen for NOSPEC. We constructed the shutters for both instruments which are made out of boron containing absorber plates and added also a new concrete shielding. In addition to this unforeseen work, we finally improved the radiation shielding of the polarizing part of the neutron guide NL 5b (total length 65 m, polarizing part 40 m, bending radius 1640 m), to the total thickness of 14.5 cm, in order to reduce the gamma background level sufficiently. In the meantime, a gamma shutter, a beam monitor, and three movable attenuators have been constructed and fixed at the end of the neutron guide in front of the spectrometer. High radiation background produced in the first spectrometer arm, however, prevents until now measurements with the full beam.

By using the first neutrons being available at the instrument in August 2005, the primary spectrometer arm of RESEDA was aligned with respect to the straight neutron beam, and adjusted to its vertical position. The 3He-detector was put into operation, and first measurements of the shape and intensity of the neutron beam were performed. The estimated intensity of the straight beam, measured by using beam attenuators of well-known attenuation strengths, is in agreement with theoretical predictions. First polarization

tests were performed showing that the beam polarization is lower than predicted, most likely due to polarization losses in the Ni/Ti-neutron guide. Neutron spin echo (NSE) coils containing neutron guides made of float glass, were put on stream, and first NSE polarization showed that beam polarization was partially lost also in the attenuation/monitor zone between the neutron guide and the mumetal shielding of RESEDA. The guide field in this region was hence modified in the reactor pause of September and October, and the attenuator shielding was improved.

At the same time, the RF circuits were finished and put into operation with the new RF amplifiers. The impedance and the resonance frequencies of the RF circuits were tested under different conditions, and the software controlling the RF parameters was adapted to the amplifiers. In November, the Neutron Resonance Spin Echo (NRSE) coils were put into operation, and the first NRSE echo groups could be detected. Though the beam polarization is not perfect, the NRSE data - a typical echo group plot is shown in Fig. 2.67 demonstrate that all the components of RESEDA work properly. The mean neutron wavelength of the primary beam, as extracted from the NRSE data, is 5.3 Å in good agreement with the value predicted from the selector frequency, and the width of the wavelength band amounts to 13% (FWHM). We finally investigated the dependence of the NRSE polarization from several parameters, as the magnetic fields in the coupling coils and the solenoids fixed at the mural shielding, and as a function of the RF frequency. Besides the predominantly expected results from these tests, it turned out that the polarization depends on the position of the neutron guide hall crane, and on the set value of the FRM-II sample oven. Further test measurements, especially of the polarization as a function of the beam divergence, are in preparation, because re-



Figure 2.66: The image shows the two secondary spectrometer arms of RESEDA. The open mumetal shielding gives free view on the NSE and NRSE coils.

cent tests gave hints that the polarization is decreasing with increasing divergence.

In 2005, the progress at RESEDA was again very remarkable, as in 2004. Within less than 2 years essential parts of the instrument have been modified, including neutron guide shielding, selector housing, beam shutters and attenuators, NRSE coils, cooling and security systems, complete cabling of the instrument, completely new instrument control software etc. Commissioning of RESEDA will presumably take some time still in 2006.

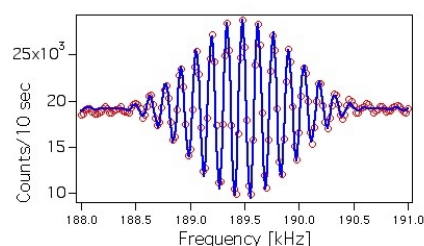


Figure 2.67: A typical NRSE echo group. The RF frequency in the first spectrometer arm is fixed to 189.5 kHz. The RF frequency in the second arm is scanned around the same value. The mean neutron wavelength extracted from the fit with the theoretical function is 5.3 Å, the width of the wavelength band is 13 % (FWHM).





## 3 Scientific Highlights

### 3.1 Magnetic-field induced instability in the A-Phase of MnSi: Bulk and SANS measurements

D. Lamago<sup>2,1</sup>, R. Georgii<sup>2,1</sup>, P. Böni<sup>1</sup>, C. Pfleiderer<sup>1</sup>

<sup>1</sup>Physics Department, E21, TU München,

<sup>2</sup>ZWE FRM II, TU München

MnSi develops itinerant-electron magnetism below  $T_c = 29$  K that supports a long wavelength helical modulation. In recent years the properties of MnSi have attracted great scientific interest [1, 2]. Motivated by recent efforts [3] we revisit reorientational processes of the helical modulation in MnSi at ambient pressure as function of field. We combine small-angle neutron scattering with AC susceptibility data. This provides unexpected new insights into the nature of the helical modulation and its possible connection to the NFL phase and the partial magnetic order at high pressure [2].

The AC susceptibility of a single crystal of MnSi have been measured by means of a 9 T Quantum Design PPMS System. SANS-experiments were carried out at the diffractometer MIRA at FRM II in Garching.

Fig. 3.1(a) shows typical AC-susceptibility data as measured in the A-phase used for determining the phase boundaries of the A-phase. As function of magnetic field, the AC susceptibility displays an abrupt change of slope and a minimum that signifies the A-phase. The onset of this minimum has been mapped out as function of temperature and is shown in the phase diagrams in Fig. 3.1(b), (c) and (d).

Typical small-angle neutron scattering data are shown in Fig. 3.2. At a temperature  $T = 28.5$  K, just below  $T_c$ , we observe well defined spots of helical magnetic order (lower panel) as reported in numerous studies before. With increasing magnetic field, we observe as an additional feature a ring of scattered intensity with a radius

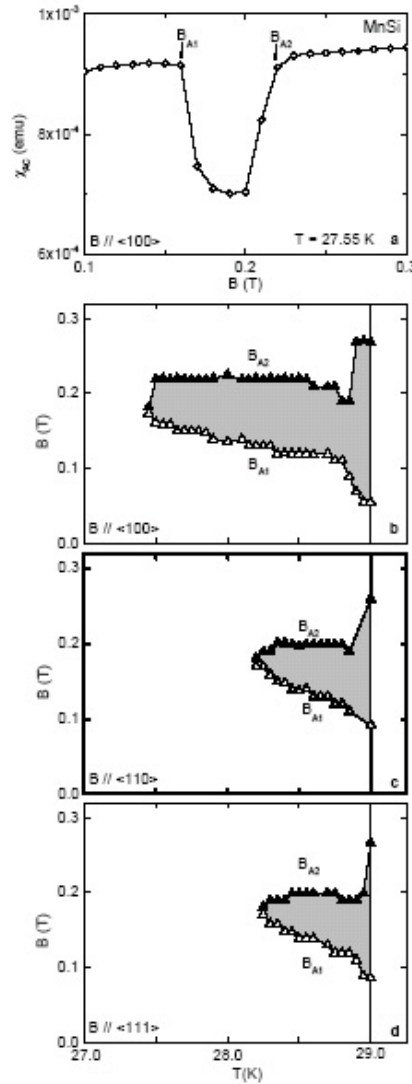


Figure 3.1: (a) AC susceptibility as measured in the A-phase of MnSi using a magnetic field with  $B \parallel \langle 100 \rangle$ . The data for  $B \parallel \langle 110 \rangle$  and  $\langle 111 \rangle$  are qualitatively similar. Panels (b), (c) and (d) show the phase boundary of the A-phase for  $B \parallel \langle 100 \rangle$ ,  $\langle 110 \rangle$ , and  $\langle 111 \rangle$ , respectively.

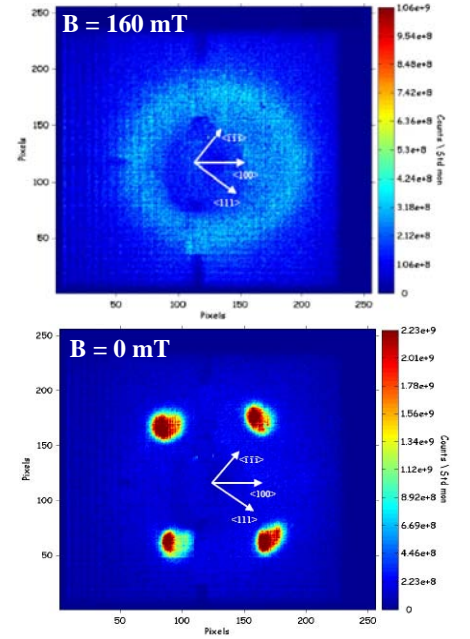


Figure 3.2: Neutron SANS intensity of MnSi at  $T = 28.5$  K (just below  $T_c$ ) recorded at the diffractometer MIRA at FRM-II. Lower panel: data at  $B = 0$ . Four resolution-limited spots are characteristic of long-range helical order, consistent with previous work. Upper panel: data at 0.16 T, where only a ring of scattering intensity appears.

corresponding to  $|\mathbf{Q}|$ , that was not present at  $B = 0$ .

The appearance of this ring of intensity is only gradual from the  $B = 0$ -phase into the A-phase. Interestingly, we observe the same qualitative behaviour also for  $B \parallel \langle 110 \rangle$  and  $B \parallel \langle 111 \rangle$  (not shown).

Therefore, the behaviour is isotropic and not related to a particular initial di-

rection of the helical order that is enforced at low  $T$  by lattice anisotropies.

The distinct change of slope of the AC susceptibility as well as the sharp peaks in the specific heat (not shown) indicate a well defined phase transition into the A-phase that shows up in the SANS-experiments as a ring of scattering intensity.

Our experiments show that combining SANS measurements at the new diffractometer MIRA at FRMII with bulk measurements helps resolving the

microscopic nature of the reorientation transition in MnSi. The results indicate the appearance of a new form of magnetic ordering that may be interpreted in terms of skyrmions. Presently, a device for 3-dimensional polarisation analysis, MuPAD, is being installed at MIRA and will help to resolve the microscopic magnetic structure in the A-phase of MnSi and distinguish between the various models.

[1] Roessli, B., Böni, P., Fischer, W., En-

doh, Y. *Phys. Rev. Lett.*, 88, (2002), 237204.

[2] Pfeleiderer, C., Reznik, D., L.Pintschovius, Löhneysen, H., Garst, M., Rosch, A. *Nature*, 427, (2004), 227.

[3] Okorokov, A., Grigoriev, S., Chetverikov, Y., Maleyev, S., Georgii, R., Böni, P., Lamago, D., Eckerlebe, H., Pranzas, K. *Physica B*, 356, (2005), 259.

## 3.2 Measurements on Mg-Alloys with the Coincident Doppler Broadening Spectrometer CDBS

M. Stadlbauer<sup>2</sup>, C. Hugenschmidt<sup>1</sup>, K. Schreckenbach<sup>1</sup>, P. Böni<sup>2</sup>

<sup>1</sup>ZWE FRM II, TU München

<sup>2</sup>TU München, Physikdepartment E21

### Experimental Setup

During 2004 a new coincident Doppler broadening spectrometer (CDBS) was set into operation at the high intense positron source NEPOMUC. The positron beam is guided in a longitudinal magnetic field to the analysis chamber and nonadiabatically released from this field by a magnetic field termination. After passing an aperture of 3 mm diameter, electrical lenses focus the divergent positron beam onto the sample where a focus diameter of 1 mm was achieved.

Since the high momenta of the electrons in the sample endue high momenta compared to the thermalized positrons, the 511 keV annihilation radiation is Doppler shifted. By measuring this Doppler shift with high purity germanium detectors, the electron momentum distribution at the annihilation site can be investigated. At high Doppler shifts, i.e. regions of the annihilation line with very low count rate, information about the chemical surrounding of the annihilation sites - for example open volume defects - can be revealed [1]. Therefore, the CDBS is equipped with two facing germanium detectors in coincidence in order to reduce background.

### Characterization of the Focus

In order to investigate the focus parameters at the sample position, an aluminum sample with glued on tungsten stripes was investigated with the CDBS since aluminum and tungsten have very different electron momentum distributions. The S-parameter - a quantity that measures the width of the annihilations line - was recorded depending on the position of the positron beam spot on the sample at a potential of -20 kV. The result is shown in figure 3.3.

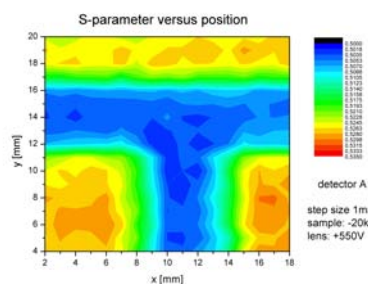


Figure 3.3: S-parameter vs. position of the focused positron beam on an aluminum sample with glued on tungsten stripes. This picture was recorded at a sample potential of 20 kV with a focal diameter of 2 mm

The sharp edges of the borders between aluminum and tungsten become smooth transitions in the S-parameter picture since the beam diameter shows a certain extension. The area of this transitions allows to estimate the beam diameter in the x and y direction. Figure 3.3 shows clearly a beam diameter of about 2 mm. By inserting an additional aperture, a focus of 1 mm was achieved.

### Measurements on Mg-Alloys

Mg-alloys experience an increasing interest for industrial applications due to their very low specific weight, high elasticity and mechanical strength. The CDBS is an ideal tool for investigating the behaviour of the alloy constituents, i.e. aluminum and zinc. If the concentration of one of the alloy constituents changes in the vicinity of open volume defects, the structure of the annihilation line should change in the high momentum region. First measurements were recorded of the pure and annealed metals aluminum, zinc and magnesium in order to get reference spectra. These annihilation lines were compared with AZ31, a diecast Mg-alloy consisting of 1% wt. zinc and 3% wt. aluminum and normalized to magnesium (see figure 3.4).

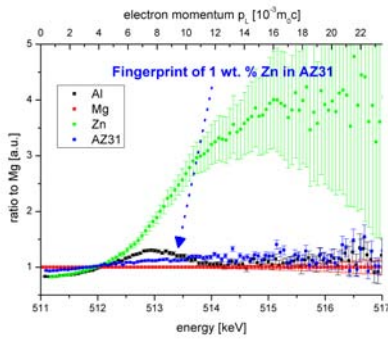


Figure 3.4: Annihilation lines of annealed aluminum, zinc, magnesium and AZ31-samples, normalized to magnesium. The line of AZ31 is shifted towards the line of zinc, which proves that even in defect free material, 1% wt. of zinc can be detected.

The lines of the pure elements can be clearly separated from each other. Especially zinc shows a large deviation compared to magnesium and aluminum at high momenta. The structure of the AZ31-line is clearly shifted towards the line of zinc due to the 1% wt. zinc atoms in the sample. Consequently even in defect free samples zinc can be detected.

- [1] Asoka-Kumar, P., Alatalo, M., Ghosh, V. J., Krusemann, A. C., Nielsen, B., Lynn, K. G. *Phys. Rev. Lett.*, 77, (1996), 2097–2100.

### 3.3 A study of oil lubrication in a rotating engine using stroboscopic neutron imaging

Burkhard Schillinger<sup>1,2</sup>, Johannes Brunner<sup>1,2</sup>, Elbio Calzada<sup>1,2</sup>

<sup>1</sup>TU München, Physics Department, E21

<sup>2</sup>ZWE FRM II, TU München

Even at modern high-flux neutron sources, the required exposure time for one neutron radiography image with high counting statistics is in the order of one second. Continuous time-resolved imaging of objects in motion is thus very limited in time resolution and signal dynamics. However, repetitive motions can be recorded with a stroboscopic technique: A trigger-able accumulating detector is triggered for many identical time windows of the cyclic motion until sufficient fluence is accumulated for one image. The image is read out, the delay for the time window is shifted and the recording repeated until a complete movie of the cyclic motion can be put together. We report about a study of oil flux in a running, electrically driven BMW engine out of current production.

#### Introduction

The neutron radiography facility ANTARES at FRMII of TU München delivers a cold flux of 108 n/cm<sup>2</sup>s at

a collimation ratio of L/D=400. Considering a time window as long as one millisecond and a scintillator detection efficiency of 30%, only 3.3 x 10<sup>5</sup>n/cm<sup>2</sup>s are detected on a square centimeter. If an area of 0.3 mm x 0.3 mm is imaged onto one pixel of the detector, only 300 are detected on a single pixel. This signal is not sufficient for a useful radiography image with attenuations from zero to a factor of 1000. The only way to increase the counting statistics is to use a stroboscopic imaging technique to record a periodic motion. The signal of many time windows identical within the cycle of the examined motion is accumulated on a trigger-able detector before the signal is digitized and read out, until sufficient counting statistics is achieved.

#### Experimental setup

For our studies, we obtained a NG4 BMW engine out of current production. The engine was stripped of the intake and exhaust system and was coupled

to a 2kW electro motor with a transmission belt. The spark plugs were removed, so that the engine would not generate compression in its cylinders. Only this way, the comparatively weak electro motor was capable of turning the engine at low rotation speeds, and due to the reduced heat production, the water cooling could be omitted. Instead of using the sparc distributor to generate a synchronization signal, we mounted a hall sensor close to the transmission wheel on the camshaft. The generated pulse was used to trigger the image intensifier of a cooled CCD camera. With the camera electronics and software, the trigger signal could be delayed in order to shift the time window within the cycle of the engine.

#### Measurements at ANTARES

The detection system was an Andor iStar MCP intensified CCD camera with 1024 x 1024 pixels [1, 2]. Of special interest is the visualization of the oil cooling of the piston bottoms. Since

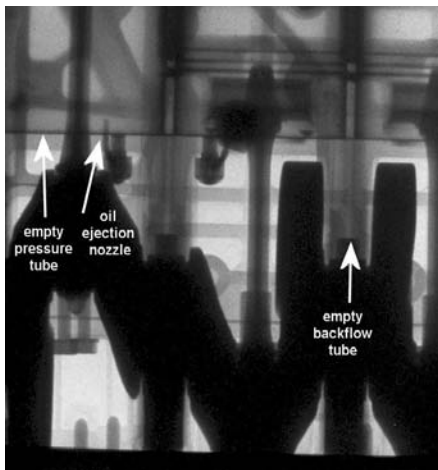


Figure 3.5: Static neutron radiography image of the engine.

the pistons are only connected to the engine body via the piston rings with very low heat dissipation, a continuous oil jet is directed from below at the piston bottoms, lowering the piston temperature by more than 200 degrees C. Because of the limited flux, the time window was selected as high as one millisecond, the rotation speed was selected as 600 rpm, which is well below the nominal idle speed of the engine. The images thus show motion unsharpness, but good definition on the stationary parts. At this rotation speed, the oil pump did not produce its nominal pressure, the oil pressure was pulsed and produced blobs in the cooling oil jet. In the field of view of 25 cm x 25 cm, the nozzles for the cooling oil jets were

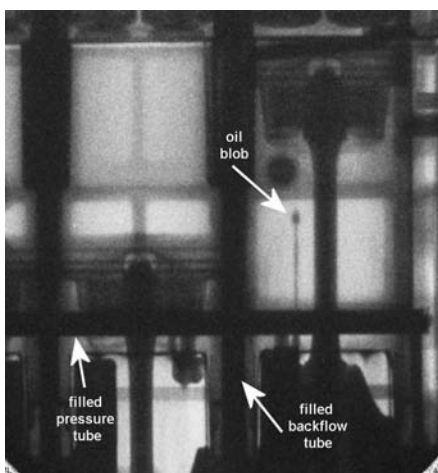


Figure 3.6: Dynamic neutron radiography image of the engine.

visible along with the horizontal pressure tube. The area between the pistons contains the vertical tubes for the pressure-free backflow of oil from the camshaft on top to the oil pan at the bottom of the engine. In the car, these tubes are mostly empty, because the engine is mounted at a 30 degree tilt angle. On our test stand, the engine was mounted vertically, resulting in a fill-up of these tubes.

Fig. 3.5 shows a static radiography of the engine, showing valves, pistons, piston rods, piston pins and piston rings, with the pressure tubes and backflow channels empty. Fig. 3.6 shows one single frame of the engine in motion, viewing different cutouts. An oil blob is visible on its way to the piston bottom, the horizontal pressure tube for the supply of the oil ejection nozzles and the vertical backflow tubes are filled up.

Fig. 3.7 and 3.8 show a static and dynamic cutout for comparison. The vertical backflow tubes which are mounted on the outside of the engine block extend beyond the edges of the cylinder bore and cover the edges of the pistons, making impossible to observe the oil film on the pistons in motion in this 90 degree view.

In the running engine, the transmission through the free areas besides the crankshaft is only half of the static transmission, meaning non-repetitive oil splashes and foams obstruct the view. As repetitive phenomenon, curtains of oil are visible flowing down the cylinder walls. The lubrication of



Figure 3.7: Static neutron radiography image cutout.

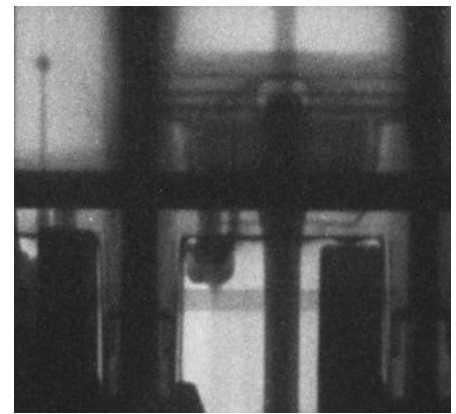


Figure 3.8: Dynamic neutron radiography cutout.

the camshaft bearings would also have been of interest, but the engine has a plastic cover on top which obstructs the neutron view to this area. Further tests will be performed with an Aluminium replacement cover.

## Outlook

Stroboscopic neutron radiography has proved its potential for further examinations of the lubrication of running engines. In a realistic experiment with compression, heat generation will cause difficulties, as filling the cooling system with water will obstruct part of the view. A partial solution may be the use of heavy water in the cooling system. To avoid exhaust fumes in the reactor hall, an external electro motor will be required which must equal the nominal power of the engine to drive it at high rotational speeds.

[1] iStar. [www.andor.com](http://www.andor.com).

[2] Schillinger, B., Brunner, J., Calzada, E. *Physica B*. Acc. pub.

## 3.4 Small-angle scattering effects in neutron radiography and tomography

Burkhard Schillinger<sup>1,2</sup>, Elbio Calzada<sup>1,2</sup>, Roland Gähler<sup>3</sup>, Hongyun Li<sup>1,4</sup>, Martin Mühlbauer<sup>1,2</sup>, Michael Schulz<sup>1,2</sup>

<sup>1</sup>TU München, Physics Department, Institute E21

<sup>2</sup>ZWE FRM II, TU München

<sup>3</sup>Institut Laue-Langevin, Grenoble, France

<sup>4</sup>Northwest Institute of Nuclear Technology, Xi'an, P. R. China

Due to the very parallel beam collimation at the neutron radiography facility ANTARES, the distance between sample and detector can be increased up to two meters distance while still obtaining unblurred images. At these large distances, small angle scattering effects in otherwise homogeneous and plane samples build up to intensity variations that can be detected in a radiography image. We have examined different Aluminium and steel samples with texture variations induced by plastic deformation.

### Motivation

Quantitative stress measurements are performed with the Stress-Spectrometer STRESS-SPEC, where crystal lattice reflexes can be examined to a depth of several centimeters. By using small diaphragms, the incoming and outgoing neutron beam is focused to a measuring volume of about one cubic millimeter. By scanning the sample volume, the internal stress is mapped due to shift of the reflexes compared to the unperturbed material. Scanning of a large volume may take hours up to days. With neutron radiography and tomography, it is intended to do a qualitative scan of the sample as a whole and to determine regions of interest to be scanned quantitatively by STRESS-SPEC.

### Working principle

The beam at ANTARES has a very high parallel collimation ratio of  $L/D=800$ . With the use of a selector wheel with pinhole apertures, this collimation can be increased to 2300 up to 16000. Small texture changes in an otherwise flat and homogeneous sample will lead to locally increased small angle scattering, deviating neutrons from their straight

path. The effect is not visible in standard radiography with the detector close to the sample. If the sample to detector distance is increased to 0.5 to 2 meters, even faint effects become visible in a radiography or tomography.

### Radiographic examination of smooth-polished car chassis numbers in steel plates

The German Federal Police brought us test samples of steel plates which had contained car chassis numbers hammered into the metal. Fig. 3.9 shows a photo of the steel plates with a size of about 5 cm. The plates were grinded to a smooth surface, no trace of the chassis numbers is visible by eye. Fig. 3.10 shows a standard neutron radiography with a few centimeters distance to the detector, revealing nothing but homogeneous material. The distance was then increased to two meters, the collimation ratio to 2300. Fig. 3.11 and 3.12 show enhanced images of the plates with most of the original imprinted numbers visible.

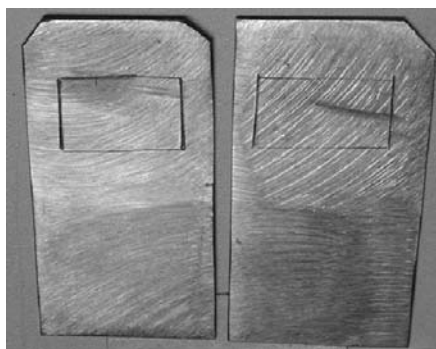


Figure 3.9: Photo of the sanded steel plates.

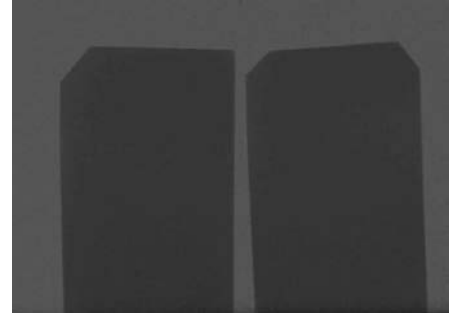


Figure 3.10: Standard neutron radiography.



Figure 3.11: Large distance radiography.

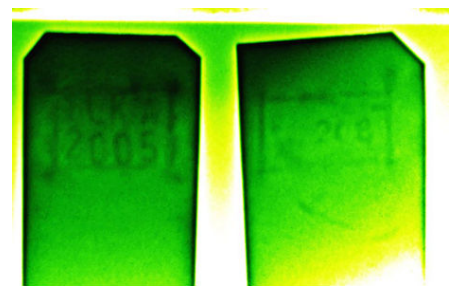


Figure 3.12: False colours of the radiography image.

### Tomographic examination of a cold-expanded rivet hole in Aluminium

Aircraft parts are riveted, not welded together. The rivet holes are subjected

to high stress during operation. To increase their stability, holes are drilled to less than the required diameter, then cold expanded by about 4% by a mandrel. This process introduces plastic deformation and a negative pre-stress into the hole edges. If pulling forces are introduced by the rivets during aircraft operation, the negative stress is first compensated before positive stress may lead to cracks. As a test sample, we examined a rolled-out Aluminium sheet with a cold expanded hole with neutron computed tomography. The sample was put in a distance of half a meter to the detector. The computed tomography returns a certain range of attenuation values or grey values for the material Aluminium. For three-dimensional visualisation, we set most of that grey-value range to transparent and examined only the most attenuating upper greyvalue range. Fig. 3.13 show a standard view of the Aluminium sheet, Fig. 3.14 shows the same sheet with only the most attenuating parts set visible.

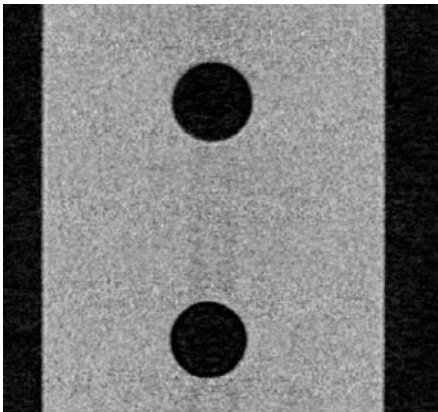


Figure 3.13: Standard tomographic view of the Aluminium sheet.

The tomography first reveals a wave structure originating from the rolling-out of the metal sheet. Furthermore, the edge of the cold-expanded hole shows a significant increase in attenuation compared to the surrounding material (Fig. 3.15).

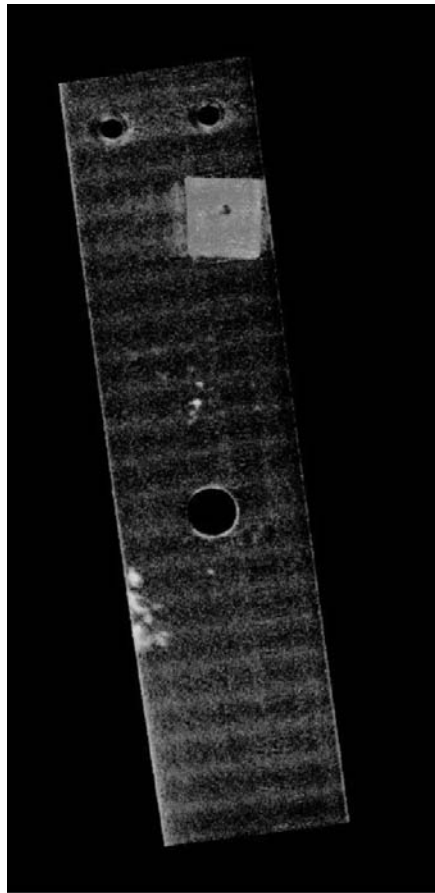


Figure 3.14: Only the most attenuating areas visible.

The Figures 3.16, 3.17 and 3.18 show better that it is a true 3D tomography. Ordinary holes in the same samples were drilled later and re-examined. They did not show the increased attenuation at the edge. This measurement was performed at a time when the above-mentioned pinhole selector wheel had not yet been available. The experiment will be repeated with even higher collimation soon.

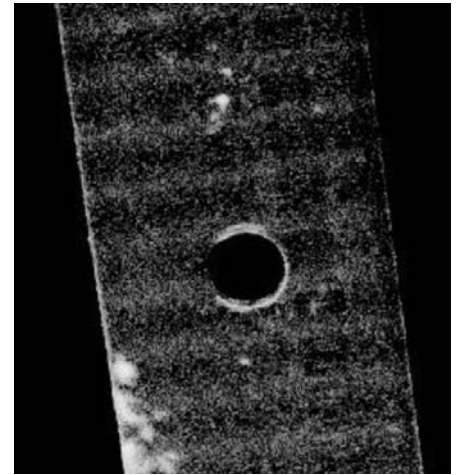


Figure 3.15: Increased attenuation at the hole edges.

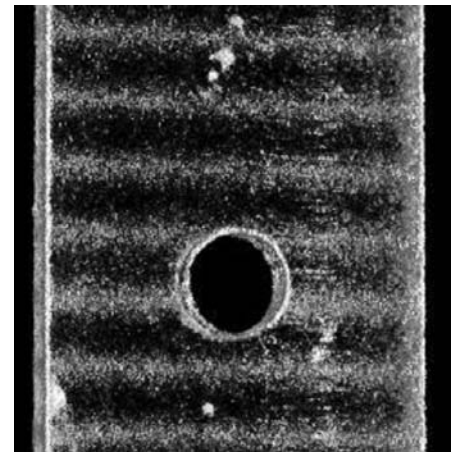


Figure 3.16: This image proves that it is a true 3D tomography.

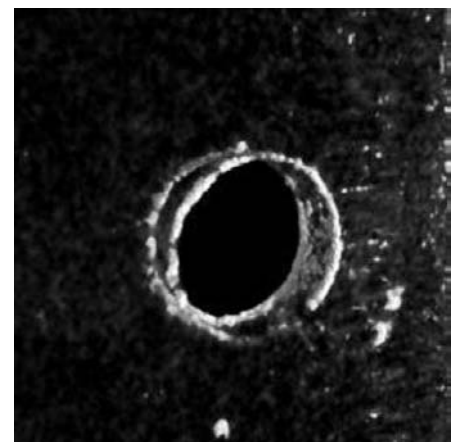


Figure 3.17: Another 3D view with the wave structure invisible.

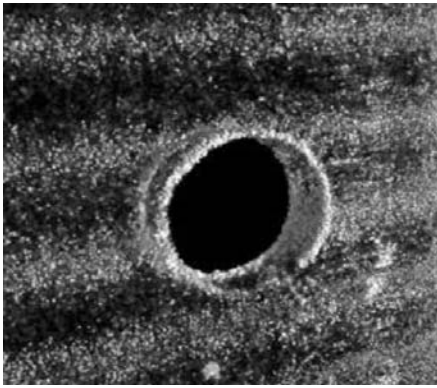


Figure 3.18: All hard structures together.

## Conclusion

A very high collimation of the neutron radiography beam allows for the examination of small-angle scattering effects in neutron radiography and tomography and thus extends the range of examination methods considerably. More experiments will be done soon.

## 3.5 Mechanisms of mass transport in multicomponent melts

A. Meyer<sup>1</sup>, F. Kargl<sup>1</sup>, S. Mavila Chathoth<sup>1</sup>, T. Unruh<sup>2</sup>

<sup>1</sup>Physik Department E13, TU München

<sup>2</sup>ZWE FRM II, TU München

We investigate the atomic motion in multicomponent metallic and oxidic melts with inelastic neutron scattering in order to clarify the microscopic transport mechanisms. The high-resolution energy and momentum information emerging from inelastic neutron scattering experiments allows to study the interplay between intermediate range structure, viscous flow and the atomic diffusion of particular components. With a high neutron flux on the sample, an excellent energy resolution and an outstanding signal to noise ratio, the neutron time-of-flight spectrometer TOFTOF is especially suited for the investigation of atomic diffusion in high temperature melts where measuring times are limited due to sample evaporation and/or interdiffusion between sample and sample holder.

On TOFTOF an incident neutron wavelength of  $\lambda = 5.4 \text{ \AA}^{-1}$  in combination with choppers rotating at 12.000 rpm yields an accessible wavenumber range at zero energy transfer of  $q = 0.2 - 2.2 \text{ \AA}^{-1}$  and an energy resolution of  $85 \mu\text{eV}$  (FWHM) at  $90^\circ$  scattering angle. A hollow cylindrical Vanadium standard with a diameter of 23 mm, a Vanadium wall thickness of 0.88 mm ( $\approx 10\%$  scatterer) and a height

of 40 mm gives a count rate of 2900 cps summed over all 640 detectors.

Beside surface energies, the precise knowledge of diffusion coefficients represents an important input for a modelling of the solidification of multicomponent materials and hence a virtual materials design. However, especially due to convection effects diffusion coefficients are in general not known in high melting alloys. Since with inelastic neutron scattering atomic motion is probed on a 10 picosecond time scale at interatomic distances, convection effects that cause a macroscopic flow on microsecond time scales, do not alter the quasielastic signal.

Figure 3.19 shows the quasielastic signal of a liquid  $\text{Fe}_{90}\text{Ni}_{10}$  alloy at 1855 K. For the measurements the alloy was melted in an alumina can that provides a hollow cylindrical sample geometry with 1.2 mm sample wall thickness. The line represents a fit with a Lorentz function. Below the first structure factor maximum the signal is governed by the contribution of the incoherent scattering on the Nickel atoms. From the  $q$  dependence of the width of quasielastic line a Ni self diffusion coefficient can be obtained on an absolute scale. Interestingly with  $3.4 \pm 0.1 \cdot 10^{-9} \text{ m}^2/\text{s}$  the resulting self diffusion coefficient of

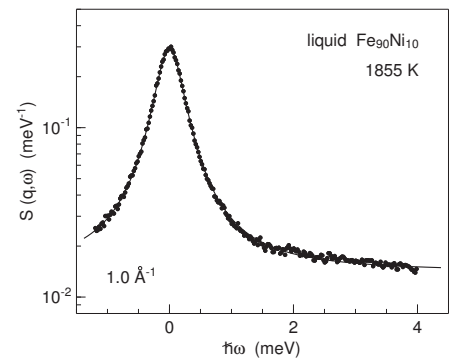


Figure 3.19: Quasielastic neutron scattering on a  $\text{Fe}_{90}\text{Ni}_{10}$  melt at 1855 K.

Nickel is slightly smaller than in dense packed pure liquid Nickel[1] or Nickel rich NiAl alloys[2].

In multicomponent hard sphere like viscous metallic melts, where diffusion coefficients of the various components exhibit similar values above the melting point, the relaxational dynamics is in quantitative agreement with the universal mode coupling scaling functions[3] and mixing effects only play a minor role for the mass transport[1]. In sodium silicates[4] and sodium borates the time scales for the Na  $\alpha$  relaxation and the Si(B)-O network structural relaxation are separated. The long range atomic transport of sodium is faster by orders of magnitude as compared to

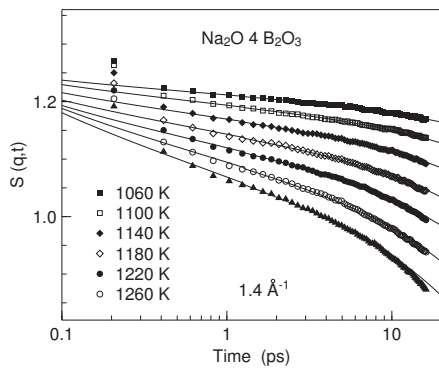


Figure 3.20: Density correlation function of a viscous sodium tetra borate melt obtained by quasielastic neutron scattering. The lines are fits with the  $\beta$  scaling function of mode coupling theory.

the transport of the silicon (boron) and oxygen atoms.

In an experiment on TOFTOF we investigated sodium tetra borate in order to address the question how far the relaxational dynamics in such a system can be described with universal mode coupling scaling functions. We

used a Platinum sample can that provides a hollow cylindrical sample geometry with a sample wall thickness of 1.2 mm. With these sample dimensions multiple scattering is negligible. In the low  $q$ -region incoherent neutron scattering on sodium is the dominant contribution to the signal, whereas around the first sharp diffraction peak at  $q \approx 1.5 \text{ \AA}^{-1}$  coherent scattering on B and O dominates. Therefore, the  $q$  dependence of amplitude and time scale of a fast  $\beta$  relaxation process should display the coupling to the two distinct  $\alpha$  relaxation processes.

Figure 3.20 shows density correlation functions. The lines are fits with the mode coupling  $\beta$  scaling law. The full set of data can consistently be described with a temperature and  $q$  independent line shape parameter  $\lambda$  and a  $q$  independent cross over time  $t_\sigma$  as found in one component viscous liquids. The amplitude  $h_q$  of the fast relaxation is found to be in phase with static structure factor for all  $q$ .  $h_q^2$  plotted as

a function of temperature extrapolates to one  $T_c$  value for all  $q$ . Since toward small  $q$  the signal is dominated by incoherent scattering on the sodium atoms, the resulting  $q$  dependence of the amplitude  $h_q$  demonstrates that sodium contributes to the fast relaxation process. Therefore, the Na ion diffusion in sodium borates is prepared by a fast  $\beta$  relaxation process as described by Mode Coupling Theory (MCT).

- [1] Chathoth, S. M., Meyer, A., Schober, H., Juranyi, F. *Appl. Phys. Lett.*, 85, (2004), 4881.
- [2] Das, S. K., Horbach, J., Koza, M. M., Chathoth, S. M., Meyer, A. *Appl. Phys. Lett.*, 86, (2005), 011918.
- [3] Meyer, A. *Phys. Rev. B*, 66, (2002), 134205.
- [4] Meyer, A., Horbach, J., Kob, W., Kargl, F., Schober, H. *Phys. Rev. Lett.*, 93, (2004), 027801.

### 3.6 Influence of the superconducting energy gap on phonon linewidths in Pb – a high resolution study at TRISP

P. Aynajian<sup>1</sup>, K. Buchner<sup>1</sup>, K. Habicht<sup>2</sup>, T. Keller<sup>1,3</sup>, M. Ohl<sup>1</sup>, B. Keimer<sup>1</sup>

<sup>1</sup>Max-Planck-Institut für Festkörperforschung, Stuttgart

<sup>2</sup>BENSC, HMI Berlin

<sup>3</sup>ZWE FRM II, TU München



Figure 3.21: The spin echo triple axis spectrometer TRISP at the FRM-II

The broadening of the linewidths of transverse phonons resulting from the electron-phonon interaction in superconducting Pb was resolved for the first time at the triple axis neutron

spectrometer TRISP at the FRM-II. The electron-phonon ( $ep$ ) interaction is responsible for the formation of Cooper pairs in conventional BCS superconductors. Therefore detailed knowledge of the  $ep$  coupling parameters is required to understand fundamental properties of these materials. The  $ep$  interaction provides a decay channel for phonons and broadens the phonon linewidth (shortens the phonon lifetime). Thus phonon linewidth measurements using neutron spectroscopy obviously offer direct access to the  $ep$  coupling parameters of each single phonon and thus can extend the range of conventional spectroscopy methods, which are restricted to phonons at the center of the Brillouin zone (light scattering) or take an average over

the whole phonon spectrum (tunneling spectroscopy). Allen [1] first derived a simple relation between the phonon linewidth and the  $ep$  coupling parameter, but he also pointed out that except for some rare cases where phonon linewidth broadening is exceptionally large, the energy resolution of neutron spectrometers is generally too low to resolve these phonon linewidth effects.

In early studies, conventional triple axis spectrometers were used to investigate  $ep$  interaction in the superconductors  $\text{Nb}_3\text{Sn}$  [2, 3] and Nb [4], which show such unusually large phonon linewidth broadening. As the phonon linewidth is also broadened by other decay processes such as phonon-phonon scattering or by instrumental effects and sample imperfections, in general thor-



ough data analysis is required to separate the electron-phonon contribution  $\Gamma_{ep}$  from the total phonon linewidth. Axe and Shirane [2, 3] used an elegant approach to directly extract  $\Gamma_{ep}$ . The basic principle of their method is that phonons with energy smaller than the width of the superconducting energy gap,  $2\Delta(T)$ , cannot decay by breaking Cooper-pairs and thus have a smaller linewidth (longer lifetime) than phonons with energy above  $2\Delta$ . By scanning the temperature,  $2\Delta(T)$  is varied across the phonon energy, and the change in phonon linewidth directly gives the electron-phonon contribution  $\Gamma_{ep}$ . Using conventional triple axis spectrometers under favorable focusing, typical  $\Gamma_{ep}$  in the order of 1meV for transverse acoustic phonons in  $\text{Nb}_3\text{Sn}$  and  $200\mu\text{eV}$  in Nb were observed. For superconducting Pb,  $\Gamma_{ep}$  is in the order of  $5\mu\text{eV}$ , which is far beyond the resolution limits of conventional neutron spectrometers. Attempts to resolve  $\Gamma_{e-ph}$  on triple axis spectrometer thus failed [5].

Using the high-resolution spectrometer TRISP [6] at the FRM-II, we were for the first time able to observe the momentum and temperature dependence of the linewidths of transverse acoustic phonons around  $T_c = 7.2\text{K}$  and to extract the electron-phonon broadening  $\Gamma_{ep}$ . TRISP is a triple axis spectrometer with polarized incident beam and polarisation analysis of the scattered beam combined with a resonance spin echo (NRSE) spectrometer. The NRSE uses small radio frequency (RF) spin flippers to define precession regions in the incident and scattered beam [7, 8]. By rotating the RF spin flip coils with respect to the neutron beam and proper setting of the frequencies, the spin echo resolution function is tuned to the phonon group velocity and energy (for details, see [9] and references therein). If the phonon has zero linewidth, the polarisation of the scattered beam vs. the applied RF stays constant as function of the spin echo time. A finite linewidth  $\Gamma$  results in a decay of the polarisation, where for a Lorentzian lineshape the polarisation decays exponentially  $P(\tau) = \exp(-\Gamma \cdot \tau)$ .  $\tau$  is the *spin echo time*, which is proportional to the applied RF.

For the present experiment, we used

a cylindrical single crystal ( $\varnothing 3 \times 5\text{cm}^3$ , cylinder axis along [100]) with a low mosaic spread of  $4.2'$ . The temperature dependence of the phonon linewidth was determined by measuring the polarisation for six different values of  $\tau$ . The linewidth is obtained by fitting exponentials to these data points (Fig. 3.23). The typical counting time for one linewidth was 4 hours.

Two sample scans are shown in Fig. 3.23. The data in the plot were taken for a [2.32 1.68 0]T1 phonon with an energy of  $2.37\text{meV}$  (horizontal line) at the temperatures 3.7 and 6K indicated by the vertical arrows in Fig. 3.22. As the superconducting energy gap is temperature dependent, the phonon energy lies below  $2\Delta$  at 3.7K and above at 6K. The additional broadening of the phonon linewidth of  $7 \pm 1\mu\text{eV}$  (a smaller slope of the data in Fig. 3.23 indicates a narrower linewidth), which occurs when the gap energy  $2\Delta$  crosses falls below the phonon energy, can be identified with influence of the electron-phonon part  $\Gamma_{ep}$  of the phonon linewidth. Changes of the phonon linewidth resulting from phonon-phonon scattering are negligible at these low temperatures.

Detailed linewidth data was also collected for other transverse branches in Pb [10]. This allows a comparison with modern ab-initio calculations, which are able to predict  $\Gamma_{ep}$  for each single phonon branch.

We thank H. Kolb and J. Peters for getting the cryogenics running and C.T. Lin for preparing the Pb crystal.

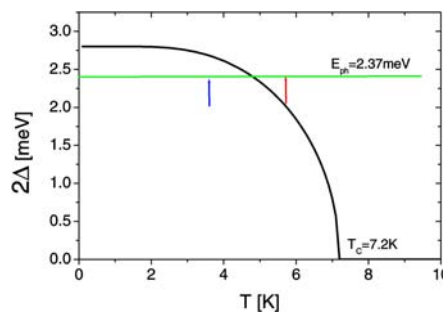


Figure 3.22: Temperature dependence of the superconducting energy gap in Pb. The horizontal line corresponds to the energy of the [0.32 0.32 0]T1 phonon, the arrows indicate the two temperature points corresponding to the data in Fig. 3.23.

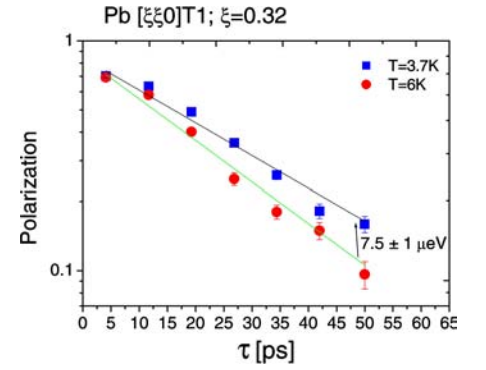


Figure 3.23: Spin echo linewidth data for a [0.32 0.32 0]T1 phonon in superconducting Pb. The slope of the curves is proportional to the linewidth. An additional broadening of  $7 \pm 1\mu\text{eV}$  appears when the gap energy  $2\Delta$  gets smaller than the phonon energy.

- [1] Allen, P. B. *Phys. Rev.*, B6, (1972), 2557.
- [2] Axe, J., Shirane, G. *Phys. Rev. Lett.*, 30, (1972), 214.
- [3] Axe, J., Shirane, G. *Phys. Rev.*, B8, (1973), 1965.
- [4] Shapiro, S., Shirane, G., Axe, J. *Phys. Rev.*, B12, (1975), 4899.
- [5] Youngblood, R., Noda, Y., Shirane, G. *Sol. State Comm.*, 21, (1978), 1433.
- [6] Keller, T., Habicht, K., Klann, H., Ohl, M., Schneider, H., B. Keimer. *Appl. Phys. A*, 74, (2002), S332.
- [7] Golub, R., Gähler, R. *Phys. Lett.*, A123, (1987), 42.
- [8] Golub, R., Gähler, R. *J. Phys. (Paris)*, 49, (1988), 1195.
- [9] Habicht, K., Golub, R., Mezei, F., Keimer, B., Keller, T. *Phys. Rev.*, B69, (2004), 104301.
- [10] Keller, T., Aynajian, P., Habicht, K., Boeri, L., Bose, S., Keimer, B. To be published.

## 4 Facts and Figures

### 4.1 Experiments and user program

J. Neuhaus<sup>1</sup>, U. Kurz<sup>1</sup>, B. Tonin-Schebesta<sup>1</sup>, W. Wittowitz<sup>1</sup>, E. Jörg-Müller<sup>1</sup>

<sup>1</sup>Forschungsneutronenquelle Heinz Maier-Leibnitz (FRM II), TU München

#### The user office

In the year 2005 the user office has started routine operation in parallel with the neutron source. Right from the beginning external users were using the neutron and positron beams at the FRM II. The first call for proposals was launched already in November 2004, experiments started in May 2005.

After serving the first *friendly users* we made the second call for proposals with deadline in July 2005. The referee meeting took place in September. Here we could establish 3 scientific groups evaluating the proposals. This scientific classification will be more fine grained in the future with an increasing number of instruments in routine operation. Already in the second round we could ask for proposals for 15 instru-

ments. We received 160 proposals demanding for 1236 days of beam time. In total 638 days could be distributed in the second round. The proposals originate from 16 different countries, where by far the most (62%) stem from Germany. About one third of the proposals originate from European countries which are eligible for funding within the 6th frame work program of the EU, i.e. the access program of the NMI3 consortium.

The experiments for the first two calls for proposals could be performed in the reactor cycles 2 to 5. Here 235 experiments were taken all together using 1543 days of beam time. These experiments include the internal use of the instrument groups as well as the beam time for industrial use.

The user office software developed

in-house has proven to be a reliable and user friendly system. Continuous improvement of the functionality is still going on. The underlying content management system, however, has shown several significant limits for the future development. We therefore decided to make a major break and rewrite the software for the system typo3. By this we will merge our public Internet pages with the user office system in order to further improve the usability for internal and external users.

Proposals can be submitted twice a year. In order to spread out the deadlines in relation to other European neutron centers the future deadlines will be mid January and mid August every year. The deadlines for 2006 are January 20 and August 11. The referee meetings will take place about 4 weeks later.

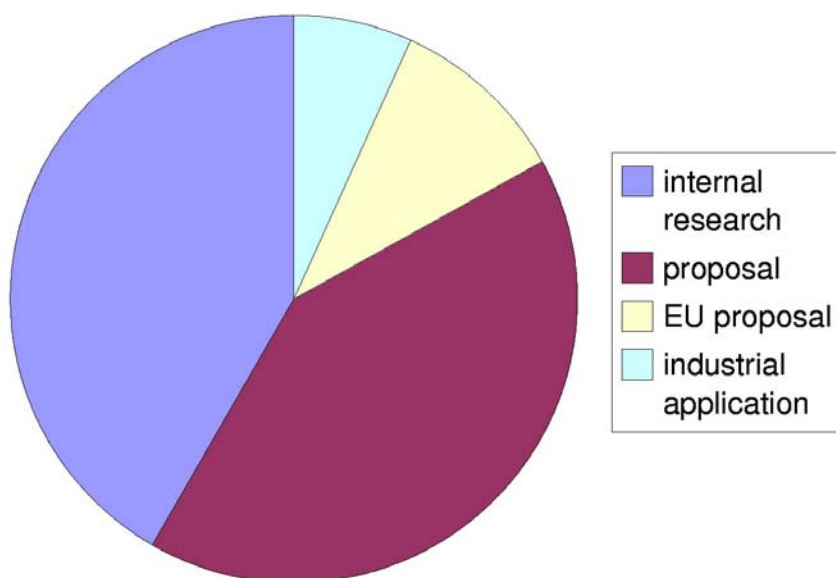


Figure 4.1: Usage of beam time in cycles 2-5.



The proposal submission is done online in the user office system (<http://user.frm2.tum.de>). Each proposer has to register for a personal account in the system. Using the module Proposal the user is guided through a questionnaire concerning the experimental parameters. In addition a written scientific motivation in form of a pdf file with a length of maximal two A4 pages is required. A detailed guideline for proposal submission is given in the section *user guide* in the online system.

In addition to the proposal submission the user office system collects experimental reports which are requested for each experiment. The reports can be uploaded in form of a pdf file up to two written pages. In addition questions concerning the user satisfaction can be filled in. The experimental re-

ports will be published online on our Internet pages.

## Instruments

In the year 2005 commissioning and testing of the instruments dominated the scientific work to a large extent. This took place to a large extent simultaneously during the first experiments. A large number of the 19 instruments (positron source Nepomuc with 3 experiment places is counted as one instrument) presented at the FRM II could already demonstrate their performance, delivering fully scheduled experiments. The number given in table 4.1, column *position* corresponds to the position number in figure 4.3.

### 4.1.1 User support

The user office helps to organise the stay at the FRM II for external visitors. If required support for hotel booking and organisational help is provided. A central e-mail (userinfo@frm2.tum.de) and phone number (+49 899 289 14313) is reachable during normal office hours.

Unfortunately a guest house is available on site up to now.

All visitors are asked to register their stay within the online user office system (module Arrival\_Departure). Here, special requirements can be asked for. The users are normally contacted by e-mail. As well, bookings of hotel rooms and others can be seen in the online system, which is helpful in case an e-mail gets lost.

Instrument	position	operated by	experiments
<b>Experimental hall</b>			
Panda	SR2 (17)	TU Dresden	26, 140 days
Stress-Spec	SR3 (18)	HMI	20, 140 days
Antares	SR4b (19)	TU München	44, 115 days
Trisp	SR5b (21)	MPI Stuttgart	14, 205 days
Puma	SR7 (22)	Univ. Göttingen, TU München	16, 108 days
Spodi	SR8a (23)	TU Darmstadt, LMU München	26, 98 days
Resi	SR8b (24)	Univ. Augsburg, LMU München	12, 57 days
Heidi	SR9b (25)	RWTH Aachen	17, 122 days
Nectar	SR10h (26)	TU München	11, 62 days
Medapp	SR10v (27)	TU München	commissioning
Nepomuc*	SR11 (28)	TU München, Univ. Bundeswehr	17, 130 days
<b>Neutron guide hall</b>			
N-Rex <sup>+</sup>	NL1 (1)	MPI Stuttgart	commissioning
TofTof	NL2au (3)	TU München	14, 104 days
Refsans	NL2b (4)	GKSS, LMU München	commissioning
Mephisto	NL3a (5)	TU München	2, 208 days**
PGAA	NL4b (10)	Univ. Köln, TU München	commissioning
Reseda	NL5ao (11)	TU München	commissioning
Spheres	NL6	FZ-Jülich	commissioning
Mira	NL6 (16)	TU München	29, 184 days

Table 4.1: List of instruments at the FRM II in December 2005. Experiment in cycles 2-5 until March 2006. (\*Nepomuc 3 Instruments, \*\* including setup of the experiments)

In order to provide working space to our external users, we have installed a terminal room for public use. In the former seminar room of the *Projekthaus* 6 personal computers are available 24h a day. The user gets a temporary account to use these computers. Here Internet access via different browsers and office programs are available. Own mobile computers can be connected by an Ethernet cable.



Figure 4.2: Terminal room for users.

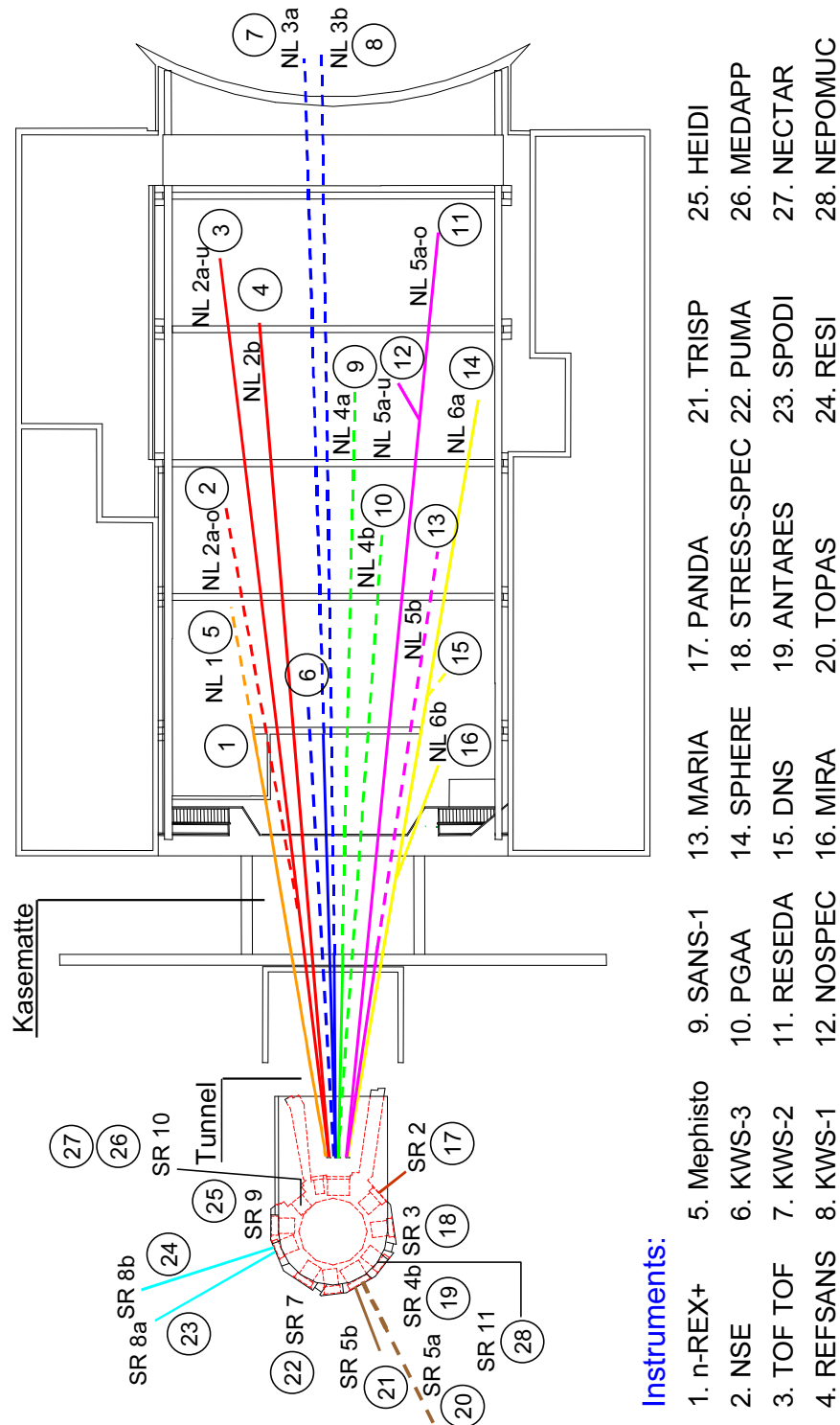


Figure 4.3: Position of the instruments in the experimental and neutron guide hall.

## 4.2 Public relations and visitor service at the FRM II

J. Neuhaus<sup>1</sup>, U. Kurz<sup>1</sup>, B. Tonin-Schebesta<sup>1</sup>, I. Scholz<sup>2</sup>

<sup>1</sup>Forschungsneutronenquelle Heinz Maier-Leibnitz (FRM II), TU München

<sup>2</sup>Presse & Kommunikation, TU München, Bereich Garching

The high demand to visit the FRM II is still a good indicator for the public interest in our institute. Due to the heavy overload of duties for our staff members we had to restrict the visits for general groups to 3 days a week. Nevertheless, in the year 2005 we could welcome 2535 visitors among them 326 pupils and 203 students from universities all over Germany. Especially the guided tours for students hopefully create an interest to use neutron beams for their own future research. On the other hand we are strong engaged to demonstrate the fascination of science for our youngest visitors, namely pupils in higher classes close the final secondary-school examinations.

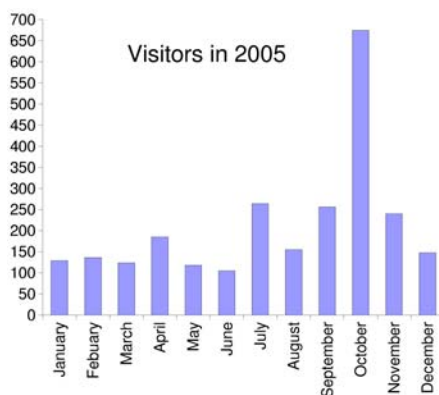


Figure 4.4: Visitors in 2005.

A highlight for the visitors is clearly the annual day of open doors which took place on October 22<sup>nd</sup> in 2005. Together with the institutes of the campus in Garching several thousand people came to Garching. As usual the demand to visit the FRM II was larger than the number of people we could welcome. In total this day 491 visitors came to see the reactor installations and the scientific instruments in the experimental and neutron guide hall.



Figure 4.5: Registration desk with heavy overload on the day of open doors.

Already in the early morning a long queue was built up to register for the guided tour through the reactor. In addition an exposition on natural radioactivity and measuring instruments to monitor radioactivity was organised by our radiation protection group. Lively discussions and a continuous run during the whole day clearly demonstrated the interest of the general public for this issue. During the discussions our experts could explain the security measures of our installation to minimise the release of activity to the environment.



Figure 4.6: Our radiation protection group explaining how to measure natural activity.

The presentation of the FRM II was completed by 3 talks in the lecture hall of the physics department. Winfried Petry explained in two sessions how neutrons are used for scientific and industrial purposes. First experiments taken at the FRM II, especially those for applied sciences fascinated the audience. In another talk Klaus Schreck-enbach explained how to operate a neutron source, which at that time had just started the routine service.



Figure 4.7: Fascinating the public with neutrons.

Besides the personal visits a large number of press releases concerned the FRM II and special experiments which are of public interest. A short impression is given on the next pages where a collection of headlines were put together.

A highlight for our public relations was clearly the film of the Bavarian television on the FRM II, which was broadcasted on the 21st of February. In the weekly series *α-Campus* a 30-minute-presentation on the building of the neutron source as well on selected instruments were presented. The film covered the scientific use as well as the industrial applications of the neutron beams.

**„Helios“ polarisiert Neutronen**  
 Am Forschungsreaktor FRM 2 der TU München in Garching, so die Wissenschaftler. Um magnetische Eigenschaften zu untersuchen, werden Neutronen genutzt.

Münchner Merkur 01.03.05

**Reaktorbetrieb rechtens**  
 Letzte Beschwerde gegen den FRM II abgewiesen

Süddeutsche Zeitung 5./6.03.05

**Forschungsneutronenquelle Heinz Maier-Leibnitz (FRM-II)**



Standard.at 03.03.05

**Umstritten, aber zugelassen: Der Forschungsreaktor Garching**  
 Als Hochleistungs-Neutronenquelle vorgesehen - Betriebserlaubnis nach zurückgewiesenen Anrainerbeschwerden rechtskräftig

**Hamburger Abendblatt**

Hamburger Abendblatt 16.03.05

Wissen

**Was macht Neutronen für die Forscher nur so attraktiv?**

CHANCEN MARKTPLATZ

HOCHSCHULE UND WISSENSCHAFT

**Hochfluss-Neutronenquelle jetzt im Routinebetrieb**

Zur Verfügung gestellt vom Informationsdienst Wissenschaft idw

04.05.05

Forschungs-Neutronenquelle Heinz Maier-Leibnitz:

**Garchinger Reaktor gestartet**

Münchner Merkur 06.05.05

**Reaktor hat Routinebetrieb aufgenommen**

TU München jetzt verantwortliche Betreiberin

Garching. (dpa) Im atomaren USA sehen dadurch die internationalen Bemühungen torpediert, die Verbreitung des Bombenstoffes zu verhindern.

**Industrielles Anwenderzentrum bereit für Hightech-Unternehmen**

www.uni-protokolle.de

20.06.2005 - (idw) Technische Universität München

Mit dem neu errichteten Industriellen Anwenderzentrum (IAZ) steht die Forschungs-Neutronenquelle Heinz Maier-Leibnitz ab sofort auch Industrie- und Dienstleistungsunternehmen für Forschungszwecke offen. Vor

**i Life Sciences**

30.08.05

Pharmaforschung in Garching eröffnet neue Möglichkeiten

Nanodisperse Arzneistoffträgersysteme werden mit der Neutronenspektroskopie untersucht

Garching/26.08.2005. Die Forschungs-Neutronenquelle Heinz Maier-Leibnitz (FRM-II) der TU München in Garching wird künftig verstärkt auch Projekten aus dem Bereich Pharmaforschung offen stehen. Langfristig soll sich hieraus ein eigener, exponierter Forschungsschwerpunkt entwickeln, der von den außergewöhnlichen technischen Gegebenheiten, dem hohen Neutronenfluss und der modernsten Instrumentierung der Garchinger Neutronenquelle profitiert. Wie die Universität München am 26. August

Figure 4.8: Headlines of articles in public journals and news papers.

**Ein Meilenstein  
in der Forschung**

TU präsentiert neuen Neutronenreflektor

Münchner Merkur 16.09.05

**Eine Reise in  
den Motor**

AUTO BILD  
14.10.05

Forscher der TU München sind sensationelle Einblicke ins Herz des Autos gelungen: Mit Neutronenstrahlen können sie einen Motor durchleuchten – während er läuft

**Details dünnster Schichten**

**Neutronenreflektometer in Garching eingeweiht**

Garching Ein weltweit einmaliges Gerät, mit dem dünnste Schichten - zum Beispiel auf Transplantaten - untersucht werden können, ist am gestrigen Mittwoch an der Forschungsneutronenquelle Heinz Maier-Leibnitz am Campus Garching der TU eingeweiht worden. Dieses weltweit einmalige und vom Bundesministerium für Forschung mit 3,3 Millionen Euro finanzierte Gerät ermöglicht besonders die Strukturforschung an komplexen biologischen aber auch magnetischen Grenzschichten, die zwischen einem Nano- bis hin zu wenigen Mikrometern klein sind. Zu diesen Grenzschichten gehören beispielsweise bioverträgliche Oberflächen aus synthetischen Polymeren, die Entzündungen auf Transplantaten verhindern können. Süddeutsche Zeitung 15.09.05

Östlich des Garchinger Reaktors entsteht neue Halle

**Jülicher Neutronenforscher ziehen an die Isar**

Sieben wissenschaftliche Großgeräte im Wert von 45 Millionen Euro werden verlagert / „Atom-Ei wird wiederbelebt“

Süddeutsche Zeitung – LKN 21.10.05

„Wir sind Opfer unseres Erfolgs“ Süddeutsche Zeitung 27.10.05

**Am Reaktor wird rund um die Uhr geforscht**

1000 Experimente laufen jährlich an der Neutronenquelle / Auftakt der neuen SZ-Serie

**Warum Metall leitet** Süddeutsche Zeitung 03.11.05

**Neutronen machen Materialeigenschaften sichtbar**

„Als ob Sie ein Fernsehstudio mit einem Kerzenlicht betreiben“ Süddeutsche Zeitung 08.12.05

**Bilder vom Inneren laufender Motoren**

Burkhard Schillinger macht mit Neutronenstrahlen Dinge sichtbar, die so noch keiner gesehen hat

**Arbeit im Grenzbereich von Physik und Chemie**

Tobias Uruh sucht an seinem Spektrometer mit Hilfe von Neutronen nach Trägerstoffen für Arzneimittel

Süddeutsche Zeitung 22.12.05

Figure 4.9: Headlines of articles in public journals and news papers.

## 4.3 Committees

### Strategierat FRM II

#### Chairman

Prof. Dr. Gernot Heger  
Institut für Kristallographie  
RWTH Aachen

#### Members

MRin Dr. Ulrike Kirste  
Bayerisches Staatsministerium für Wissenschaft, Forschung  
und Kunst

Dr. Rainer Koepke  
Bundesministerium für Bildung und Forschung

Prof. Dr. Georg Büldt  
Institut für Biologische Informationsverarbeitung  
Forschungszentrum Jülich

Prof. Dr. Dosch  
Max-Planck-Institut für Metallforschung

Prof. Dr. Dieter Richter  
Institut für Festkörperphysik  
Forschungszentrum Jülich

Prof. Dr. Dirk Schwalm  
Max-Planck-Institut für Kernphysik, Heidelberg

Prof. Dr. Helmut Schwarz  
Institute of Chemistry  
Technische Universität Berlin

Prof. Dr. Dr. Michael Wannemacher  
Radiologische Klinik und Poliklinik  
Abteilung Strahlentherapie  
Universität Heidelberg

Dr. Heinz Voggenreiter  
Director  
Institute of Structures and Design  
German Aerospace Center (DLR) Stuttgart

Prof. Dr. Götz Eckold  
Institute of Physical Chemistry  
Universität Göttingen  
(Speaker Instrumentation Advisory Board)

#### Honorary Member

MDgt i.R. Jürgen Großkreutz

#### Guests

Prof. Dr. Dr. h.c. mult. Wolfgang A. Herrmann  
Präsident der Technischen Universität München

Dr.-Ing. Rainer Kuch  
Hochschulleitung  
Technische Universität München

Dr. Michael Klimke  
Hochschulleitung Technische Universität München

Prof. Dr. Winfried Petry  
ZWE FRM II  
Technische Universität München

Prof. Dr. Klaus Schreckenbach  
ZWE FRM II  
Technische Universität München

Guido Engelke  
ZWE FRM II  
Technische Universität München



## Instrumentation Advisory Board (Subcommittee of the Strategierat)

### Chairman

Prof. Dr. Götz Eckold  
Institute of Physical Chemistry  
Georg-August-Universität Göttingen

### Members

Prof. Dr. Dieter Habs  
Sektion Physik  
Ludwig-Maximilian-Universität München

Prof. Dr. Peter Böni  
Physik Department E21  
Technische Universität München

Prof. Dr. Dirk Dubbers  
Physikalisches Institut  
Universität Heidelberg

Dr. Hans Graf  
Abteilung NE  
Hahn-Meitner-Institut, Berlin

Prof. Dr. Andreas Magerl  
Chair of Crystallography and Structural Physics  
Friedrich-Alexander-Universität Erlangen-Nürnberg

Prof. Dr. Gottfried Münzenberg  
Gesellschaft für Schwerionenforschung mbH, Darmstadt

Prof. Dr. Wolfgang Scherer  
Lehrstuhl für Chemische Physik  
Universität Augsburg

Dr. habil. Dieter Schwahn  
Institut für Festkörperforschung  
Forschungszentrum Jülich

Prof. Dr. Markus Schwaiger  
Lehrstuhl für Nuklearmedizin  
Technische Universität München

Prof. Dr. Andreas Türler  
Institut für Radiochemie  
Technische Universität München

Dr. habil. Regine Willumeit  
GKSS Forschungszentrum, Geesthacht

### Guests

Dr. Michael Klimke  
Referent der Hochschulleitung  
Technische Universität München

Dr. Klaus Feldmann  
BEO-PFR  
Forschungszentrum Jülich

MRin Dr. Ulrike Kirste  
Bayerisches Staatsministerium für Wissenschaft, Forschung  
und Kunst

Prof. Dr. Gernot Heger  
Institut für Kristallographie  
RWTH Aachen

Dr. Jürgen Neuhaus  
ZWE-FRM II  
Technische Universität München

Prof. Dr. Winfried Petry  
ZWE-FRM II  
Technische Universität München

Guido Engelke  
ZWE FRM II  
Technische Universität München

Prof. Dr. W. Press  
Institut Laue Langevin  
Grenoble, France

Prof. Dr. Klaus Schreckenbach  
ZWE FRM II  
Technische Universität München

Prof. Dr. Tasso Springer

**Secretary**

Dr. Peter Link  
ZWE FRM II

**Committee for Industrial and Medical Use  
(Subcommittee of the Strategierat)****Members**

*Automobile Industry*  
Dr.-Ing. Rainer Simon  
BMW AG München

Dr.-Ing. Maik Broda  
Ford Forschungszentrum Aachen

*Aerospace Industry*  
Dr.-Ing. Rainer Rauh  
Airbus Deutschland Bremen

*Chemistry and Environment*  
Dr. Jens Rieger  
BASF AG Ludwigshafen

Dr. Ralph Gilles  
TU München ZWE FRM II  
<http://wwwnew.frm2.tum/en/industry.html>

Dr. Heinz Voggenreiter  
German Aerospace Center (DLR) Stuttgart

**Scientific Committee - Evaluation of Beamtime Proposals  
(Subcommittee of the Strategierat)****Members**

Prof. Dr. Hartmut Abele  
Ruprecht-Karls-Universität  
Heidelberg

Prof. Heinz-Günther Brokmeier  
Institut für Werkstofforschung  
GKSS - Forschungszentrum Geesthacht

Prof. Dr. Matthias Ballauf  
Universität Bayreuth

Prof. Dr. Thomas Brückel  
IFF  
FZ-Jülich

Prof. Dr. John Banhart  
Hahn-Meitner-Institut  
Berlin

Dr. Olwyn Byron  
Div. of Infection and Immunity  
University of Glasgow

Dr. Philippe Bourges  
Laboratoire Léon Brillouin  
CEA Saclay

PD Mechthild Enderle  
Institut Laue Langevin  
Grenoble

Prof. Markus Braden  
Physikalisches Institut  
Universität zu Köln

Prof. Nikolaus Froitzheim  
Geologisches Institut  
Universität Bonn

Dr. Hermann Heumann  
MPI für Biochemie  
Martinsried bei München

Prof. Jan Jolie  
Institute of Nuclear Physics  
Universität zu Köln

Prof. Bernhard Keimer  
Max-Planck-Institut für Festkörperforschung  
Stuttgart

Prof. Dr. Andreas Magerl  
LS für Kristallographie und Strukturphysik  
Universität Erlangen

Prof. Karl Maier  
Helmholtz-Institut für Strahlen- und Kernphysik  
Bonn

Dr. Joël Mesot  
ETH Zürich & PSI  
Villigen, Schweiz

Prof. Dr. Kell Mortensen  
Risoe National Laboratory  
Danish Polymer Center  
Denmark

Prof. Dr. Krause-Rehberg  
Department of Physics  
Universität Halle

Dr. Stéphane Longeville  
Laboratoire Léon Brillouin  
Laboratoire de la Diffusion Neutronique  
CEA Saclay

Prof. Dr. Andreas Meyer  
Physik-Department E13  
TU München

Prof. Michael Monkenbusch  
Institut für Festkörperforschung  
Forschungszentrum Jülich

Prof. Werner Paulus  
Structures et Propriétés de la Matière  
Université de Rennes 1

Dr.-Ing Anke Pyzalla  
Institut für Werkstoffkunde und Materialprüfung  
TU Wien

Prof. Dr. Joachim Rädler  
Department für Physik  
Ludwig-Maximilians-Universität München

Dr. Louis-Pierre Regnault  
CEA Grenoble

Dr. Rodriguez-Carvajal  
Institut Laue-Langevin  
Grenoble

Prof. Günther Roth  
Institut für Kristallographie  
RWTH Aachen

Prof. Michael Ruck  
Institut für Anorganische Chemie  
TU Dresden

Prof. Wolfgang Scherer  
Institut für Chemische Physik  
Universität Augsburg

Prof. Wolfgang Schmahl  
LS für Strukturforschung  
Ludwig-Maximilians-Universität München

Prof. Jeremy Smith  
Fachbereich Computational Molecular Biophysics  
Universität Heidelberg

Prof. Dr. Manfred Stamm  
Institut für Polymerforschung  
Dresden

Prof. Bernd Stühn  
Institut für Festkörperphysik  
TU Darmstadt

Prof. Monika Willert-Porada  
Lehrstuhl für Werkstoffverarbeitung  
Universität Bayreuth

PD Katharina Theis-Bröhl  
Festkörperphysik  
Ruhr-Universität Bochum

### Scientific Secretaries

Dr. Christoph Hugenschmidt  
ZWE FRM II

Dr. Martin Meven  
ZWE FRM II

Dr. Peter Link  
ZWE FRM II

Dr. Tobias Unruh  
ZWE FRM II

### TUM Advisory Board

#### Chairman

Prof. Dr. Ewald Werner  
Lehrstuhl für Werkstoffkunde und -mechanik  
Technische Universität München

#### Members

Prof. Dr. Peter Böni  
Physik Department E21  
Technische Universität München

Prof. Dr. Bernhard Wolf  
Heinz Nixdorf-Lehrstuhl für medizinische Elektronik  
Technische Universität München

Prof. Dr. Andreas Türler  
Institut für Radiochemie  
Technische Universität München

Prof. Dr. Arne Skerra  
Lehrstuhl für Biologische Chemie  
Technische Universität München

Prof. Dr. Markus Schwaiger  
represented by Prof. Dr. Senekowitsch-Schmidtke  
Nuklearmedizinische Klinik und Poliklinik  
Klinikum Rechts der Isar  
Technische Universität München

#### Guests

Dr. Michael Klimke  
University Management  
Technische Universität München

Prof. Winfried Petry  
ZWE FRM II  
Technische Universität München

Guido Engelke  
ZWE FRM II  
Technische Universität München

Prof. Klaus Schreckenbach  
ZWE FRM II  
Technische Universität München

## Scientific Steering Committee

### Chairman

Dr. Hans Boysen  
Sektion Kristallographie  
Ludwig-Maximilians-Universität München

Prof. Dr. Bernhard Keimer  
MPI für Festkörperforschung Stuttgart

Prof. Dr. Dieter Richter  
IFF FZ-Jülich

Prof. Dr. Winfried Petry  
ZWE FRM II  
TU München

## 4.4 Staff

### Board of Directors

#### Scientific Director

Prof. Dr. W. Petry

#### Technical Director

Prof. Dr. K. Schreckenbach

#### Administrative Director

G. Engelke

### Experiments

#### Head

Prof. Dr. W. Petry

#### Secretaries

W. Wittowetz

E. Jörg-Müller

#### Coordination

Dr. J. Neuhaus

H. Türck

H. Bamberger

#### Instruments

P. Aynajian (MPI-Stuttgart)

Dr. S. Bayrakci (MPI-Stuttgart)

J. Brunner

K. Buchner (MPI-Stuttgart)

M. Bröll(MPI-Stuttgart)

W. Bünten (JCNS)

E. Calzada

Chr. Daniel (LMU München)

D. Etzdorf

J. Franke (MPI-Stuttgart)

Dr. U. Garbe (GKSS)

Dr. A.-M. Gaspar

Dr. R. Georgii

Dr. R. Gilles

Dr. M. Haese-Seiller (GKSS)

Dr. W. Häußler

F. Hibsich

Dr. M. Hofmann

Dr. M. Hölzel (TU Darmstadt)

Dr. K. Hradil (Univ. Göttingen)

Dr. C. Hugenschmidt

Dr. V. Hutano (RWTH Aachen)

S. Kampfner

R. Kampmann (GKSS)

Dr. T. Keller (MPI-Stuttgart)

Dr. V. Kudryaschov(GKSS)

B. Krimmer

D. Lamago

Dr. P. Link

Dr. Loeper-Kabasakal

C. Loistl

K. Lorenz

R. Lorenz

A. Mantwill

F. Maye (MPI-Stuttgart)

T. Mehadene

Dr. M. Meven

S. Mühlbauer

Qi Ning (Visiting Scientist from China)

M. Nülle (MPI-Stuttgart)

Dr. A. Ostermann

Dr. B. Pedersen

C. Piochacz

Dr. J. Rebelo-Kornmeier (HMI Berlin)

Dr. A. Radulescu (JCNS)

R. Repper

Dr. D. Rich

J. Ringe

Dr. P. Rottländer (JCNS)

Dr. A. Rühm (MPI Stuttgart)

A. Sazonov

Dr. B. Schillinger

Dr. M. Schlapp (TU Darmstadt)

H. Schneider (Univ. Göttingen)

Dr. A. Schneidewind (TU Dresden)

R. Schwikowski

Dr. A. Senyshyn (TU Darmstadt)

G. Seidl

C. Smuda

M. Stadlbauer

B. Straßer

Dr. T. Unruh

H. Wagensonner

EM. Wagner

Dr. W. Waschkowski

Dr. U. Wildgruber (MPI-Stuttgart)

Dr. R. Wimpory (HMI Berlin)

Dr. H.-F. Wirth

Dr. Joachim Wuttke (JCNS)

Prof. O. Zimmer

#### Detectors and electronic

Dr. K. Zeitelhack

Dr. I. Defendi

S. Egerland

Dr. A. Kastenmüller

D. Maier

M. Panradl

Th. Schöffel

#### Sample environment

Dr. J. Peters

H. Kolb

A. Pscheidt

A. Schmidt

J. Wenzlaff

#### Neutron optics

Prof. Dr. G. Borchert

C. Breunig

H. Hofmann

E. Kahle

O. Lykhvar

Dr. S. Masalovich

A. Ofner

A. Urban

R. Valicu

#### IT Services

J. Krüger

H. Wenninger

L. Bornemann

J. Ertl

J. Dettbarn

S. Galinski

H. Gilde

J. Mittermaier

R. Müller

J. Pulz

C. Rajaczak

S. Roth

M. Stowasser

B. Wildmoser

#### Konstruktion

K. Lichtenstein

## Administration

### Head

G. Engelke

### Secretary

C. Zeller

### Members

B. Bendak  
B. Gallenberger  
I. Heinath  
K. Lüttig  
R. Obermeier

### Public relations

I. Scholz (ZV TUM)  
A. Schaumlöffel

### Visitorservice

U. Kurz  
Dr. B. Tonin-Schebesta

## Reactor operation

### Head

Prof. Dr. K. Schreckenbach  
Dr. Ingo Neuhaus,  
designated Technical Director

### Secretaries

M. Neuberger  
S. Rubsch

### Management

Dr. H. Gerstenberg (irradiation and  
sources)  
Dr. J. Meier (reactor projects)  
Dr. C. Morkel (reactor operation)

### Shift members

F. Gründer  
A. Bancsov  
A. Benke  
M. Danner  
J.-M. Favoli  
M. Flieher  
H. Groß  
L. Herdam  
F. Hofstetter  
K. Höglauer  
T. Kalk  
G. Kaltenegger  
U. Kappenberg  
F. Kewitz  
M. G. Krümpelmann  
J. Kund  
A. Lochinger  
G. Mauermann  
A. Meilinger  
M. Moser  
L. Rottenkolber  
G. Schlittenbauer

### Technical services

N. Waasmaier  
K. Pfaff  
J. Aigner  
D. Bahmet

R. Binsch  
H. Gampfer  
W. Glashauser  
J. Groß  
G. Guld  
B. Heck  
N. Hodzic  
M. Kleidorfer  
W. Kluge  
H. Kollmannsberger  
J.-L. Kraus  
R. Maier  
K. Otto  
A. Schindler  
R. Schlecht jun.  
J. Schreiner  
C. Strobl  
G. Wagner  
A. Weber  
J. Wetzl  
N. Wiegner  
C. Ziller

### Electrics and electronics

R. Schätzlein  
G. Aigner  
W. Buchner  
Ü. Sarikaya  
H. Schwaighofer  
U. Wildgruber

### Irradiation and sources

Dr. H. Gerstenberg  
Dr. E. Gutmiedl  
Dr. X. Li  
C. Müller  
M. Oberndorfer  
D. Päthe  
W. Lange  
G. Langenstück  
V. Loder  
A. Richter  
H. Schulz  
E.-M. Wagner

A. Wirtz

### Reactor projects

Dr. J. Meier  
M. Schmitt  
M. Ullrich

### Documentation

V. Zill  
J. Jung

### Instrument Safety

R. Lorenz

### Technical design

F.-L. Tralmer  
J. Fink  
H. Fußstetter  
J. Jüttner  
K. Lichtenstein

### Workshops

C. Herzog  
U. Stiegel  
A. Begic  
M. Fuß  
A. Huber  
A. Scharl  
R. Schlecht sen.  
M. Tessaro

### Radiation protection

Dr. H. Zeising  
S. Dambeck  
W. Dollrieß  
H. Hottmann  
B. Neugebauer  
D. Kugler  
H.-J. Werth  
S. Wolff

### Chemical laboratory

Dr. F. Dienstbach  
U. Jaser  
C. Auer  
R. Bertsch

**Reactor physics**

Prof. Dr. K. Böning  
Dr. A. Röhrmoser

N. Wieschalla  
C. Bogenberger

R. Jungwirth

**Security department**

L. Stienen

J. Stephani



## 4.5 Publications

- [1] Schneidewind A., Link P., Etzdorf D., Schedler R., Rotter M., Loewenhaupt M. *PANDA: first results from the cold three axes spectrometer at FRM-II, (proceedings of ICNS 2005). Physica B*. In press.
- [2] Affouard F., Cochin E., Danede F., Decressain R., Descamps M., Häussler W. *Onset of slow dynamics in difluorotetra-chloroethane glassy crystal. Journal of Chemical Physics*, **123/8**, (2005), 084501.
- [3] Brunner M., J. Engelhardt, Frei G., Gildemeister A., Lehmann E., A. H., Schillinger B. *Characterization of the image quality in neutron radioscopy. Nucl. Instr. & Meth.*, **A542**, (2005), 123–128.
- [4] Böning K. *The New FRM-II Research Reactor in Munich. The 2005 Frederic Joliot/Otto Hahn Summer School on Nuclear Reactors, Karlsruhe (Germany) August 24 - September 2, 2005, Proceedings of the Summer School*, 14 pages.
- [5] Cadogan J., Moze O., Ryan D., Suharyana, Hofmann M. *Magnetic ordering in DyFe<sub>6</sub>Sn<sub>6</sub>. Physica B*. In press.
- [6] Calzada E., Schillinger B., F. G. *Construction and assembly of neutrons radiography and tomography facility ANTARES at FRM-II. Nucl. Instr. & Meth.*, **A 542**, (2005), 38–44.
- [7] Fei Y., Kennedy S., Campell S., Hofmann M. *Neutron polarisation analysis of nanostructured ZnFe<sub>2</sub>O<sub>4</sub>. Physica B*, **356**, (2005), 264.
- [8] Gapinski J., Wilk A., A. P., Häussler W. *Diffusion and microstructural properties of solutions of charged nanosized proteins: Experiment vs Theory. Journal of Chemical Physics*, **123 (5)**, (2005), 054708.
- [9] Gilles R. *Neutron scattering, a powerful tool in material science exemplary on superalloys. Zeitschrift für Metallkunde*, **96, 4**, (2005), 325–334.
- [10] Gilles R., Schlapp M., Hölzel M., Krimmer B., Boysen H., Fuess H. *SPODI - the new Structure Powder Diffractometer at the FRM-II. Zeitschrift für Kristallographie - Suppl.*, **22, 45**.
- [11] Grigoriev S., Maleyev S., Okorokov A. I., Chetverikov Y. O., Georgii R., Böni P., Lamago D., Eckerlebe H., Pranzas K. *Critical fluctuations in MnSi near T<sub>c</sub>: A polarized neutron scattering study. Physical Review*, **B 72**, (2005), 134420–1–5.
- [12] Gutmiedl E., Petry W., Schreckenbach K. *Status of the new research reactor FRM-II. Proceedings of the International Symposium on Research Reactor and Neutron Science - In Commemoration of the 10th Anniversary of HANARO Daejeon, Korea, April 2005*.
- [13] Hofmann M., Campell S., Link P., Fiddy S., Goncharenko. *Valence and Magnetic Transitions in YbMn<sub>2</sub>Ge<sub>2</sub> - Pressure and Temperature. Physica B*. In press.
- [14] Hofmann M., Schneider R., Seidl G., Kornmeier J., Wimpory R., Garbe U., Brokmeier H. *The New Materials Science Diffractometer STRESS-SPEC at FRM-II. Physica B*. In press.
- [15] Hugenschmidt C., Mayer J., Stadlbauer M. *Investigation of the near surface region of chemically treated and Al-coated PMMA by Doppler-broadening spectroscopy. Radiat. Phys. Chem.* In press.
- [16] Hugenschmidt C., Schreckenbach K., Stadlbauer M., Straßer B. *First positron experiments at NEPOMUC. Appl. Surf. Sci.*, **252**, (2006), 3098 – 3105.
- [17] Hugenschmidt C., Schreckenbach K., Stadlbauer M., Straßer B. *Low energy positrons of high intensity at the new positron facility NEPOMUC. Nucl. Instr. Meth.*, **A 554, 1-3**, (2005), 384–391.
- [18] Häussler W., Schmidt U. *Effective field integral subtraction by the combination of spin echo and resonance spin echo. Physical Chemistry Chemical Physics*, **7/6**, (2005), 1245 – 1249.
- [19] Jarousse C., Lemoine P., Petry W., Röhrmoser A. *Monolithic UMO Full Size Prototype Plates Manufacturing Development. The International Meeting on Reduced Enrichment for Research and Test Reactors RERTR, Boston (Mass. USA), November 6-10, 2005; to be published in the RERTR 2005 Proceedings*.
- [20] Jobic H., Karger J., Krause C., Brandani S., Gunadi A., Methivier A., Ehlers B., G. and Farago, Häussler W., Ruthaven D. *Diffusivities of n-alkanes in 5A zeolite measured by neutron spin echo, pulsed-field gradient NMR, and zero length column techniques. Adsorption Journal of the International Adsorption Society*, **11, Suppl. 1**, (2005), 403–407.

- [21] Köper I., Bellissent-Funel M.-C., Petry W. *Dynamics from picoseconds to nanoseconds of trehalose in aqueous solutions as seen by quasielastic neutron scattering*. *J. of Chemical Physics*, **122**, (2005), 014514–1–6.
- [22] Lamago D., Georgii R., Böni P. *Magnetic susceptibility and specific heat of the itinerant ferromagnet MnSi*. *Physica*, **B 359**, (2005), 1171–1173.
- [23] Masalovich S., Ioffe A., Schlapp M., von Seggern H., Küssel E., Brückel T. *Optimization of a neutron image plate detector with low gamma-sensitivity*. *Nuclear Instruments and Methods in Physics Research*, **A 539**, (2005), 236–249.
- [24] Mühlbauer M., Calzada E., Schillinger B. *Development of a system for neutron radiography and tomography*. *Nucl. Instr. and Meth.*, **A 542**, (2005), 324–328.
- [25] Nienhaus K., Ostermann A., Nienhaus G., Parak F., Schmidt M. *Ligand migration and protein fluctuations in myoglobin mutant*. *Biochemistry*, **44**, (2005), 5095–105.
- [26] Okorov A., Grigoriev S., Hugenschmidt C., Chevertikov Y., Maleyev S., Georgii R., Böni P., Lamago D., Eckerlebe H., Pranzas K. *The effect of the magnetic field on the spiral spin structure in MnSi studied by polarized SANS*. *Physica*, **B 356**, (2005), 259–263.
- [27] Ostermann A., Parak F. *Hydrogen Atoms and Hydration in Myoglobin: Results from High Resolution Protein Neutron Crystallography*. in: *Hydrogen- and Hydration Sensitive Structural Biology*, ISBN4-87805-061-6 C3045, 111–122.
- [28] Röhrmoser A., Petry W., Wieschalla N. *Reduced Enrichment Program for the FRM-II, Status 2004/05*. *Proceedings '9th International Meeting on Reduced Enrichment for Research and Test Reactors (RERTR)', Budapest, April 10 - 13, 2005*.
- [29] Schillinger B., Abele H., Brunner J., Frei G., Gähler R., Gildemeister A., Hillenbach A., Lehmann E., Vontobel P. *Detection systems for short-time stroboscopic neutron imaging and measurements on a rotating engine*. *Nucl. Instr. and Meth.*, **A542**, (2005), 142–147.
- [30] Schillinger B., Brunner J. *Stroboscopic and continuous fast imaging with neutrons*. *Internal Publication of PSI on the occasion of the International Workshop 'Imaging with cold neutrons' held on Oct 13th -14th, 2005 at Paul-Scherrer- Institute*.
- [31] Schillinger B., Brunner J., Calzada E. *A study of oil lubrication in a rotating engine using stroboscopic neutron imaging*. *Physica B*. In press.
- [32] Schillinger B., Calzada E. *Proposed combination of CAD data and discrete tomography for the detection of coking and lubricants in turbine blades of engines*. *Electronic Notes in Discrete Mathematics; Proceedings of the Workshop on Discrete Tomography and its Applications*, **20**, (2005), 493–499.
- [33] Schreckenbach K. *Nukleare Inbetriebnahme des FRM-II* (Jahrestagung Kerntechnik, 10.-12. Mai 2005, Nürnberg, 2005).
- [34] Schreckenbach K., Gerstenberg H. *Status Report on the Nuclear Start-up of FRM-II*. *ENS RRFM Transactions - 9 th International Topic Meeting on Research Reactor Fuel Management, Budapest, 10-13 April 2005*, 114 – 118.
- [35] Stadlbauer M., Hugenschmidt C., Schreckenbach K., Straßer B. *Spatially Resolved Investigation of Thermally Treated Brass with a Coincident Doppler-Spectrometer*. *Appl. Surf. Sci.*, **2006**, (2005), 3269 – 3273.
- [36] Stampanoni M., Borchert G., Abela R. *Progress in Microtomography with the Bragg Magnifier at SLS*. *Radiation Physics and Chemistry*. In press.
- [37] Stampanoni M., Borchert G., Abela R. *Nanotomography employing asymmetrical Bragg diffraction*. *Nucl. Instr. Meth.*, **A 551**.
- [38] Wieschalla N., Böning K., Petry W., Röhrmoser A., Böni P., Bergmaier A., Dollinger G., Grossmann R., Schneider J. *Heavy Ion Irradiation of U-Mo/Al Dispersion Fuel*. *The International Meeting on Reduced Enrichment for Research and Test Reactors RERTR, Boston (Mass. USA), November 6-10, 2005; to be published in the RERTR 2005 Proceedings*.
- [39] Zeitelhack K., Schanzer C., Kastenmüller A., Röhrmoser, Daniel C., Franke J., Gutmiedl E., Kudryashov V., Maier D., Päthe D., Petry W., Schöffel T., Schreckenbach K., Urban A., Wildgruber U. *Measurement of neutron flux and beam divergence at the cold neutron guide system of the new Munich research reactor FRM-II*. *Nuclear Instruments and Methods in Physics Research A*. In press.

# Imprint

.....

Publisher:  
Technische Universität München  
Forschungsneutronenquelle Heinz Maier-Leibnitz (FRM II)  
Lichtenbergstr. 1  
85747 Garching  
Germany  
Phone: +49 89-289-14965  
Fax: +49 89-289-14995  
Internet: <http://www.frm2.tum.de>  
email: [userinfo@frm2.tum.de](mailto:userinfo@frm2.tum.de)

.....

Editors:  
J. Neuhaus  
B. Pedersen

.....

Photographic credits:  
All images: TUM

.....

Design:  
B. Pedersen, TUM  
J. Neuhaus, TUM  
E. Jörg-Müller, TUM

.....

Typesetting(L<sup>A</sup>T<sub>E</sub>X<sub>2 $\epsilon$</sub> ):  
B. Pedersen, TUM  
E. Jörg-Müller, TUM

.....